COMPUTATIONAL MODELING OF STATIC AND DYNAMIC EARTH PRESSURE AGAINST RETAINING WALLS BASED ON LOCALIZED DEFORMATION

Hemanta Hazarika

COMPUTATIONAL MODELING OF STATIC AND DYNAMIC EARTH PRESSURE AGAINST RETAINING WALLS BASED ON LOCALIZED DEFORMATION

A dissertation submitted in partial fulfillment of the
requirements for the Degree of Doctor of Engineering

Hemanta Hazarika

DEPARTMENT OF GEOTECHNICAL AND ENVIRONMENTAL ENGINEERING
NAGOYA UNIVERSITY
NAGOYA, JAPAN

MARCH 1996

ACKNOWLEDGMENTS

This dissertation presents the author's three years of research works after completion of the master course. The author here wishes to acknowledge the supervision, guidance, support, encouragement and assistance, received from the faculties, colleagues, family as well as the friends.

The author extends his sincere gratitude to his supervisor Dr. Minoru Matsuo, Professor, Department of Geotechnical and Environmental Engineering, Nagoya University for admitting the author as doctoral student in his laboratory, offering the research opportunity in a new environment, for his sincere advice and encouraging suggestions.

The author expresses his profound gratitude to his academic advisor Dr. Akira Asaoka, Professor, Department of Civil Engineering, Nagoya University for his valuable advice, able guidance, personal encouragement and continuous moral support. The dynamic and inspiring personality in him, helped the author a lot during this tumultuous period. It was a matter of great pleasure to have him as academic advisor.

The author also takes this opportunity to express his heartfelt gratitude to Dr. Hiroshi Matsuzawa, former Associate Professor at the Department of Geotechnical and Environmental Engineering, Nagoya University and currently at Ohyo Corporation Ltd., Nagoya for his non-ending support, infallible guidance and continuing advice in the research from the very start of the author's study at Nagoya University.

Great pleasure is also felt by the author in extending appreciation to doctoral course jury member Dr. Satoru Ohtsuka, Associate Professor at the Department of Geotechnical and Environmental Engineering, Nagoya University for reading the text painstakingly, and making valuable suggestions for improvement of this thesis, as well as for his personal interest and concern in author's research.

Sincere thanks and gratitude are due to Dr. Yoshitsugu Hayashi, Professor, Department of Geotechnical and Environmental Engineering, Nagoya University for serving in the examination committee and his encouragement.

Thanks and appreciation are also due to Mr. Masahiro Sugimura, formerly Research Associate at the Department of Geotechnical and Environmental Engineering, and currently consulting engineer at Tamano Sogo Corporation Ltd., Nagoya for his helpful advice and invaluable suggestions in the numerical computations as well as in conducting the experiments during this study.

The author expresses his gratitude to Dr. Kano Ueshita, Retired Professor, Department of Geotechnical and Environmental Engineering, Nagoya University, and now at Department of Civil Engineering, Chubu University for serving as his supervisor for the first two years of author's doctoral research.

The author also expresses his appreciation to all the faculty members of the Department of Geotechnical and Environmental Engineering as well as the Department of Civil Engineering for their direct and indirect help and encouragement in the course of the author's study at Nagoya University. The lectures of these eminent faculty members were of great help to authors in his research.

Special thanks go to Dr. Masaki Nakano, Assistant Professor, Department of Geotechnical and Environmental Engineering and to Dr. Toshihiro Noda, Research Associate, Department of Civil Engineering for helping the author in all the official affairs as well as in the daily affairs concerning author's academic life.

Thanks are also due to Ms. Noriko Itoh, officer of Civil Engineering Department and Ms. Akiko Tsunekawa, officer of Geotechnical and Environmental Engineering Department for their kind help concerning official matters. The author also would like to thank Ms. Kimiko Kamigaito, Librarian, Department of Civil Engineering for her kind gesture in times of need.

Thanks and appreciation are extended to Dr. Gyaneswor Pokharel of Yahagi Corporation Ltd., Nagoya, Japan, the friendly discussion with whom benefited the author a lot in his research. Mr. Dimitri Blanis of Kyoto University, Kyoto, Japan deserves special acknowledgment for proofreading the manuscript painstakingly.

The author likes to thank Dr. Yuzuru Matsuoka, Professor at the Department of Geotechnical and Environmental Engineering for the kind gesture in letting use the computer facilities in his laboratory. The author also appreciates the direct or indirect help extended by Dr. Kenji Daito, Assistant Professor at Department of Geotechnical and Environmental Engineering, by the past students of Environmental Geotechnics Laboratory, the students of Matsuo-Asaoka Laboratory, and the students of Matsuoka Laboratory, in particular Messrs. Sekiguchi, Mizuno, Tajima, Hayashi, Yahata and Geshi.

The financial support from the Ministry of Education and Culture (MONBUSHO), Japanese Government, deserves special acknowledgment, without which the author's stay in Japan would not have been possible.

The author takes this opportunity to extend appreciation to his friends from overseas at Nagoya University and the Japanese friends, in particular, to Miss Fumie Sasa for providing moral support and encouragement.

Last but not the least, the authors heartfelt thanks go to his beloved parents, sister Ila, and brother Pronob for their mental and emotional support as well as abiding understanding during his stay in Japan. This piece of work is dedicated to author's mother Ms. Swarnalata Hazarika and father Mr. Sreemanta Ram Hazarika, who taught him the value of education.

Hemanta Hazarika
Nagoya University, Japan

CONTENTS

CHAPTER
ONE

Introduction

A journey of a million miles
starts with the first step

Confucius

1.1 GENERAL ISSUES

The determination of forces acting on geotechnical engineering structures, which are in indirect or direct connection with earth masses, is of paramount importance in applied soil mechanics. A sound knowledge of these forces (both the static and dynamic) is essential for the safe and economical design of such structures as retaining walls, footings, tunnels etc.

A retaining wall is a structure designed to maintain a difference in the elevations of the ground surfaces on each side of the structure. Retaining walls are extensively used in connection with railways, highways, bridges, canals and many other engineering works. Some of the more common uses are illustrated in Fig. 1.1. The examples given in the figure give an insight as to how the retaining walls as civil engineering structures are intimately involved in the day to day life of human beings. Hence, proper analysis and design of these structures assume utmost importance. The stability analysis of the retaining walls necessitates the determination of earth pressures acting against the walls. Fig. 1.2 shows the various parameters involved in the analysis and design of a retaining wall-backfill system when the wall moves in active mode. The figure is for the sole purpose of illustration, since retaining walls of simple trapezoidal section are rarely constructed. The resultant active force P_A acts at an angle δ to the back of the wall. The wall friction angle δ is more often expressed as $\tan\delta$, the coefficient of wall friction. The point of application of the resultant force is conveniently expressed as a dimensionless quantity (h/H), called the relative height of point of application.

The Classical earth pressure theory, enunciated by Coulomb, is widely used in the earth pressure analysis and design of the retaining structures within the validity of the assumptions of that theory. The theory, however, paid no attention whatsoever to the modes of movement

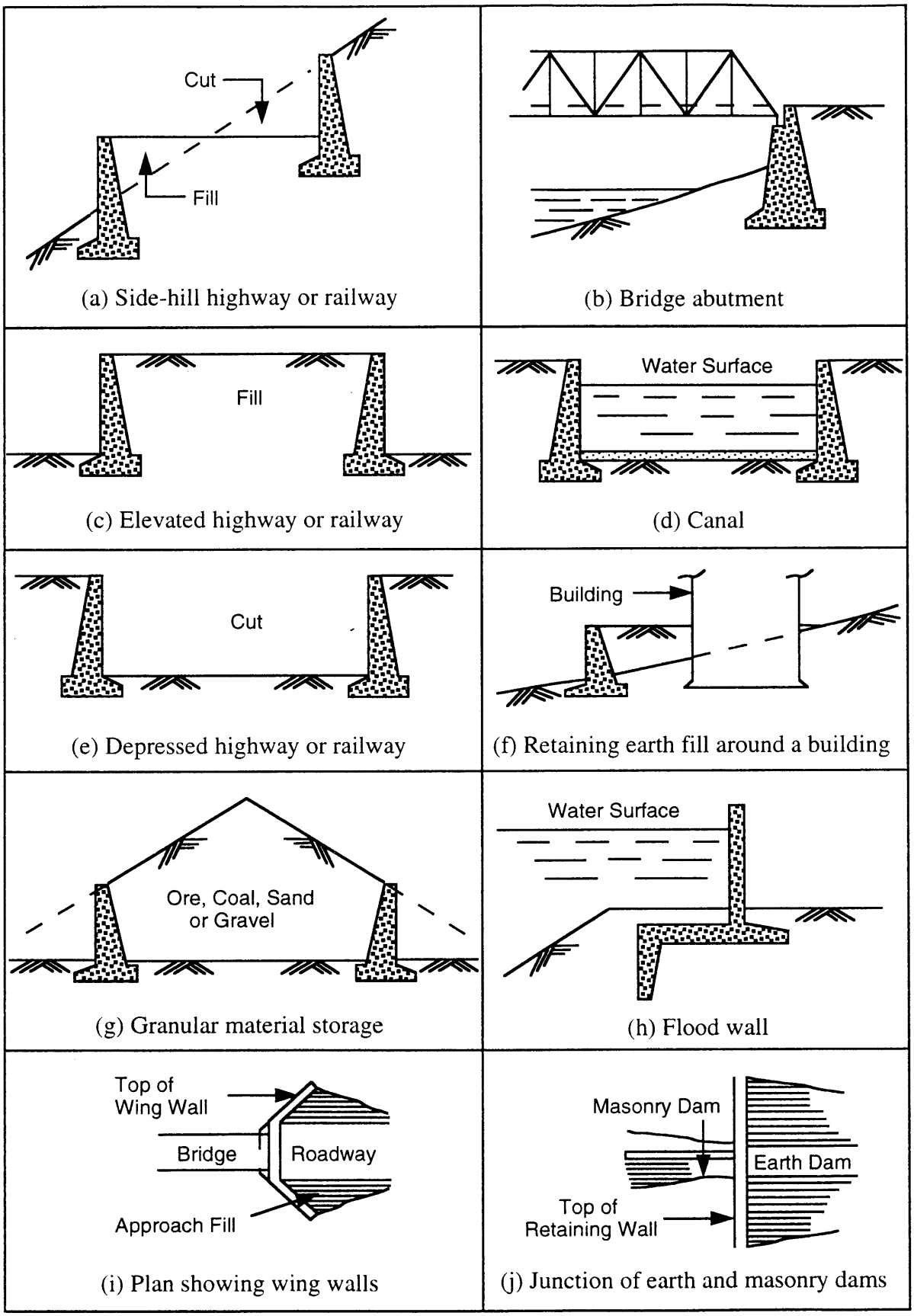

Fig. 1.1 Common uses of retaining wall (*After* Huntington, 1957)

of the wall (Translation, Rotation about the base, Rotation about the top, Rotation about the base as well as Translation etc.) and assumed the lateral earth pressure distribution to be simply hydrostatic. Mononobe-Okabe's dynamic earth pressure theory too has similar drawback as it is based on Coulomb's static earth pressure theory.

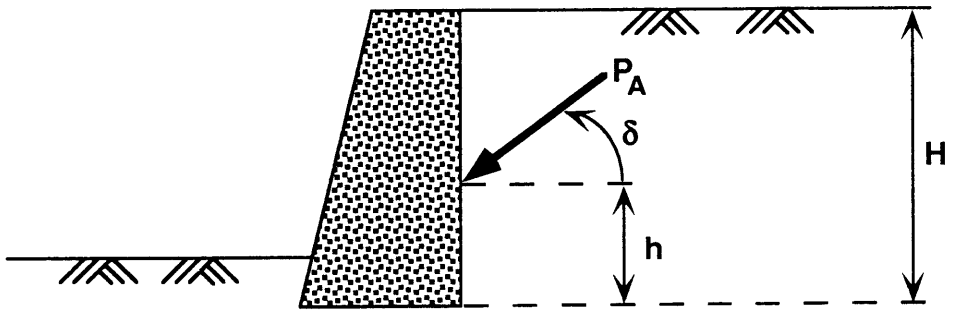

Fig. 1.2 Main parameters of interests in earth pressure calculations

Ever since Terzaghi (1936) pointed out the fallacies in Coulomb's theory, the attention of the research community in the field of earth pressure has been focused on the earth pressure dependent on the wall movement modes. Experimental observations by various researchers (Roscoe (1970), Ichihara and Matsuzawa (1973), Sherif et. al (1982), Sherif et. al (1984), Sherif and Fang (1984), Fang and Ishibashi (1986), Ishibashi and Fang (1987), Kawamura et al (1983), Ohara (1970)) have led to the conclusion that the magnitude and the distribution of the earth pressure as well as the point of application of the resultant are influenced by the kinds of movement the wall experiences in various situations. Analytical expressions have been proposed (Dubrova (1962), Saran and Prakash (1977), Dimarogona (1983), Bang (1985)) explaining the nonlinear distribution of the earth pressure for different modes of wall displacement under static as well as dynamic loading.

However, the analytical methods can not explain the real phenomenon associated, as they are unable to truly capture the progressive deformation characteristics of the backfill, and hence, its consequences on the active or passive state parameters. Nevertheless, the basis of these methods is the classical Coulomb theory which gives only the upper bound solution. On the other hand, development of an efficient numerical model to treat this dependency of earth pressure on the wall movement modes (thus enabling the practicing engineers to translate the results into the design) is still at its infancy. This research is a step forward in the direction towards the development of a numerical model.

Fig. 1.3 shows the various components which are part and parcel of the numerical modeling of a retaining wall, namely: (1) the backfill and (2) the interface between the wall and the backfill. In this dissertation, the emphasis is given to the modeling of these two components, with special consideration to the wall deformation modes, which will be discussed in detail in subsequent chapters.

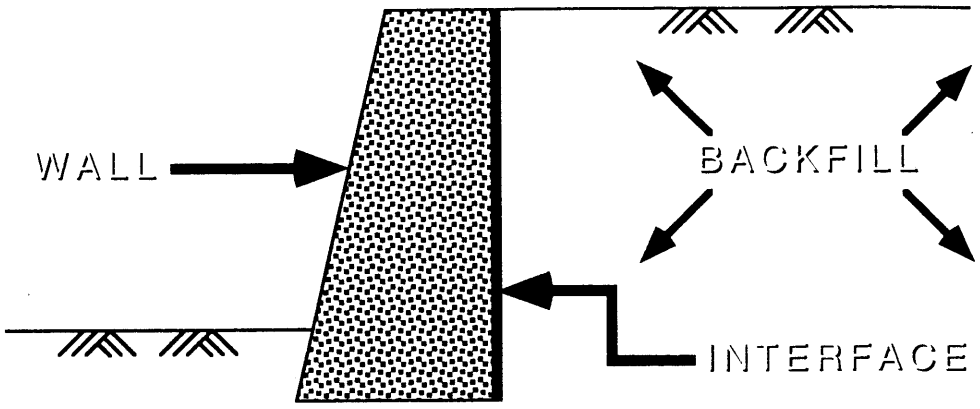

Fig. 1.3 Components involved in the modeling of a retaining wall-backfill system

Fig. 1.4 shows the different approaches usually adopted for the computational modeling of a retaining wall-backfill system. The topics with shaded blocks connected by thick arrows are of special interest to this research, and much attention is focused on these topics. The three main issues of interests extensively considered in this thesis are:

(1) Modeling of the Backfill

(2) Modeling of the Interface

(3) How the Earth Pressure (both Static and Dynamic) is influenced by the Wall Displacement Modes?

1.2 OBJECTIVES AND SCOPE OF THIS RESEARCH

1.2.1 Overview

As mentioned earlier, the analytical methods based on the classical theory and other theories with rigid-plastic assumption, are not sufficient to capture the progressive deformation phenomenon such as earth pressure development against a retaining wall. Hence, researchers resort to numerical methods. Researches galore can be found relating to the numerical computations of the static and dynamic earth pressure, using different approaches. However, these works seem to ignore the progressive deformation characteristics of the backfill soil such as localization. When deformed sufficiently into the plastic range, the deformation within the granular materials tends to localize along concentrated bands, named *Shear Bands,* resulting in non-uniform stress state within an element. The modeling of this localization phenomenon is of immense practical importance since the failure of many engineering structures is indeed characterized by the formation and propagation of shear bands. In particular, failure and post-failure analyses are important in earthquake, mining and petroleum engineering design problems, where one is typically interested in the ultimate

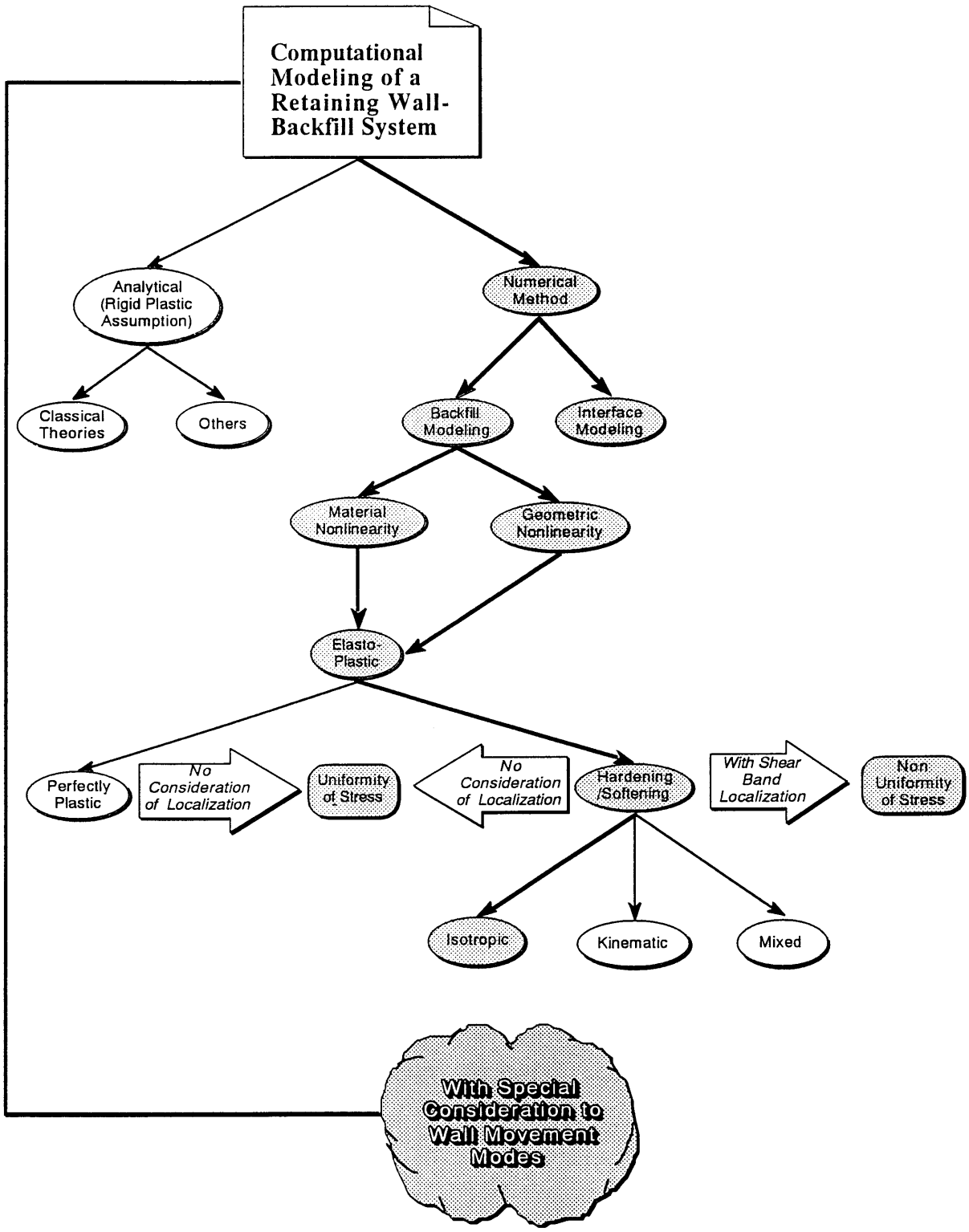

Fig. 1.4 Various approaches of modeling the retaining wall-backfill system

and residual bearing capacities of the various analyzed structures. In process of earth pressure generation, the initiation of the active or the passive state from the at-rest state is a phenomenon which involves progressive failure. Thus, the simultaneous mobilization of the peak strength at various locations along the slip surface, as assumed in most of the analyses,

is not encountered frequently. Hence the numerical analysis of the earth pressure calls for the consideration of the effects of the incepted shear bands.

Most of the numerical works on seismic earth pressure use equivalent linear stress-strain relation for defining the constitutive properties of the backfill. These researches paid attention only to the dynamic component of the earth pressure, not the total earth pressure. The lion's share of this research was devoted to the development of the constitutive relation of the backfill, for modeling the static and the dynamic earth pressure, considering the localized deformations. The developed model can be applied to analyze both the earth pressures (total static and total dynamic).

The modeling of the interface is an integral part of the earth pressure analysis as it involves the interaction of the retaining structures and the backfill soil. Various interface models with varying degree of complexity are available in the literature to date. A new simplified interface model, from the point of view of the earth pressure analysis, is also presented in this thesis.

1.2.2 Objectives

The principal elements of the present study are already illustrated in Fig. 1.4. The purpose of this study is to treat the previously mentioned three topics of interest (i.e. backfill modeling, interface modeling and how the earth pressure is influenced by the wall displacement modes). Accordingly, the objectives of this research are in three folds: (1) To develop a numerical model for the analysis of a retaining wall-backfill system; (2) To apply the developed model to analyze the active earth pressure generation against a rigid wall supporting dry backfill sand for various modes of deformation of the wall and (3) To bring to light the various governing mechanisms involved in the backfill deformations.

The first objective involves the modeling of the backfill as well as the interface. Consequently, the development of a new constitutive law for the backfill material considering the localized deformation, and the idealization of the interface, which fits well the physical mechanism involved in the wall-backfill interaction, form the foundation of this research.

1.2.3 Scope

As of the present, the application of the developed methodology is restricted only to the experimental model. As a first step, if a fundamental methodology can be developed through simulation of the experimental models, in future this methodology can be refined and used in practical problems instead of directly applying it to the field problems which have no reliable data. Nevertheless, it is assumed that the inferences derived from this research can be easily carried over to other retaining wall problems.

1.3 ORGANIZATION OF THE THESIS

This chapter gives a general view of the issues related to the earth pressure research. The scope and the objectives of the research are also indicated. The organizational structure of the thesis is schematically shown in Fig. 1.5.

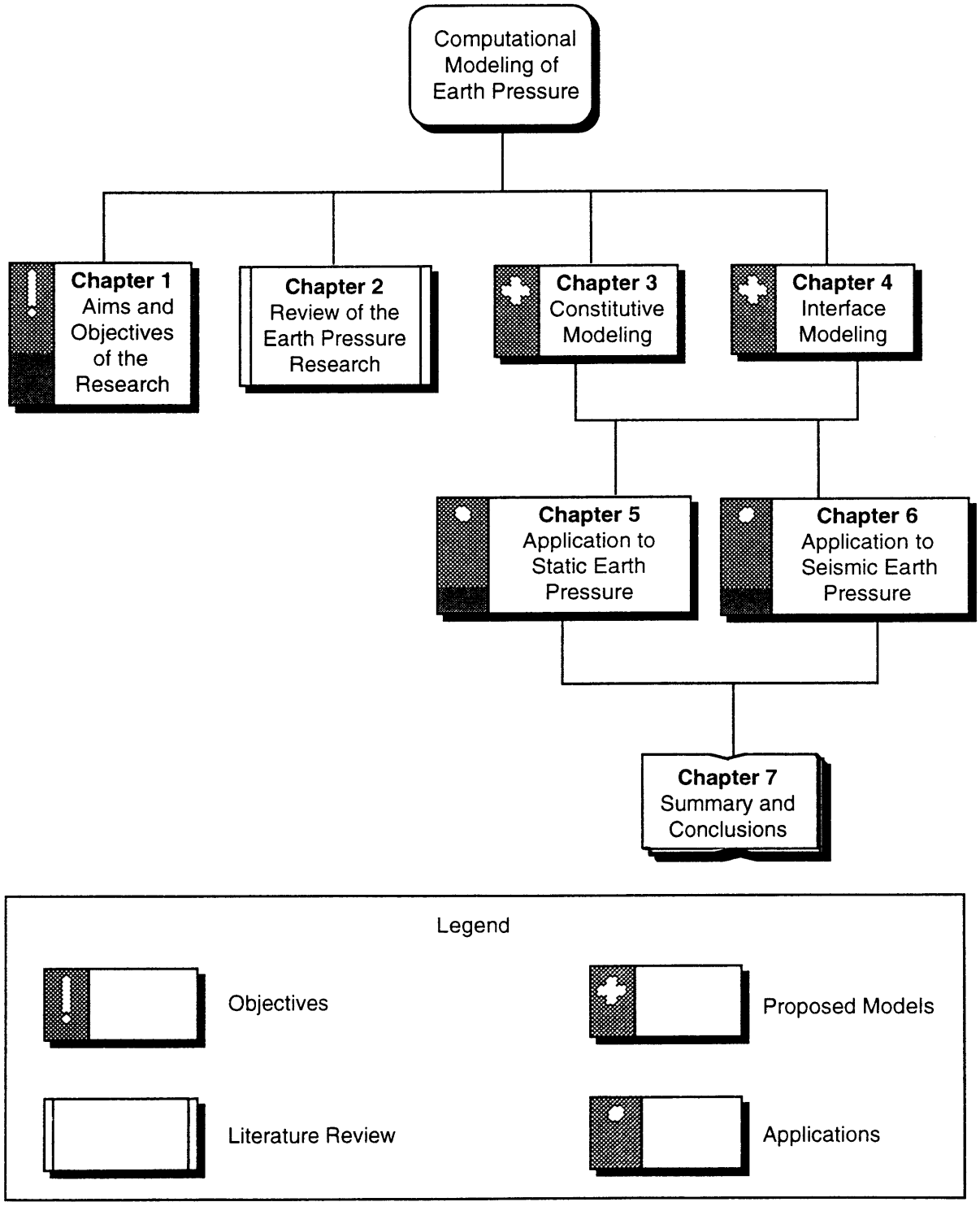

Fig. 1.5 Thesis organization

In Chapter 2, a review of the earth pressure research (experimental, analytical and numerical) to date is presented. The limitations of the existing methods of the earth pressure analysis are discussed. The influence of the wall displacement modes on the earth pressure against a rigid retaining wall, was given particular attention, and the need of the present research is highlighted.

Chapter 3 presents two constitutive laws for modeling the backfill. One is the conventional formulation using Drucker-Prager model with a hyperbolic strain hardening function. The other is a new constitutive formulation which is derived based on smeared shear band technique utilizing two shear bands (named here as *Coupled Shear Band Method*) in order to capture the progressive nature of deformation of the backfill mass. In contrast to the conventional shear band analyses, the *Coupled Shear Band Method* considers two shear bands inside a localized element. The constitutive relation, which is formulated by coupling the two bands, incorporates the width of the shear bands in order to represent the "geometric softening".

Chapter 4 is devoted to the interface between the soil and the structure. The interface models developed by the researchers for various applications have been reviewed. A new interface model is presented that can take care of the problem of crossing and separation. The merit of this model lies in its simplicity and minimum parameters involved in its application. The simulation capability of the model becomes apparent in Chapter 5 and Chapter 6, where the model is applied in the analysis of two earth pressure problems.

In Chapter 5 the numerical models presented in Chapter 3 (Backfill Model) and in Chapter 4 (Interface Model) have been applied to analyze the static earth pressure against a rigid retaining wall subjected to various modes of its movement. An experimental model has been simulated in the analyses. The progressive failure modes of the backfill are observed for each wall displacement mode, and the active state is defined based on the failure zone progressions. Comparisons of the numerical results have been made with experimental results, classical theories, analytical methods, and with numerical results obtained using the strain hardening theories of plasticity.

Chapter 6 deals with the seismic earth pressure problems. The backfill has been modeled based on the formulation described in Chapter 3. Under seismic loading conditions, when the wall moves away from the backfill, and the inertia force acts away from the backfill, momentary separation of the wall and the backfill is imminent. Hence, the interface model presented in Chapter 4 is modified to allow for the relative motions of the interface. The progressive deformation of the backfill mass as well the various earth pressure parameters are numerically evaluated for a model retaining wall. In addition, wall-movement-mode dependent seismic active earth pressure problems are also addressed. A comparative discussion of the numerical results is made with Mononobe-Okabe's theory, Logarithmic Spiral Method (see Appendix A for detail) and Dimarogona's analytical method, and the drawbacks of these methods are pointed out.

Concluding remarks are made at the end of each chapter. A summary and the overall conclusions of this research are presented in Chapter 7.

REFERENCES

[1] Bang, S. (1985), "Active Earth Pressure Behind Retaining Walls", *Journal of Geotechnical Engineering Division, ASCE*, Vol. 111, 3, pp. 407-412.

[2] Dimarogona, P.D. (1983), "Distribution of Lateral Earthquake Pressure on a Retaining Wall", *Soils and Foundations, JSSMFE*, Vol. 23, 4, pp. 1-10.

[3] Fang, Y.S. and Ishibashi, I. (1986), "Static Earth Pressure with Various Wall Movements", *Journal of Geotechnical Engineering Division, ASCE*, Vol. 112, 3, pp. 317-333.

[4] Hansen, B. (1953), *Earth Pressure Calculation*, Danish Technical Press, Copenhagen.

[5] Harr, M.E. (1966), *Foundations of Theoretical Soil Mechanics*, McGraw-Hill Book Co., New York, USA.

[6] Huntington, W.C. (1957), *Earth Pressure and Retaining Wall*, John Wiley and Sons, New York, USA.

[7] Ichihara, M. and Matsuzawa, H. (1973), "Earth Pressure During Earthquake", *Soils and Foundations, JSSMFE*, Vol. 13, 4, pp. 75-86.

[8] Ishibashi, I. and Fang, Y.S. (1987), "Dynamic Earth Pressure with Different Wall Movement Modes", *Soils and Foundations, JSSMFE*, Vol. 27, 4, pp. 11-22.

[9] Kawamura, M., Kuribayashi, E. and Shiga, K. (1987), "Effect of Interactions on Dynamic Active Earth Pressures", In *Development in Geotechnical Engineering- Soil Dynamics and Liquefaction*, Ed. A. S. Cakmak, Elsevier, Amsterdam, Holland, pp. 103-110.

[10] Kerisel, J. (1972), "The Language of Models in Soil Mechanics", *Proceedings of the Fifth International Conference of Soil Mechanics and Foundation Engineering*, Madrid, Spain, pp. 1-49.

[11] Kezdi, A. (1974), *Handbook of Soil Mechanics - Soil Physics*, Elsevier Scientific Publications, Amsterdam, Holland.

[12] Leonards, G.A. (1962), *Foundation Engineering*, Mc-Graw Hill, New York, USA.

[13] Ohara, S. (1970), "Experimental Studies of Seismic Active and Seismic Passive Earth Pressure", *Proceedings of the Third Japan Earthquake Engineering Symposium*, Tokyo, Japan, pp. 137-144.

[14] Roscoe, K.H. (1970), "The Influence of Strains in Soil Mechanics", *Geotechnique*, Vol. 20, 2, pp. 129-170.

[15] Saran, S. and Prakash, S. (1977), "Effect of Wall Movement on Lateral Earth Pressure", *Proceedings of the Sixth World Conference on Earthquake Engineering*, New Delhi, India, pp. 2371-2372.

[16] Sherif, M.A., Ishibshi, I. and Lee, C.D. (1982), "Earth Pressure Against Rigid Retaining Walls", *Journal of Geotechnical Engineering Division, ASCE*, Vol. 108, GT 5, pp. 679-695.

[17] Sherif, M.A., Fang, Y.S. and Sherif, R.I. (1984), "K_A and K_0 Behind Rotating and Nonyielding Walls", *Journal of Geotechnical Engineering, ASCE*, Vol. 110, GT 1, pp. 41--56.

[18] Sherif, M.A. and Fang, Y.S. (1984), "Dynamic Earth Pressure on Walls Rotating about the Top", *Soils and Foundations, JSSMFE*, Vol. 24, 4, pp. 109-117.

[19] Terzaghi, K. (1936), "A Fundamental Fallacy in Earth Pressure Computations", *Journal of Boston Society of Civil Engineers*, Vol. 23, pp. 71-88.

[20] Terzaghi, K. and Peck, R.B. (1967), *Soil Mechanics in Engineering Practice*, John Wiley and Sons, New York, USA.

[21] Terzaghi, K. (1934), "Large Retaining-Wall Tests. I-Pressure of Dry Sand", *Engineering News Record*, Vol. 112, pp. 136-140.

CHAPTER
TWO

Earth Pressure - A Retrospect

Believe nothing, no matter where you read it
or who said it, no matter if I have said it,
unless it agrees with your own reason
and your own common sense

Gautama Buddha

2.1 INTRODUCTION

Earth pressure, in the broadest sense of the word, denotes forces or stresses that occur either in the interior of an earth mass or on the contact surface of soil and structure. Its magnitude will be determined by the physical interaction between soil and structure, the value as well as character of absolute and relative displacements and deformations.

Taking this general definition into consideration, one may state that the problem of earth pressure is one of the basic and essential topics of Civil Engineering. Karl Terzaghi, the father of Soil Mechanics, has contributed tremendously to the field of earth pressure. His experimental as well as theoretical contribution to the earth pressure problems is a real eye opener to the researchers. Following Terzaghi's footstep enormous research has already been done. Therefore, instead of going to the pre-Terzaghi era, here an attempt is made to review the existing researches on the earth pressure from the point where Terzaghi has left behind.

Earlier investigations in the field of earth pressure can be broadly divided into two major areas, i) Analytical/Numerical and ii) Experimental. The present research involves only the computational (numerical) aspect of the earth pressure. However, for the sake of completeness, the pertinent works done by various investigators in all the areas are reviewed herein.

2.2 ANALYTICAL STUDIES

Practically every known method of earth pressure calculation belongs to one or another of the following five groups (Kezdi, 1974).

(1) Theories of elasticity: In this method three stresses and two displacements are determined by two equations of equilibrium and the compatibility equation assuming the validity of Hooke's law. The ultimate failure can not be detected by this method. Boussinesq's method comes under this group.

(2) Theories of plasticity: This method is based on the assumption that the condition of plastic failure is fulfilled at every point of the mass or along specified surfaces. Two equations of equilibrium plus the failure condition is used to determine the three stresses. Rankine's earth pressure theory belongs to this group.

(3) Equilibrium method: In this method, slip surfaces are assumed to develop in the earth mass; along these surfaces, at every point, the condition of failure is fulfilled. A single equation is formed by combining the two equations of equilibrium and the condition of failure, which explains the variation of stress along any rupture plane. An additional requirement is that the solution must be kinematically admissible. Ohde's theory is a classic example of this method.

(4) Extreme method: In this method, one part of the earth mass behind the wall is considered. The conditions of equilibrium and the failure conditions, in this case, are not sufficient to determine the earth pressure; the missing equations will be furnished by an extreme condition: the value of the earth pressure has to be a minimum or a maximum. It is essential that the stresses acting on the sliding surfaces do not enter into the calculations. This group contains e.g. the widely used earth pressure theory of Coulomb, assuming a plane surface of sliding and the methods of Rendulic, Fellenius and others.

(5) Empirical method: The models tests and experiences come under this group.

2.2.1 Static Earth Pressure Research

All the customary methods to earth pressure computation can be traced back either to Coulomb's or to Rankine's theory of earth pressure. It is worth mentioning at this point that Rankine's earth pressure theory is a classic one as far as the mechanism of earth pressure generation is concerned. However, the theory fails to claim much practical merit since in practice it is almost impossible to encounter a retaining wall that is smooth. Coulomb's method gives what is now termed an *upper bound* solution (equilibrium plus a mechanism of failure) whereas the Rankine method gives a *lower bound* solution (equilibrium plus failure criterion). Under specific circumstances the correct solution lies between these two bound solutions.

In the post-Terzaghi era, many models based on the theory of plasticity were developed for solving the static earth pressure problems. Notable contribution came from Hansen (1958), Sokolovski (1960), Rowe (1963) and Davis (1968). A summary of the application of the concepts to earth pressure problems was given by Roscoe (1970) in his Rankine lecture. Roscoe gave another dimension to the earth pressure research through his method of associated fields. Based on the test results at Cambridge, James and Bransby (1970) proposed a simple zero extension line field for predicting passive displacements in sands behind a retaining wall. Habibagahi and Ghahramani (1979) extended the zero extension line theory to predict stress patterns in the backfill behind a vertical wall. Alternative approaches have been developed by Lee and Herington (1972) by using the theory of plasticity. The applicability of various theories of earth pressure based on the theory of plasticity has been discussed extensively by Lee (1975).

It is evident that the accuracy of the values predicted by the plasticity theory are determined by the effectiveness of the particular soil model. Lee (1975) has shown that the numerical values for active or passive parameters determined by alternative methods are commonly very close, and therefore, one can not claim that the Coulomb method is widely inaccurate. Use of plasticity theory has, however, as well as taking into account the type of wall movement, resolved some basic issues. One of the most significant contributions is the prediction of the values of wall-soil adhesion and friction to be used in the Coulomb analysis. It was shown that the common assumption of the wall friction angle as two thirds of the soil values leads to a good approximation to theoretical values derived by the use of plasticity theory.

2.2.2 Dynamic Earth Pressure Research

Mononobe-Okabe's theory is a stepping stone in the analytical research of dynamic earth pressure. The theory is an extension of Coulomb's sliding wedge theory in which earthquake effects are taken into account by the addition of horizontal and vertical inertia terms. Mononobe-Okabe analysis gives satisfactory results only if the wall displacements are sufficient to fully mobilize the shear strength. Despite some advancement in the field of dynamic earth pressure in the last seventy years, the state-of-the-art today is not in a stage where reasonably accurate predictions of dynamic lateral earth pressures can be made. Nevertheless, it is becoming increasingly important to predict accurately the dynamic lateral soil pressures on essential structures, such as basement walls of nuclear power facilities and quay walls. A review, how the study has progressed over these years, follows.

Matsuo and Ohara (1960) have found an approximate elastic solution for the dynamic soil pressure on a rigid wall for translational motions using a two-dimensional analytical model. The basic equations were derived using classical wave theory, assuming that the wall was stationary, with the wave traveling in the soil media and impinging on the surface of the

wall. A comprehensive review on the state-of-art of dynamic earth pressure was given by Seed and Whitman (1970).

Scott (1973) treated the soil as a one-dimensional shear beam attached to the wall by springs representing the soil-wall interaction and arrived at the conclusion that the pressures and moments are significantly higher than those calculated by Mononobe-Okabe's Method. The points of application of the earth pressures are, in general, found to be around two thirds of the wall height above the base. Details of Scott's model illustrating the rigid wall system are shown in Fig. 2.1.

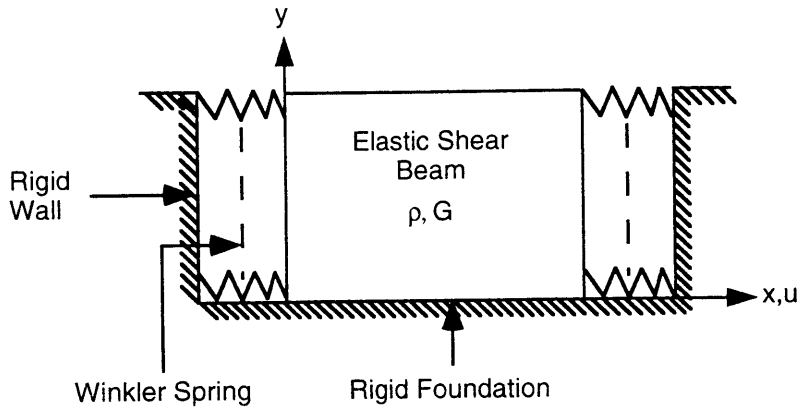

Fig. 2.1 Scott's (1973) analytical model

Tajimi (1973) used two-dimensional wave propagation theory in homogeneous elastic body to determine the dynamic earth pressure on walls displaced either in translation or rotation. The mathematical model consists of a quarter-infinite field, whose vertical boundary undergoes lateral displacement due to movement of the basement wall. The distribution of earth pressure on the wall is expressed by the real and imaginary components varying with frequency.

Jakovlev (1977) derived several expressions for the active and the passive earth pressures under earthquake conditions. Two approaches, one based on Coulomb's theory and the other based on the safe-stress static theory of Sokolovski (1960), were described including the surcharge effects.

Having recognized that wall movements are expected during earthquakes, Richards and Elms (1979) suggested a procedure to calculate the total displacement of the wall. The wall undergoes a displacement relative to the soil whenever a relative velocity exists between the wall and the soil.

Prakash (1981) summarized pertinent literature regarding the analytical and experimental works on dynamic earth pressure. The problems of earth pressure variation due to the earthquake motion, the point of application of the dynamic increment and the displacement of the wall have been highlighted in that state-of-art report.

Prakash (1981) describes a single degree of freedom (SDOF) model to investigate the behavior of retaining wall in translation (Fig. 2.2). The deformation of the soil and the relative displacement between the wall and the soil were not considered separately. However, the total displacement from the original equilibrium position of the wall is computed using the spring-mass-dashpot system (Fig. 2.2a). The equivalent spring constant represents backfill soil resistance and base friction. The equivalent mass includes the retaining wall mass and 0.8 times the mass of the soil contained in a Rankine failure wedge. The force-displacement relation is elasto-plastic, with higher values of stiffness and yield on the compression side. It is stated that, for a selected amplitude and natural period, larger slip occurs when the natural period of the wall-soil system coincides with the period of excitation.

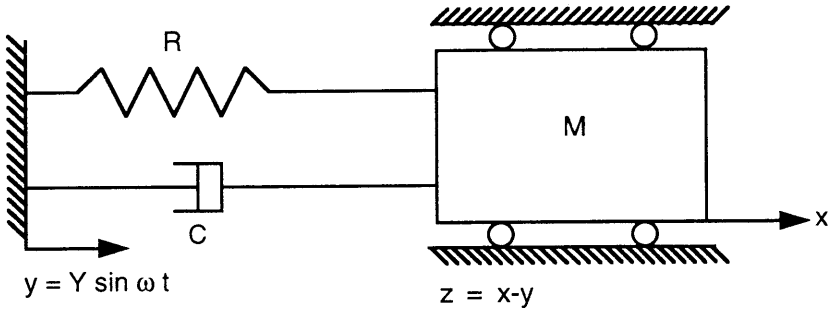

(a) Mathematical model

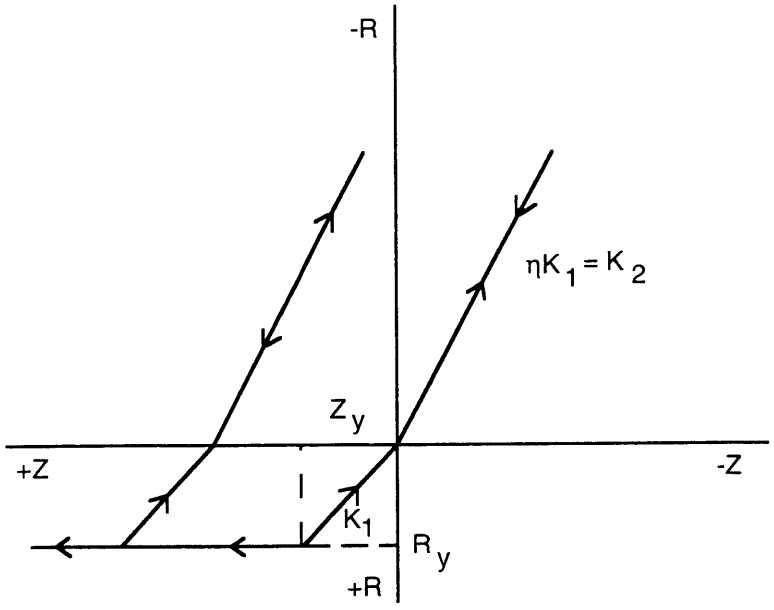

(b) Force-displacement relationship

Fig. 2.2 SDOF model for dynamic analysis of retaining walls (*After* Praksh, 1981)

Nadim and Whitman (1984) computed the amount of permanent tilting and sliding of a gravity retaining wall due to the earthquake loading. Limiting accelerations, where the wall begins to tilt or slide, were evaluated by considering the dynamic equilibrium of the wall. The equilibrium and continuity conditions of the wall and the backfill were written. The total force on the wall and its line of action were evaluated by considering the equilibrium of a slice of the backfill and integrating the force increment along the wall-backfill interface.

Siddarthan et al (1990) proposed an analytical model based on the model of Nadim and Whitman (1984) for predicting the seismic displacements of rigid retaining walls supporting dry backfill. The sliding and tilting were coupled in calculating the response. By performing a parametric study on the position of center of rotation along wall base, they conclude that when the center of rotation is away from the wall toe, a coupled mode of deformation occurs and the total horizontal movement can be as much as 78% higher than those given by considering sliding alone.

2.3 EFFECT OF THE WALL DISPLACEMENT MODES

2.3.1 Fallacies of the Classical Theories

Coulomb's theory provided no analytical basis for the distribution of earth pressure. He simply assumed the pressure distribution to be quasi-hydrostatic and considered the resultant earth force to apply at one-third the height of the wall. Same is the case for Mononobe-Okabe's theory for the dynamic earth pressure. However, a retaining wall can undergo various kinds of movement depending on the situations as mentioned elsewhere. For instance, when relatively deep fills or adjacent structures exist in front of the toe section of a retaining wall, the passive earth pressure from the fills or the adjacent structures prevent the movement of the wall at its lower part. In this case the wall undergoes rotational movement about the base (RB). On the other hand, for bridge abutments, only the lower portion can move since the outer movement at the top is restrained by the relatively rigid superstructures. In such situations, the mode of displacement is rotation about the top (RT). Other probable modes that a wall may be subjected to are Translation (T), Rotation about the center (RC) and combination of Rotation about the Base as well as Translation (RB-T). In Figs. 2.3(a)-(e), the aforementioned modes are shown for the active displacement of the wall. Results of large-scale model tests by Terzaghi and Tschebotarioff (in Chapter 5 of Ref. [26]) have demonstrated that for very rigid retaining walls experiencing rotation about the base (RB), the earth pressure (sandy backfill) distribution is more or less hydrostatic. However, for the other modes of motion, the test results indicate a parabolic type distribution of the earth pressure. Thus, in contrast to Coulomb's theory (Static Case) and Mononobe-Okabe's theory (Dynamic Case), the earth pressure distribution pattern (Figs. 2.3(b)-(e)) is nonlinear

and the distribution pattern depends on the modes of displacement of the wall, resulting in differences in the values of the resultant thrust and its point of application.

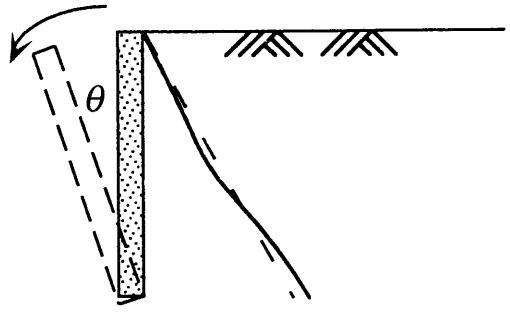

(a) Rotation about base (**RB**)

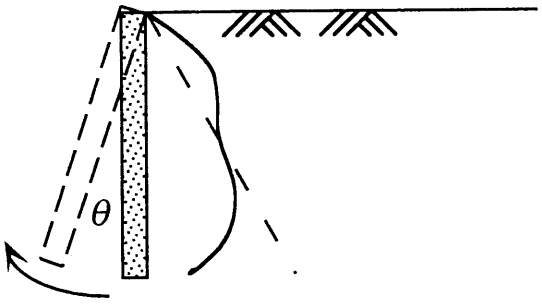

(b) Rotation about top (**RT**)

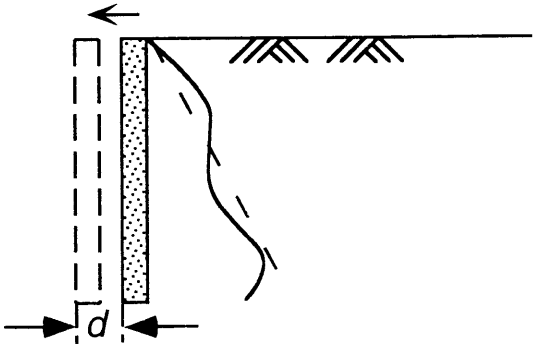

(c) Translation (**T**)

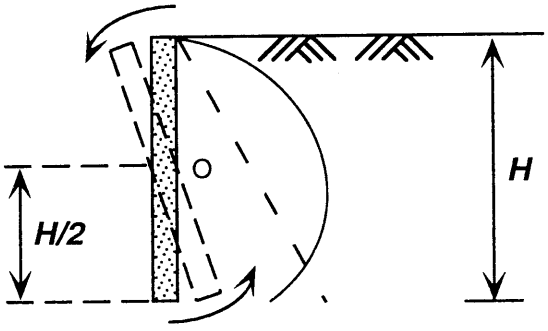

(d) Rotation about center (**RC**)

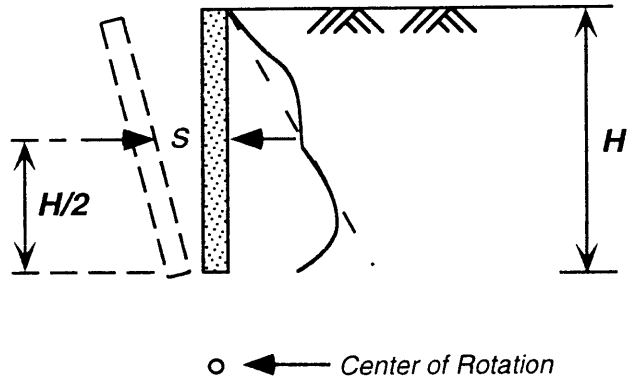

Distribution Assumed by Classical Theories

Probable Distribution

(e) Rotation about base + Translation (**RB-T**)

Fig. 2.3 Various wall displacement modes

2.3.2 Experimental Investigations

2.3.2.1 Static Earth Pressure

Many Researchers in the recent past have conducted small-scale as well as large-scale model tests aiming at finding out the distribution of earth pressure, the resultant earth pressure at the critical state (Active or Passive) and its point of application for different wall movement modes. The extensive work by Roscoe (1970), for the passive case, has demonstrated that the magnitude, the direction and the position of the applied point of the resultant force of earth pressure are generally dependent on the mode of movement of the wall.

Ichihara and Matsuzawa (1973) conducted model tests on a wall translating as well as rotating about a point located 20 cm below the base of a 55 cm high wall. Their experiments have shown that the point of application of the resultant and the mobilized angle of wall friction are functions of the mean wall displacement.

The experimental work by Fang and Ishibashi (1986) for various wall displacement modes suggests that the lateral earth pressure distribution pattern differs depending on the wall movement modes; consequently, the point of application of the total active thrust has no unique value, and it increases with increasing soil density.

2.3.2.2 Dynamic Earth Pressure

Ohara (1970) conducted shaking table tests on retaining wall for four different types of wall movement, namely, RB, RT, T and RB-E (Rotation about the base with elastic supported wall). Both the seismic active and passive pressures were measured. It was concluded that the vertical distribution of the seismic earth pressure acting on the wall depends on the mode of wall movement and it is similar to the static one. The angle of internal friction of the dry sand layer was found to decrease with increasing seismic coefficient.

Ichihara and Matsuzawa (1973) used a large scale vibrating soil bin to estimate the active earth pressure as well as the at-rest pressure during vibration. The frequency of excitation was 3.3 Hz with 600 gals of acceleration amplitude. The mode of movement of the wall was RB-T. They concluded from the test results that the point of application of the resultant active thrust moves upward with increasing acceleration and the Mononobe-Okabe theory can be used to predict earth pressure using the static angle of internal friction. It is stated that the active state develops when the angle of friction between the wall and the backfill reaches its maximum value.

Sherif et al (1982) used shaking table tests to find the neutral, active static as well as dynamic stresses and their points of application for rigid retaining walls supporting dry sandy backfill. The University of Washington's shaking table and retaining wall assembly was used. The wall could move in three modes: T, RB and RT. They presented an equation

based on the test results to calculate the displacement necessary to initiate active earth pressure as a function of the wall height and the backfill soil strength.

Matsuzawa et al (1985) reviewed different dynamic earth pressure and water pressure theories as well as available experimental investigations. They concluded that the point of application of the lateral earth pressure depends on the mode of wall movement. They proposed a generalized apparent angle of seismic coefficient to calculate the dynamic lateral earth pressure and the water pressure.

Ishibashi and Fang (1987) investigated the dynamic active earth pressure developed against rigid retaining structures with dry cohesionless backfill based on the observations of the shaking table model experiment with different wall movement modes. It was found that the dynamic active earth pressure distribution is strongly influenced by the wall movement modes particularly at a low level of horizontal acceleration, while inertial body effect becomes dominant at a higher acceleration level.

Kawamura et al (1987) conducted shaking table investigations on a gravity wall with sandy backfill to find the effect of the wall displacements on dynamic active earth pressure acting against the wall of 50 cm in height. It was concluded that the magnitude and the point of application of the resultant force are dependent on the mode of wall movement, which is a function of the wall height and the backfill density.

2.3.3 Analytical Approach

2.3.3.1 Static Earth Pressure

Dubrova (1963) proposed analytical expressions for the nonlinear distribution of earth pressure for different modes of the wall movement using the *method of redistribution of pressure*, a brief discussion of which follows. For detailed discussion of the method the readers are referred to Harr (1966).

Fig. 2.4a shows a condition representing a rigid wall that rotates about the middle height (point O). Fig. 2.4b shows a mechanistic model of the interaction of the soil and the wall. Dubrova simply assumed that (for this case) the limiting passive condition exists only at the very top of the wall, the limiting active state only at the bottom and that both occur simultaneously. Denoting the angle between the force and the normal on any line ψ (bounded by two values $-\phi$ and $+\phi$), Dubrova assumed that the variation of this angle with z, is linear and is given by:

$$\psi = \frac{2\phi z}{H} - \phi \qquad (2.1)$$

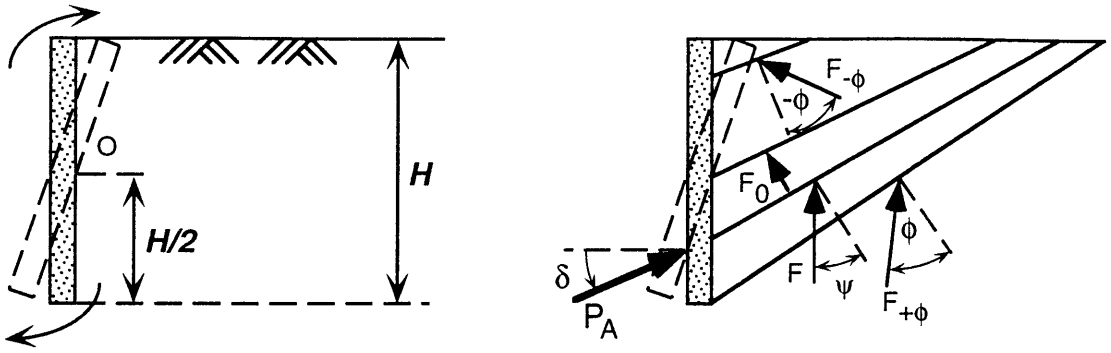

(a) (b)

Fig. 2.4 Dubrova's method of redistribution of pressure (*After* Harr, 1966)

Dubrova then assumed the validity of Coulomb's solution. Hence, the angle that the quasi-rupture line makes with the horizontal for any z will be

$$\theta = \frac{\pi}{4} - \frac{\phi}{2} + \frac{\phi z}{H} \tag{2.2}$$

Using Coulomb's equation, the force against the wall at any z is given by

$$P = \frac{\gamma}{2\cos\delta}\left[\frac{z}{(1/\cos\delta) + \sqrt{\tan^2\psi + \tan\psi\tan\delta}}\right]^2 \tag{2.3}$$

The distribution of the pressure against the wall is given by:

$$p(z) = \frac{dP}{dz} = \frac{\gamma}{\cos\delta}\left[\frac{z\cos^2\psi}{(1+m\sin\psi)^2} - \frac{2z^2\phi\cos\psi}{H(1+m\sin\psi)^3}\left(\sin\psi + \frac{1+m^2}{2m}\right)\right] \tag{2.4}$$

where $m = [1 + (\tan\delta / \tan\psi)]^{1/2}$.

Dubrova further simplified the equation by taking m to be constant; hence the modified equation takes the form,

$$p(z) = \frac{\gamma}{\cos\delta}\left[\frac{z\cos^2\psi}{(1+m\sin\psi)^2} - \frac{2z^2\phi\cos\psi}{H(1+m\sin\psi)^3}(\sin\psi + m)\right] \tag{2.5}$$

where $m = [1 + (\tan\delta / \tan\phi)]^{1/2}$. The development followed in Eq. (2.5) provide the basis for Dubrova's method; that is, for any modes of displacement of the wall, once ψ is

specified, p(z) can be determined. For the case of a wall rotating about its top (RT mode), Dubrova found the following expression for the distribution.

$$p(z)_{RT} = \frac{\gamma}{\cos\delta}\left[\frac{z\cos^2\psi}{(1+m\sin\psi)^2} - \frac{z^2\phi\cos\psi}{H(1+m\sin\psi)^3}(\sin\psi+m)\right]; \quad \psi = \frac{\phi z}{H} \qquad (2.6)$$

For the case of the wall rotating about the base (RB mode), Dubrova found the Coulomb solution for the active case to be correct, thus

$$p(z)_{RB} = \frac{\gamma z}{\cos\delta}\left[\frac{\cos\phi}{1+m\sin\phi}\right]^2; \quad \psi = \phi - \frac{\phi z}{H} \qquad (2.7)$$

For pure translation (T mode), Dubrova treated the case as the average of RB and RT mode and thus mathematically can be expressed as:

$$p(z)_T = 0.5[p(z)_{RB} + p(z)_{RT}] \qquad (2.8)$$

Dubrova's method provides no means of assessing the pressure distribution for any arbritary surfaces other than the assumed straight surfaces. As Roscoe (1970) has pointed out, this method of predicting the stress distribution at failure in the case of a translating wall is open for criticism.

Bang (1985) extended Dubrova's method by introducing the concept of *Intermediate Active State,* and proposed expression for the distribution of earth pressure for a wall undergoing rotation about base, which can express the effect of both the magnitudes of the wall displacement and the modes of displacement.

2.3.2.2 Dynamic Earth Pressure

Saran and Prakash (1977) using the same philosophy of Dubrova, developed an analytical formulation for a general case of an inclined wall supporting inclined cohesionless backfill. Solutions were obtained for both the active and passive cases for all the possible modes of wall movement, namely, RB, RT and T.

Dimarogona (1983) proposed an analytical method for the distribution of earth pressure against a retaining wall caused by an earthquake loading for any mode of wall movement, based on Dubrova's method of *redistribution of pressure.*

Fig. 2.5 shows the mechanical model used by Dimarogona (1983) with infinite number of failure lines. Considering one of the failure surface, the forces acting on it, during earthquake, are shown in Fig. 2.6. In the figure, α is the seismic coefficient, and λ_i expresses the direction of earthquake. The total force, P_{di} acting on the wall is given by:

$$P_{di} = W'_{di} \frac{\sin(\theta_{di} - \psi_{di} + \lambda_i)}{\cos(\theta_{di} - \psi_{di} - \delta_{di})} \tag{2.9}$$

where W'_{di} and λ_i are given by the following equations.

$$W'_{di} = W_{di}(1 + \alpha^2 + 2\alpha\cos(\lambda'_i))^{1/2} \tag{2.10}$$

$$\lambda_i = \tan^{-1}\left(\frac{\alpha \sin\lambda'_i}{(1 + \cos\lambda'_i)}\right) \tag{2.11}$$

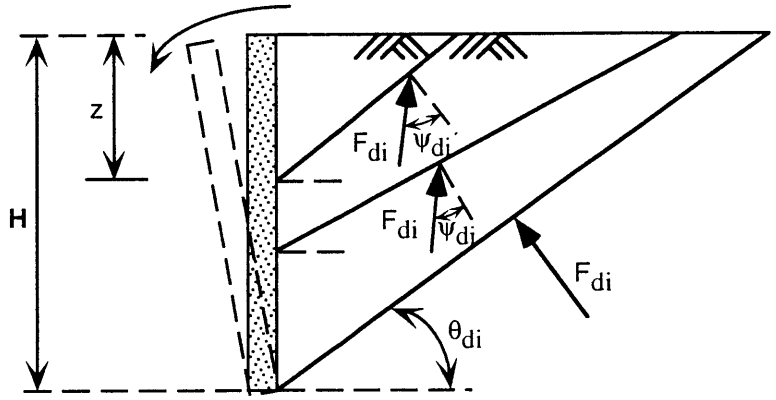

Fig. 2.5 Mechanical model of soil-wall interaction during an earthquake (*After* Dimarogona, 1983)

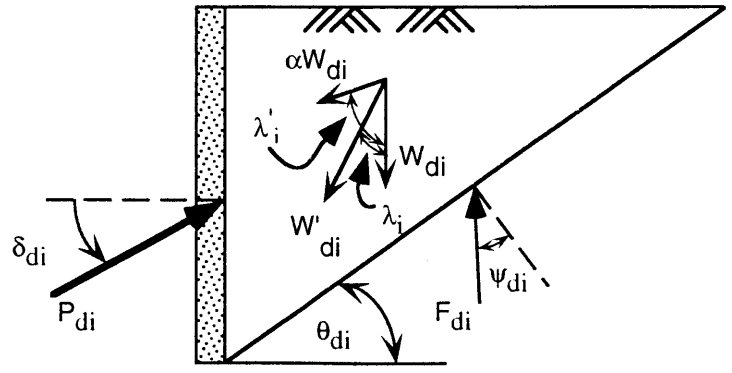

Fig. 2.6 Forces acting on a wall during earthquake (*After* Dimarogona, 1983)

The pressure distribution along the wall is computed as

$$p_{di} = \frac{\partial P_{di}}{\partial z} = \gamma z R^{1/2} BC + \frac{1}{2}\gamma z^2 R^{-1/2}\left(-\alpha \sin\lambda_i' \frac{3}{2} d\psi\right) BC + \frac{1}{2}\gamma z^2 R^{1/2} \frac{\partial B}{\partial z} C + \frac{1}{2}\gamma z^2 R^{1/2} B \frac{\partial C}{\partial z} \tag{2.12}$$

in which,

$$B = \frac{\cos\left(\frac{\psi_{di}}{4}\right) - \sin\left(\frac{\psi_{di}}{4}\right)}{\cos\left(\frac{\psi_{di}}{4}\right) + \sin\left(\frac{\psi_{di}}{4}\right)} \tag{2.13a}$$

$$R = 1 + \alpha^2 + 2\alpha\cos\lambda_i' \tag{2.13b}$$

$$\frac{\partial B}{\partial z} = -\frac{d\psi}{2\left[\cos\left(\frac{\psi_{di}}{4}\right) + \sin\left(\frac{\psi_{di}}{4}\right)\right]^2} \tag{2.13c}$$

$$C = \frac{\cos\left(\frac{3\psi_{di}}{4} - \lambda_i\right) - \sin\left(\frac{3\psi_{di}}{4} - \lambda_i\right)}{\cos\left(\frac{3\psi_{di}}{4} + \delta_{di}\right) + \sin\left(\frac{3\psi_{di}}{4} + \delta_{di}\right)} \tag{2.13d}$$

$$\frac{\partial C}{\partial z} = [-\frac{3}{2} d\psi \cos(\delta_{di} + \lambda_i) + d\lambda\left\{\sin\left(\frac{3\psi_{di}}{2} - \lambda_i + \delta_{di}\right) + \cos(\delta_{di} + \lambda_i)\right\} - d\delta\left\{\cos(\delta_{di} + \lambda_i) - \sin\left(\frac{3\psi_{di}}{2} - \lambda_i + \delta_{di}\right)\right\}] / \left\{\cos\left(\frac{3\psi_{di}}{2} + \delta_{di}\right) + \sin\left(\frac{3\psi_{di}}{2} + \delta_{di}\right)\right\}^2 \tag{2.13e}$$

$$d\lambda = \frac{1}{4} d\psi \frac{\alpha(\cos\lambda_i' + \alpha)}{1 + \alpha^2 + 2\alpha\cos\lambda_i'} \tag{2.13f}$$

The distribution of ψ along the wall is the same as the one assumed by Dubrova for different modes of movement of the wall; θ_{di} is assumed to be given by the following equation.

$$\theta_{di} = \frac{\pi}{4} + \frac{\psi_{di}}{4} \tag{2.14}$$

The rotation of the failing retaining wall about any point was considered. For such cases of the failure mode, the slope of the failure line was determined, together with the point of application of the total force. Moreover, the pressure distribution and the critical direction of the earthquake loading were computed.

2.4 NUMERICAL STUDIES

2.4.1 Static Earth Pressure

Plasticity based models have been used extensively in recent years to describe the behavior of soils. The models based on the theory of plasticity, in general, describe the soil as an elastic-perfectly plastic, or to account for the hardening-softening behavior up to the ultimate or residual strength, as an elastic strain hardening-softening plastic material.

Clough and Duncan (1971) analyzed the soil-structure interaction problem by the nonlinear finite element method. They used hyperbolic empirical equations with material parameters determined from experiments to account for the nonlinear behavior of both the interface elements as well as the soil elements, and performed incremental analysis for a wall undergoing two modes (T and RB) of movement. However, their model still suffers from the fact that it can not describe the mobilization of the wall friction along the wall-backfill interface in each increment of the displacement. A pre-assigned value of the angle of wall friction, δ, is required to perform the incremental analysis. In other words, their model took δ as an input variable. Another drawback of their method is that the generalized Hooke's law, which form the basis of simple hyperbolic stress-strain relationship takes soil as non-dilatant material.

Ozawa and Duncan (1976) modified the model of Clough and Duncan (1971) to account for the elasto-plastic behavior instead of hyperbolic behavior by extending Lade's theory and applied it for the calculation of the passive earth pressure. However, they applied the model to analyze only smooth walls, and no attempt was made by them to incorporate wall friction. Griffith (1981) used simple numerical models to examine the influence of various stress/strain paths (both pre- and post-peak) with reference to the ultimate earth pressure conditions.

Nakai (1985) used elasto-plastic soil element as well as elasto-plastic joint element in the earth pressure analysis for different wall movement modes. The constitutive equation used in his analysis was based on the concept of *Spatial Mobilized Plane* proposed by Nakai and Matsuoka (1983). The model has the added advantage of considering the effect of the

intermediate principal stress, and the smoothening of the corners of the Mohr-Coulomb's hexagon. However, the absence of the concept of the work-hardening on one hand, and the assumption of the coincidence of the principal strain increment axes with the principal axes of stress on the other, bring it to the category of the perfect plasticity model. No explanations were also found regarding the assumptions and the physical significance of the different parameters that appeared in the material property matrix of the joint element used in the analysis.

Many other researchers (e.g. Simpson and Wroth, 1972; Bhatia and Bakeer, 1989 etc.), in the last two decades, contributed to the field of numerical computations of earth pressure under static loading conditions.

2.4.2 Seismic Earth Pressure

Numerical analysis of earth pressure under seismic loading conditions involves more complication. With the advent of computer, the Finite Element Method (FEM) became a powerful tool in analyzing seismic earth pressure problems. In the last decades, significant advancements have been achieved in the analysis of the behavior of earth retaining walls under seismic conditions.

Aggour and Brown (1973) used finite element model of a wall-backfill system excited by sinusoidal ground motion. They concluded that in flexible wall, the pressure near the top is smaller than on rigid walls, and that the dynamic pressures depend very much on the static ones. They also concluded that if the length of the backfill is greater than 10 times the height of the wall, the dynamic wall pressure approaches that of an infinite backfill.

Nazarian and Hadjian (1979) emphasize the need for a numerical model that includes a no-tension wall-soil interface, simultaneous rotation and translation of the wall base and the radiation damping effects.

Aubry and Chouvet (1981) proposed a mixed implicit-explicit nonlinear technique to analyze the soil-wall interaction while accounting for the wall inertia and the relative displacement between the wall and the soil. The behavior of the backfill sand was described by the Drucker-Prager elasto-plastic law with associated flow rule. The initial state of stress assumed to be in the active state throughout the mesh. Special interface elements, taking into account Coulomb's law of friction, were used between the soil and the wall. In view of the extremely small duration of the imparted dynamic excitation, the presented wall-soil analysis is not clear enough to draw any useful conclusion.

Nadim and Whitman (1983) assumed that all irreversible distortions in the backfill occur in thin failure surfaces, the location and orientation of which were assumed in advance. These surfaces were modeled by very thin joint elements of Goodman type (1968) that have limited shear strength. The behavior of soil in the non-failing portion of the problem was assumed to be elastic. Equivalent linear soil properties were employed. The conclusions

were: (1) The amplification of the backfill motion is important when the ratio of the dominant frequency of the ground motion and the fundamental frequency of the backfill is greater than 0.3 and (2) Due to seismically induced stress redistribution, the residual forces on the wall may be greater than the static active forces.

Bakeer and Bhatia (1985) used finite element method in the dynamic analysis of a retaining wall subjected to different modes of movement. The analysis showed that the magnitude and the distribution of the earth pressure depend on the mode of the wall displacement. It was also confirmed that the coefficient of earth pressure becomes maximum when the fundamental frequency of the wall-wedge system approaches the frequency of the input motion. The effect of the fundamental frequency of the wall-wedge system on the location of the earth pressure was found to be extremely small.

Siddharthan et al (1989) investigated the seismic response of rigid retaining walls supporting dry sandy backfill. Slip elements were incorporated at the wall-soil interface, at the base of the wall as well as along a pre-selected failure plane in the backfill (at 62^{o} to the horizontal and passing through the toe of the wall). The properties of the slip elements were assumed elastic-perfectly plastic, with failure given by the Mohr-Coulomb failure criterion. They showed that the rotational deformation (of the wall structure) might be very significant in some cases and should be accounted for in analysis procedures.

Stamatopoulos and Whitman (1990) investigated the permanent tilt behavior of retaining walls. A residual strain method was implemented, in which the calculation of the transient and the residual response was uncoupled over each cycle of loading. A hyperbolic model, for the sand backfill, with shear modulus decreasing with increasing shear stress was used.

Elgamal and Allampalli (1992) developed a simplified wall-soil computational model to investigate the permanent sliding and rotational response of cantilever and gravity retaining walls.

2.5 CLOSURE

In this chapter, literature on the existing philosophies of earth pressure from the analytical, the experimental as well as the numerical points of view have been reviewed. Similarities as well as diversities in the approaches have been seen. Even though, tremendous progress has been made in general in the field of earth pressure, however, the progress for the dynamic earth pressure has been remarkably uneven. The accuracy of the values of earth pressure predicted by the plasticity theory is determined by the particular model adopted for soil.

A retaining wall can undergo various modes of displacement depending on the situations. The distribution of the earth pressure is highly nonlinear depending on these modes. The classical theory of Coulomb or Mononobe-Okabe provided no analytical basis for the

distribution of earth pressure. The resultant active or the passive thrust and the point of application of the resultant thrust are governed by the modes of displacement of the wall.

Analytical solutions are available for expressing the distribution of earth pressure for various modes of displacement. However, they can not explain the actual phenomenon as they are unable to truly capture the progressive deformation characteristics of the backfill soil. Numerical analysis based on the finite element method (FEM) or the discrete element method (DEM) has been increasingly getting popular in analyzing earth pressure problems. However, most of the existing numerical models do not consider the localized deformation inside the backfill. In addition, an adequate interface description is also found to be lacking in those models.

The inception and propagation of shear bands, inside the backfill, need to be considered while analyzing the progressive deformation phenomenon such as earth pressure. Hence, a new constitutive model is developed for the backfill based on *smeared shear band method*, which is discussed in Chapter 3. Having recognized the importance of interface modeling in the soil-structure interaction phenomenon associated with the retaining wall behavior a simple interface model is developed and described in Chapter 4.

REFERENCES

[1] Aggour, M.S. and Brown, C.B. (1973), "Retaining Wall in Seismic Areas", *Proceedings of the Fifth World Conference on Earthquake Engineering*, Rome, Italy, pp. 2624-2627.

[2] Alampalli, S. (1990), "Earthquake Response of Retaining Walls: Full Scale Testing and Computational Modeling", *Ph.D. Thesis*, School of Engineering, Rensselaer Polytechnic Institute, New York, USA.

[3] Aubry, D. and Chouvet, D. (1981), "Numerical Computation of Earth Pressure During Earthquakes", *Proceedings of the International Conference on Recent Advances on Geotechnical Earthquake Engineering and Soil Dynamics*, Rolla, Missouri, USA, pp. 721-726.

[4] Bakeer, R.M. and Bhatia, S.K. (1985), "Dynamic Earth Pressure behind Gravity Walls Subjected to Sinusoidal Motion", *Proceedings of the Second International Conference on Soil Dynamics and Earthquake Engineering*, pp. 3-12.

[5] Bang, S. (1985), "Active Earth Pressure Behind Retaining Walls", *Journal of Geotechnical Engineering Division, ASCE*, Vol. 111, 3, pp. 407-412.

[6] Bhatia, S.K. and Bakeer, R.M. (1989), "Use of the Finite Element Method in Modelling a Static Earth Pressure Problem", *International Journal for Numerical and Analytical Methods in Geomechanics*, Vol. 13, pp. 207-213.

[7] Clough, G.W. and Duncan, J.M. (1971), "Finite Element Analyses of Retaining Wall Behavior", *Journal of Soil Mechanics and Foundation Engineering, ASCE*, Vol. 97, SM 12, pp. 1657-1673.

[8] Davis, E.H. (1968), "Theories of Plasticity and Failure of Soil Masses", In *Soil Mechanics-Selected Topics*, Ed. I. K. Lee, Butterworths, U.K., pp. 341-380.

[9] Dimarogona, P.D. (1983), "Distribution of Lateral Earthquake Pressure on a Retaining Wall", *Soils and Foundations, JSSMFE*, Vol. 23, 4, pp. 1-10.

[10] Elgamal, A-W. and Alampalli, S. (1992), "Earthquake Response of Retaining Walls: Full Scale Testing and Computational Analysis", *Proceedings of the 10th World Conference on Earthquake Engineering*, Madrid, Spain, pp. 1671-1676.

[11] Fang, Y.S. and Ishibashi, I. (1986), "Static Earth Pressure with Various Wall Movements", *Journal of Geotechnical Engineering Division, ASCE*, Vol. 112, 3, pp. 317-333.

[12] Goodman, R.E., Taylor, R.L. and Brekke, T.L. (1968), "A Model for the Mechanism of Jointed Rock", *Journal of Soil Mechanics and Foundation Engineering, ASCE*, Vol. 94, SM 3, pp. 637-659.

[13] Griffiths, D.V. (1981), "Computation of Strain Softening Behavior", *Proceedings of the Symposium on Implementation of Computer Procedures and Stress-Strain Laws in Geotechnical Engineering*, Chicago, USA, pp. 591-603.

[14] Habibagahi, K. and Ghahramani, A. (1979), "Zero Extension Line Theory of Earth Pressure", *Journal of Geotechnical Engineering, ASCE*, Vol. 105, GT 7, pp. 881-896.

[15] Hansen, B. (1958), "Lone Ruptures Regarded as Narrow Rupture Zones: Basic Equations Based on Kinematic Considerations", *Proceedings of the International Conference on Earth Pressure Problems;* Brussels, Belgium, pp. 39-49.

[16] Harr, M.E. (1966), *Foundations of Theoratical Soil Mechanics*, McGraw-Hill Book Co., New York, U.S.A.

[17] Ichihara, M. and Matsuzawa, H. (1973), "Application of Plane Strain Test to Earth Pressure", *Proceedings of the Eighth International Conference on Soil mechanics and Foundation Engineering*, pp. 185-190.

[18] Ichihara, M. and Matsuzawa, H. (1973), "Earth Pressure During Earthquake", *Soils and Foundations, JSSMFE*, Vol. 13, 4, pp. 75-86.

[19] Ishibashi, I. and Fang, Y.S. (1987), "Dynamic Earth Pressure with Different Wall Movement Modes", *Soils and Foundations, JSSMFE*, Vol. 27, 4, pp. 11-22.

[20] Jakovlev, P.I. (1977), "Coefficients of Active and Passive Pressure on Retaining Walls Under Seismic Conditions", *Proceedings of the Sixth World Conference on Earthquake Engineering*, New Delhi, India, pp. 2356-2362.

[21] James, R.G. and Bransby, P.L. (1971), "A Velocity Field for Some Passive Earth Pressure Problem", *Geotechnique*, Vol. 21, 1, pp. 61-83.

[22] Kawamura, M., Kuribayashi, E. and Shiga, K. (1987), "Effect of Interactions on Dynamic Active Earth Pressures", In *Development in Geotechnical Engineering- Soil Dynamics and Liquefaction*, Ed. A. S. Cakmak, Elsevier, Amsterdam, Holland, pp. 103-110.

[23] Kezdi, A. (1974), *Handbook of Soil Mechanics - Soil Physics*, Elsevier Scientific Publications, Amsterdam, Holland.

[24] Lee, I.K. (1975), "Application of Plasticity Theory to the Prediction of Earth Pressures", *Proceedings of the General Session of the Symposium on Soil Mechanics - Recent Developments*, New South Wales, Australia, pp 27-81.

[25] Lee, I.K. and Herington, J.R. (1972), "A Theoretical Study of the Pressures Acting on a Rigid Wall by a Sloping Earth or Rock Fill", *Geotechnique*, Vol. 22, 1, pp. 1-26.

[26] Leonards, G.A. (1962), *Foundation Engineering*, McGraw-Hill Book Co., New York, USA.

[27] Matsuo, H. and Ohara, S. (1960), "Lateral Earth Pressures and Stability of Quay Walls during Earthquakes", *Proceedings of the Second World Conference on Earthquake Engineering*, Japan, pp. 165-181.

[28] Matsuzawa, H., Ishibashi, I. and Kawamura, M. (1985), "Dynamic Soil and Water Pressures of Submerged Soils", *Journal of Geotechnical Engineering, ASCE*, Vol. 111, 10, pp. 1161-1176.

[29] Mononobe, N. and Matsuo, H. (1929), "On the Determination of Earth Pressure during Earthquake", *Proceedings of the World Engineering Conference*, pp. 177-185.

[30] Nadim, F. and Whitman, R.V. (1984), "Coupled Sliding and Tilting of Gravity Retaining Walls During Earthquakes", *Proceedings of the Eighth World Conference on Earthquake Engineering*, San Francisco, USA, pp. 477-484.

[31] Nadim, F. and Whitman, R.V. (1983), "Seismically Induced Movement of Retaining Walls", *Journal of Geotechnical Engineering, ASCE*, Vol. 109, GT 7, pp. 915-931.

[32] Nakai, T. (1985), "Analysis of Earth Pressure Problems Considering the Influence of Wall Friction and the Wall Deflection", *Proceedings of the Fifth International Conference on Numerical and Analytical Methods in Geomechanics*, Nagoya, Japan, pp. 765-772.

[33] Nakai, T. and Matsuoka, H. (1983), "Shear Behaviors of Sand and Clay under Three-Dimensional Stress Condition", *Soils and Foundations, JSSMFE*, Vol. 23, 2, pp. 26-42.

[34] Nazarian, H.N. and Hadjian, A.H. (1979), "Earthquake-Induced Lateral Soil Pressures on Structures", *Journal of the Geotechnical Engineering Division, ASCE*, Vol. 105, GT 9, pp. 1049-1066.

[35] Ohara, S. (1970), "Experimental Studies of Seismic Active and Seismic Passive Earth Pressure", *Proceedings of the Third Japan Earthquake Engineering Symposium*, Tokyo, Japan, pp. 137-144.

[36] Okabe, S. (1924), "General Theory on Earth Pressure and Seismic Stability of Retaining wall and Dam", *Journal of JSCE*, Vol. 10, 5, pp. 1277-1323.

[37] Ozawa, Y. (1973), "Elasto-Plastic Finite Element Analysis of Soil Deformation", *Ph. D. Thesis*, School of Engineering, University of California, Berkeley, USA.

[38] Ozawa, Y. and Duncan, J.M. (1976), "Elasto-Plastic Finite Element Analyses of Sand Deformations", *Proceedings of the 2nd International Conference on Numerical Methods in Geomechanics,* Blacksburg, Virginia, USA, pp. 243-263.

[39] Prakash, S. (1981), "Analysis of Rigid Retaining Walls During Earthquakes", *Proceedings of the International Conference on Recent Advances in Geotechnical Earthquake Engineering and Soil Dynamics*, Rolla, Missouri, USA, pp. 993-1019.

[40] Prakash, S. (1981), *Soil Dynamics*, McGraw-Hill Book Co., New York, USA.

[41] Richards, R. and Elms, D. (1979), "Seismic Behavior of Gravity Retaining Walls", *Journal of Geotechnical Engineering, ASCE*, Vol. 105, GT 4, pp. 449-464.

[42] Roscoe, K.H. (1970), "The Influence of Strains in Soil Mechanics", *Geotechnique*, Vol. 20, 2, pp. 129-170.

[43] Rowe, P.W. (1963), "Stress-Dilatancy, Earth Pressure and Slopes", *Journal of Soil Mechanics and Foundation Engineering, ASCE*, Vol. 89, SM 3, pp. 37-61.

[44] Saran, S. and Prakash, S. (1977), "Effect of Wall Movement on Lateral Earth Pressure", *Proceedings of the Sixth World Conference on Earthquake Engineering*, New Delhi, India, pp. 2371-2372.

[45] Scott, R.F. (1973), "Earthquake-induced Earth Pressures on Retaining Walls", *Proceedings of the Fifth World Conference on Earthquake Engineering*, Rome, Italy, pp. 1611.

[46] Seed. H.B. and Whitman, R.V. (1970), "Design of Earth Retaining Structures for Dynamic Loads", *Proceedings of the Special Conference on Lateral Stress, Ground Displacement and Earth Retaining Structures*, Ithaca, New York, pp. 103-147.

[47] Sherif, M.A., Ishibshi, I. and Lee, C.D. (1982), "Earth Pressure Against Rigid Retaining Walls", *Journal of Geotechnical Engineering Division, ASCE*, Vol. 108, GT 5, pp. 679-695.

[48] Siddharthan, R., Ara, S. and Anderson, J.G. (1990), "Seismic Displacements of Rigid Retaining Walls", *Proceedings of the Fourth US National Conference on Earthquake Engineering*, Palm Springs, California, pp. 673-682.

[49] Simpson, B. and Wroth, C.P. (1972), "Finite Element Computations for a Model Retaining Wall in Sand", *Proceedings of the Fifth Europian Conference of Soil Mechanics and Foundation Engineering*, Madrid, Spain, pp. 85-94.

[50] Sokolovski, V.V. (1960), *Statics of Soil Media*, Butterworths Scientific Publications, London, UK.

[51] Stamatopoulos, C.A. and Whitman, R.V. (1990), "Prediction of Permanent Tilt of Gravity Retaining Wall by the Residual Strain Method", *Proceedings of the Fourth US National Conference on Earthquake Engineering*, Palm Springs, California, pp. 683-692.

[52] Tajimi, H. (1973), "Dynamic Earth Pressures on Basement Wall", *Proceedings of the Fifth World Conference on Earthquake Engineering*, Rome, Italy, pp. 1560-1569.

[53] Terzaghi, K. (1936), "A Fundamental Fallacy in Earth Pressure Computations", *Journal of Boston Society of Civil Engineers*, Vol. 23, pp. 71-88.

CHAPTER
THREE

Constitutive Model for the Backfill

It is the mark of an educated man
to look for precision in each class of things
just so far as the nature of the subject admits

Aristotle

3.1 INTRODUCTION

The history of soil mechanics can be viewed as a search for the relations describing the behavior of soil as a material responsive to the laws of mechanics. Perhaps Terzaghi's greatest contribution in establishing the mechanics of soil as a discipline was to organize the diffuse literature of the achievements in the subject into a rational entity. In recent years much research effort has been devoted to the development of realistic constitutive models of soil behavior, a considerable proportion of which are based on the underlying assumptions of classical plasticity theory.

While today there are practically no limits on the capability of computational techniques, serious handicaps still exist with expressing material behavior by the proper constitutive law. Limitations in using the techniques primarily derive from our inability to describe appropriate constitutive behavior for soil and to determine the parameters needed for the constitutive models.

Advances in understanding the behaviors of granular materials, such as sand, depend upon both experimental and theoretical works. Experimental studies show what types of constitutive relations are valid for laboratory conditions; theoretical studies indicate the consequences of using various proposed constitutive relations for solving boundary value problems. A variety of quasi linear or nonlinear elastic and elasto-plastic models have been proposed for characterizing the stress-deformation behavior of such materials. Since the behavior is complex owing to the effect of factors such as the initial state of stress, stress path, change in physical state (volume) and the type of loading, it is necessary to modify or improve the models based on classical plasticity theories.

In this chapter two types of constitutive relations are derived. One is derived assuming continuity of stress throughout the entire deformation field, which is nothing but the conventional elasto-plastic strain hardening relationship using Drucker-Prager failure criterion. However, failure of the soil structures and foundations is very frequently accompanied by the development of surfaces or bands at which high gradients of strains are present. Capture of failure surfaces by standard finite element techniques is still not satisfactory as the deformation is smeared over a certain number of elements. In recent years, considerable attention has been paid to the shear band localization problem. Until now, these shear band localization analyses considered only one shear band inside an element. However, the theoretical and experimental investigations proved the existence of two bands crossing each other. Therefore, a new constitutive relation, for granular materials, is derived by considering two shear bands for the elements undergoing localization. This constitutive law is derived by coupling the two bands, and is named *Coupled Shear Band Method.*

3.2 CONVENTIONAL ELASTO-PLASTIC CONSTITUTIVE RELATION

The general form of the elasto-plastic constitutive equations for perfectly plastic, isotropic strain-hardening and anisotropic strain-hardening materials can be written as,

$$d\boldsymbol{\sigma} = \left[\mathbf{D}^e - \frac{(\mathbf{D}^e \frac{\partial g}{\partial \boldsymbol{\sigma}}) \otimes (\mathbf{D}^e \frac{\partial f}{\partial \boldsymbol{\sigma}})}{h + \frac{\partial f}{\partial \boldsymbol{\sigma}} \bullet (\mathbf{D}^e \frac{\partial g}{\partial \boldsymbol{\sigma}})} \right] d\boldsymbol{\varepsilon} \tag{3.1}$$

in which $\boldsymbol{\sigma}$ is the stress tensor , $\mathbf{D}^e$ is the elasticity matrix, f is the yield function, g is the plastic potential function, $\boldsymbol{\varepsilon}$ is the strain tensor and h is the hardening modulus. Introducing the dilatancy factor, β (Rudnicki and Rice, 1975) into the above equation yields the following expression for the constitutive relations.

$$d\boldsymbol{\sigma} = \left[\mathbf{D}^e - \frac{(\mathbf{D}^e(\mathbf{m} + \beta\mathbf{n})) \otimes (\mathbf{D}^e \frac{\partial f}{\partial \boldsymbol{\sigma}})}{h' + \frac{\partial f}{\partial \boldsymbol{\sigma}} \bullet \mathbf{D}^e(\mathbf{m} + \beta\mathbf{n})} \right] d\boldsymbol{\varepsilon} \tag{3.2}$$

Here $\mathbf{m}$ and $\mathbf{n}$ are the unit tensors in the directions of deviatoric and volumetric stress respectively; $h' = \frac{h}{\frac{\partial g}{\partial s}}$ is the hardening parameter and can be derived as,

$$h' = \frac{\partial \kappa}{\partial e^p} + \beta \frac{\partial \kappa}{\partial \bar{\varepsilon}^p} \tag{3.3}$$

here κ is the hardening function of the material during the plastic deformation. The dilatancy factor, β, is defined by the following equations:

$$\beta = \frac{d\bar{\varepsilon}^p}{de^p}: \quad d\bar{\varepsilon}^p = \sqrt{d\varepsilon_v{}^p d\varepsilon_v{}^p}, \quad de^p = \sqrt{d\mathbf{e}^p d\mathbf{e}^p} \tag{3.4}$$

in which $d\mathbf{e}^p$ and $d\boldsymbol{\varepsilon}_v{}^p$ refers to deviatoric and volumetric part of the plastic strain $d\boldsymbol{\varepsilon}^p$ respectively. The tensile force is taken as positive here and will be the same throughout the discussion of this thesis.

The Drucker-Prager criterion of perfect plasticity has been modified to account for the strain hardening properties of the backfill soil in which the yield function can be written in the form,

$$f(\boldsymbol{\sigma}, \kappa_l(\boldsymbol{\varepsilon}^p)) = \alpha\bar{\sigma} + s - \kappa_l \tag{3.5}$$

where $\kappa_l = \kappa_{in} + \kappa$, and κ_{in} is the initial value of the hardening function, $\bar{\sigma}$ and s denotes the volumetric and the deviatoric component of the stress tensor respectively. The material parameters α and κ_{in}, which are derived using Mohr's diagram under plane strain condition, are computed by employing the following equations.

$$\alpha = \sqrt{\frac{2}{3 + 4\tan^2\phi_i}}\tan\phi_i \tag{3.6}$$

$$\kappa_{in} = \sqrt{\frac{6}{3 + 4\tan^2\phi_i}}c \tag{3.7}$$

Here ϕ_i is the angle of internal friction of the backfill soil at the initial yield (Fig. 3.1), which can be determined from experimental data for the material; c denotes the cohesion. Using the above yield function (Eq. 3.5) we can obtain the following equation.

$$\frac{\partial f}{\partial \boldsymbol{\sigma}} = \mathbf{m} + \alpha\mathbf{n} \tag{3.8}$$

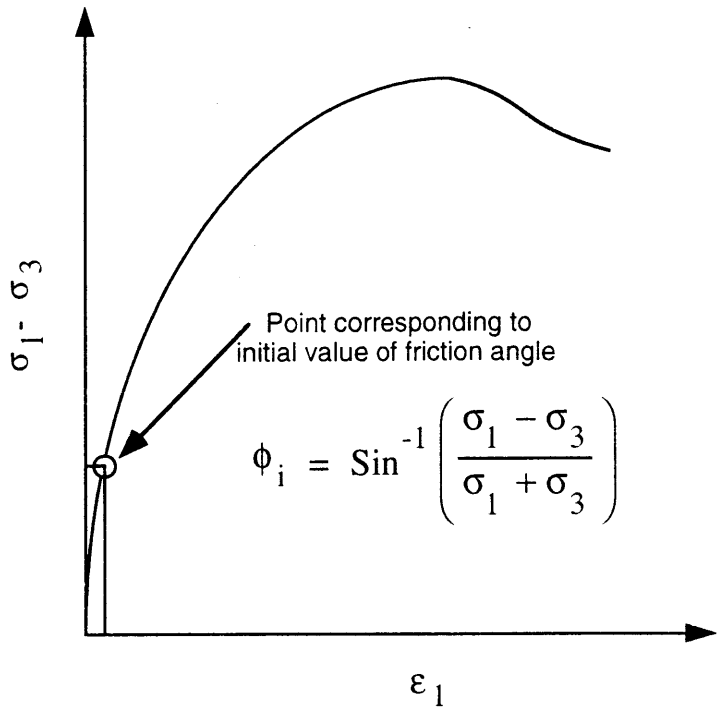

Fig. 3.1 Definition of the angle of internal friction at initial yield, ϕ_i

Hence the elasto-plastic constitutive relations can be obtained as in Eq. (3.9) by substituting the values from Eq. (3.3) and Eq. (3.8) into Eq. (3.2).

$$d\boldsymbol{\sigma} = \left[\mathbf{D}^e - \frac{(\mathbf{D}^e(\mathbf{m}+\beta\mathbf{n}))\otimes(\mathbf{D}^e(\mathbf{m}+\alpha\mathbf{n}))}{h' + (\mathbf{m}+\alpha\mathbf{n})\bullet\mathbf{D}^e(\mathbf{m}+\beta\mathbf{n})}\right]d\boldsymbol{\varepsilon} \tag{3.9}$$

A hyperbolic form of the hardening function, κ, is assumed, which is given by the following equation:

$$\kappa = \frac{\xi}{(a + b\xi)} \tag{3.10}$$

in which $d\xi = |de^p|$; a and b are the material parameters, which can be determined from the experimental results. Using Eqs. (3.3) and (3.10), the hardening parameter h' can be derived as,

$$h' = \frac{a}{(a + b\xi)^2} \tag{3.11}$$

The dilatancy factor β has been assumed to be of the form,

$$\beta = a_1 e^{-b_1 \bar{\sigma}} \tag{3.12}$$

where a_1 and b_1 are the material parameters determined from the experimental results by least-squares curve-fitting technique.

3.3 LOCALIZED DEFORMATION ANALYSIS - AN INTRODUCTION

In the quest for determining the collapse loads, it is often found that the applied or driving forces needed to cause failure in a soil mass is much less than those apparently needed to mobilize the maximum shear strength of the soil everywhere along any assume failure surface. This phenomenon called progressive failure involves non-uniform spatial stress and strain distributions. In order to obtain the solution of a progressive failure problem, it is necessary to introduce in the analysis the explicit stress-strain or constitutive relationship which describes the elasto-plastic transition from the initial elastic state to the ultimate failure. Progressive failure and localization of inelastic deformation are phenomena which are delicately intertwined. The well-defined deformation pattern in the form of a shear band to emerge from a state of previous homogeneity is indeed a very fascinating phenomenon.

3.3.1 Brief Review on Localization Research

The shear band localization is known to be a factor responsible for strain softening behavior of the granular materials. Many researchers (e.g. Mandel (1966), Rice (1976), Rice and Rudniki (1980), Anand and Spitzig (1980), Vardoulakis (1981), Ortiz et al (1987), Yatomi et al (1989)) in the last three decades have been trying to model the localized deformation phenomenon treating it as a material instability. All these treatments exhibit numerical deficiencies as they preclude the post-localization analysis. In other words, the studies were confined to the initiation of the localization.

De Borst (1988) included the post bifurcation behavior into his treatment, however, the solution could not escape the pathological mesh dependence. Desrues (1990) gave a comprehensive treatment on the subject of shear band from both the numerical and experimental points of view. Since the triggering of the shear band leads to softening, the post localization analysis involves modeling of the softening regime. Oka et al (1994) developed a visco-plastic strain softening model for clay, using the strain localization theory, which is capable of describing the plastic instability.

However, most of the existing strain softening models do not consider the geometrical effect, in the sense that the shear banding is entirely attributed to the material instability. These models show sensitivity to different factors such as the discretization of the system, the rate of strain softening etc. Pietruszczak and Mroz (1981) introduced the plastic shear band theory to analyze the behavior of strain softening material from a different perspective. They showed that the width of the shear band can be related to the type of the material; hence the rate of strain softening is significantly affected by the geometry of the specimen, which was termed *geometrical softening*. In the formulation, the *smearing technique* was applied to include a factor (the width of the shear band) in the constitutive description representing the geometrical softening. The selection of the appropriate value for the thickness of the shear band has been shown to render the analyses essentially insensitive to the details of discretization.

Pietruszczak and Stolle (1987) extended the smeared shear band approach of Pietruszczak and Mroz (1981) to include more complex strain softening model that accounts for the finite strain and rotations within the shear band using non-associated flow rule. The approach views the inception of softening as a bifurcation from an initial uniform deformation to a non-uniform deformation inside a planar band under conditions of continuing equilibrium and continued homogenous deformation outside the shear band. The hardening function employed in the formulation allows a transition from hardening to softening at the instant of strain localization.

3.3.2 Smeared Shear Band Approach

An element undergoing shear band bifurcation can be schematically represented as shown in Fig. 3.2 with two sub-elements, one with elastic response and the other with shear band response engulfing the shear band, where the strain is localized.

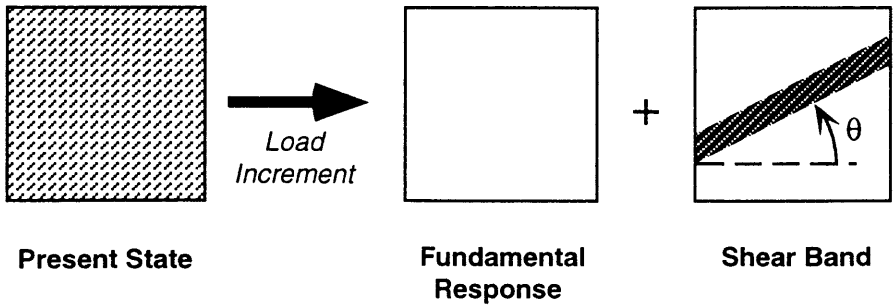

Fig. 3.2 Concept of shear band localization problem

If $\bar{\mathbf{d}}$ is the strain rate inside the shear band, the strain rate for the whole element is given by smearing the strain inside the band to the entire element. Since the thickness of the band is

small compared to the dimension of the element, large deformation generates inside the band. However, when smeared over the entire element the strain can be assumed to be small, and is given by:

$$\dot{\boldsymbol{\varepsilon}}^{P} = \zeta \bar{\mathbf{d}} \tag{3.13}$$

Here ζ is the smearing factor defined to be

$$\zeta = \frac{\text{Area of Shear Band } (A_b)}{\text{Area of Element } (A_e)} \tag{3.14}$$

The total strain in the localized element is given by:

$$\dot{\boldsymbol{\varepsilon}} = \dot{\boldsymbol{\varepsilon}}^{e} + \dot{\boldsymbol{\varepsilon}}^{P} \tag{3.15}$$

This is known as smeared shear band approach and was initially proposed by Pietruszczak and Mroz (1981).

Until now, all the shear band analyses considered only one shear band inside an element. In this research, the constitutive relations for the post-bifurcation behavior are developed using two shear bands based on the concept of smeared shear band approach. The constitutive model, named *Coupled Shear Band Method* (C.S.B. Method), is formulated by coupling the two shear bands the description of which follows.

3.4 ESSENTIALS OF THE COUPLED SHEAR BAND METHOD

Localized shearing leads to bifurcation from a uniform deformation to a non-uniform mode involving the inception of shear bands. Once localization takes place, the post bifurcation behavior can be idealized as pseudo-uniform deformation using smeared shear band approach with single band initially proposed by Pietruszczak and Mroz (1981) and later modified by Pietruszczak and Stolle (1987). However, theoretical evidence supports the existence of two bands along which the strain is localized. Experimentally too it is confirmed that if co-axiality of the ends of the sample is imposed by the apparatus generally two shear bands will be observed crossing each other (Desrues, 1990). The two bands develop simultaneously or alternately in loose sands; in dense sands the first band dominates for a while, but finally the second band appears. Above all, Mohr's diagram gives two directions of the failure planes along which failure occurs with inclinations as shown in Fig. 3.3.

Although localization is possible even in the hardening regime just before the peak, in this research, it is assumed that the localized shearing takes place only at the peak load (i.e. at

failure), which leads to softening. In order to simulate the two failure planes of Mohr's diagram, consideration of both the bands in the analysis is indispensable, since the concentrated strains in two different directions ultimately contribute to the softening of the material. The consideration of single shear band, in general, might lead to underestimation of the strain softening response. Hence, for an element undergoing the localized shearing, the effect of both the shear bands needs to be incorporated in its constitutive relation.

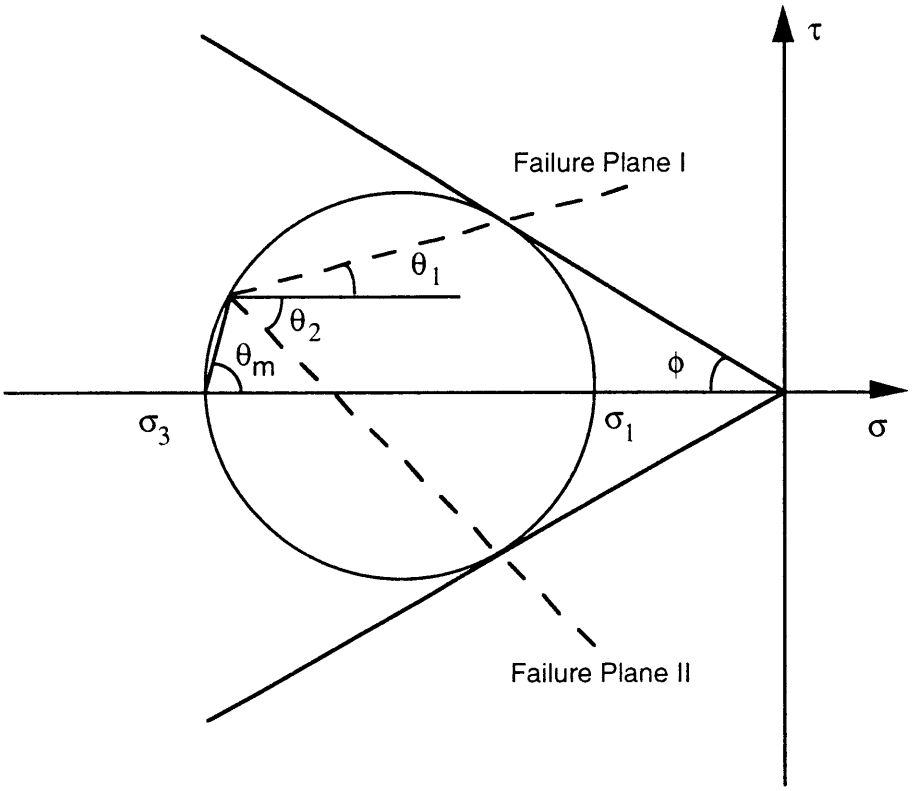

Fig. 3.3. Mohr's diagram for cohesionless soil showing the directions of the bands

3.4.1 Orientations of the Bands

As mentioned earlier, the basic assumption made here is that the localized shearing initiates at the instant of failure. Hence, when the yield surface reaches the failure surface, the element can be assumed to have *cracked* engulfing the two shear bands. At that instant, the constitutive relation for the cracked elements needs to be modified taking into the account the effect of the incepted bands.

At the localized state, the element can be assumed to be composed of three sub-elements as shown (considering a triangular element) schematically in Fig. 3.4. Such an element, containing the shear band, has been named as "cracked triangular element" by Kawamoto

and Takeda (1979). Sub-element I behaves elastically under the applied load. Sub-elements II and III entrap the shear bands, which are inclined at angles θ_1 and θ_2 to the X axis respectively. The plastic strains accumulate inside the two bands.

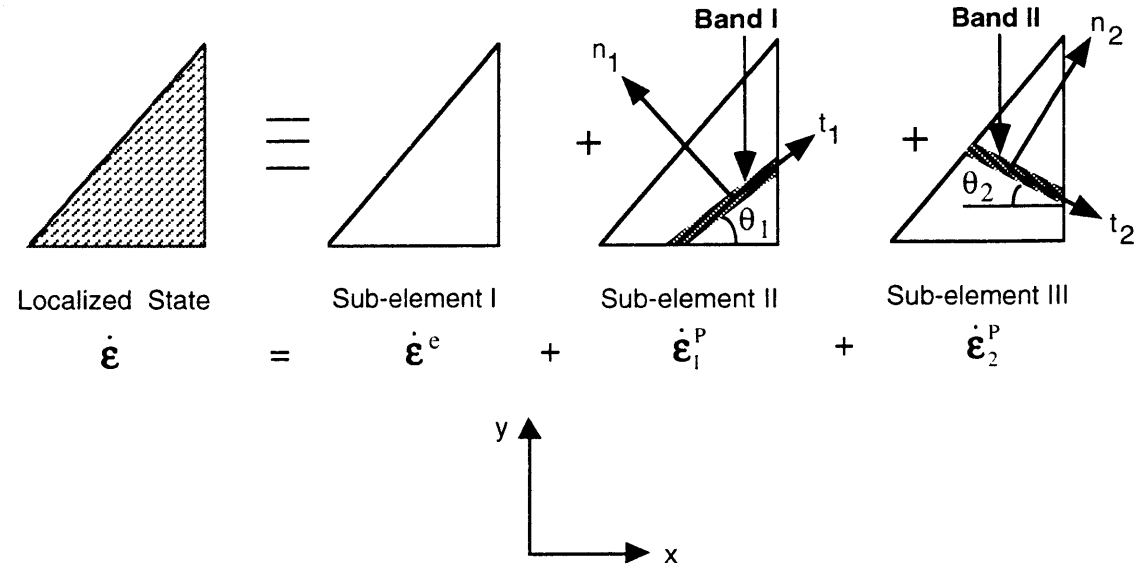

Fig. 3.4 Cracked triangular element with two shear bands

Assuming co-axiality of the stress and strain rate tensors, the inclinations of the two bands are given by the following equations.

$$\theta_1 = \theta_m - (\frac{\pi}{4} + \frac{\phi}{2}) \tag{3.16}$$

$$\theta_2 = \theta_m - (\frac{3\pi}{4} - \frac{\phi}{2}) \tag{3.17}$$

where θ_m is the angle from the X axis to the major principal axis in the Mohr diagram (Fig. 3.3); ϕ being the angle of internal friction of the material.

The Coulomb orientations, given by the above equations (Eqs. 3.16 & 3.17), are not the sole shear band orientations existing in the literature. In fact differing opinions exist regarding the orientations of the bands. The question of the orientation of the shear bands is an important one from both the practical and the theoretical point of view, since a critical orientation for the initiation of localization is one of the results of the bifurcation analysis applied to shear band mode of bifurcation. If the shear band is seen as a region of intensely shearing material where the strains are considerably greater than those in the surrounding regions, which can then be assumed to be comparatively rigid, then the compatibility indicates the coincidence of the shear bands with zero extension lines and this led to

Roscoe's (1970) orientation, $\theta = \theta_m \pm (\pi/4 - \frac{\psi}{2})$, ψ being the angle of dilation. A further possibility is to regard the formation of the shear band as an instability in the constitutive relationship that the material is following immediately before the rupture forms. This approach leads to the intermediate orientation, $\theta = \theta_m \pm [\pi/4 - \frac{1}{4}(\phi + \psi)]$ (Arthur et. al (1977), Vardoulakis (1981), Vermeer (1982)). Thus, Coulomb orientations and Roscoe orientations provide the upper and the lower bound respectively. It can be expected that the boundary conditions applied to any particular situation will influence the direction in which the shear bands choose to form. Scarpelli and Wood (1982) suggested that the degree of constraint perceived by the sand would influence the particular bifurcation (Coulomb, Roscoe or Intermediate Orientations) that it adopts at any particular location. When the sand gets the freedom of movement it may adopt the intermediate orientations. When the imposed condition is greater (i.e. in a simple shear test where the thickness of the sample is only about twice the expected shear band thickness), then the shear bands may have no choice but to follow the Roscoe orientations. However, in the formulations that follow the aforementioned Coulomb orientations (Eqs. 3.16 & 3.17) will be adopted.

3.4.2 Constitutive Relations for the Cracked Elements

The large deformation theory gives the relations (3.18) and (3.19), which connects the rate of deformation tensor $\bar{\mathbf{d}}$ and the Jaumann rate of stress tensor $\hat{\boldsymbol{\sigma}}$ inside the two bands under the plane strain condition in which f_b is the yield function and g_b is the plastic potential function.

For band I: Relative to the $\{n_I, t_I\}$ co-ordinate system the constitutive relation takes the form given below.

$$\begin{Bmatrix} \bar{d}_{n_I} \\ \bar{d}_{t_I} \\ \bar{d}_{nt_I} \end{Bmatrix} = \frac{1}{H_s} \begin{bmatrix} \frac{\partial g_b}{\partial \sigma_{n_I}} \frac{\partial f_b}{\partial \sigma_{n_I}} & 0 & \frac{\partial g_b}{\partial \sigma_{n_I}} \frac{\partial f_b}{\partial \sigma_{nt_I}} \\ 0 & 0 & 0 \\ \frac{\partial g_b}{\partial \sigma_{nt_I}} \frac{\partial f_b}{\partial \sigma_{n_I}} & 0 & \frac{\partial g_b}{\partial \sigma_{nt_I}} \frac{\partial f_b}{\partial \sigma_{nt_I}} \end{bmatrix} \begin{Bmatrix} \hat{\sigma}_{n_I} \\ \hat{\sigma}_{t_I} \\ \hat{\sigma}_{nt_I} \end{Bmatrix} \tag{3.18a}$$

The above relation in the $\{x,y\}$ co-ordinate system takes the form

$$\bar{\mathbf{d}}_I = \frac{1}{H_s} [\bar{C}_I] \hat{\boldsymbol{\sigma}}_I \tag{3.18b}$$

For band II: Relative to the $\{n_2,t_2\}$ co-ordinate system the constitutive relation is given by,

$$\begin{Bmatrix} \bar{d}_{n_2} \\ \bar{d}_{t_2} \\ \bar{d}_{nt_2} \end{Bmatrix} = \frac{1}{H_s} \begin{bmatrix} \frac{\partial g_b}{\partial \sigma_{n_2}} \frac{\partial f_b}{\partial \sigma_{n_2}} & 0 & \frac{\partial g_b}{\partial \sigma_{n_2}} \frac{\partial f_b}{\partial \sigma_{nt_2}} \\ 0 & 0 & 0 \\ \frac{\partial g_b}{\partial \sigma_{nt_2}} \frac{\partial f_b}{\partial \sigma_{n_2}} & 0 & \frac{\partial g_b}{\partial \sigma_{nt_2}} \frac{\partial f_b}{\partial \sigma_{nt_2}} \end{bmatrix} \begin{Bmatrix} \hat{\sigma}_{n_2} \\ \hat{\sigma}_{t_2} \\ \hat{\sigma}_{nt_2} \end{Bmatrix} \tag{3.19a}$$

Relative to the $\{x,y\}$ co-ordinate system the above equation takes the form.

$$\bar{\mathbf{d}}_2 = \frac{1}{H_s}[\bar{C}_2]\hat{\boldsymbol{\sigma}}_2 \tag{3.19b}$$

Here $[\bar{C}_1]$ and $[\bar{C}_2]$ are the compliance matrices (Vermeer, 1982) in the global co-ordinate system and defined by the following equations:

$$[\bar{C}_1] = [T_1]^T[\bar{C}_1^*][T_1] \tag{3.20}$$

$$[\bar{C}_2] = [T_2]^T[\bar{C}_2^*][T_2] \tag{3.21}$$

In which $[\bar{C}_1^*]$ and $[\bar{C}_2^*]$ represent the compliance matrices in the local co-ordinate systems $\{n_1,t_1\}$ and $\{n_2,t_2\}$ respectively and can be evaluated by the bracketed terms in the Eqs. (3.18a) and (3.19a). The matrices $[T_1]$ and $[T_2]$ are the transformation matrices defined by the shear band orientation angles θ_1 and θ_2 respectively, while H_s is the softening modulus. Eqs. (3.18a) and (3.19a) indicate that the rate of deformation across the shear band vanishes.

Expressing $\hat{\boldsymbol{\sigma}}_1$ and $\hat{\boldsymbol{\sigma}}_2$ in terms of Cauchy's stress rate $\dot{\boldsymbol{\sigma}}$ and then some transformations render the following equations

$$\bar{\mathbf{d}}_1 = \frac{1}{H_s}([\mathbf{I}] - \frac{1}{H_s}[\bar{C}_1]\boldsymbol{\beta}\boldsymbol{\delta}_1^T)^{-1}[\bar{C}_1]\dot{\boldsymbol{\sigma}} \tag{3.22}$$

$$\bar{\mathbf{d}}_2 = \frac{1}{H_s}([\mathbf{I}] - \frac{1}{H_s}[\bar{C}_2]\boldsymbol{\beta}\boldsymbol{\delta}_2^T)^{-1}[\bar{C}_2]\dot{\boldsymbol{\sigma}} \tag{3.23}$$

in which $\mathbf{I}$ is the unit tensor and $\boldsymbol{\beta}$ is given by the expression

$$\boldsymbol{\beta} = \{-2\sigma_{xy}, 2\sigma_{xy}, (\sigma_x - \sigma_y)\}^T \tag{3.24}$$

δ_1 and δ_2 are the transformation matrices defined by the orientation angles θ_1 and θ_2 and can be obtained by substituting the values of θ in the expression given below

$$\delta = \{-sc,\ sc,\ \frac{1}{2}(c^2 - s^2)\}^T \tag{3.25}$$

where $s = \sin(-\theta)$; $c = \cos(-\theta)$. Introducing the smearing factor ζ, the infinitesimal plastic strains in the two sub-elements can be expressed as

$$\dot{\boldsymbol{\varepsilon}}_1^P = \zeta \bar{\mathbf{d}}_1 \tag{3.26}$$

$$\dot{\boldsymbol{\varepsilon}}_2^P = \zeta \bar{\mathbf{d}}_2 \tag{3.27}$$

As shown in Fig. 3.4, the total strain in the cracked element can be written as,

$$\dot{\boldsymbol{\varepsilon}} = \dot{\boldsymbol{\varepsilon}}^e + \dot{\boldsymbol{\varepsilon}}_1^P + \dot{\boldsymbol{\varepsilon}}_2^P \tag{3.28}$$

where $\dot{\boldsymbol{\varepsilon}}^e$ is the elastic strain rate generated inside the sub-element I. Substituting the Eqs. (3.22), (3.23), (3.26) and (3.27) into the Eq. (3.28) the constitutive equation takes the following form:

$$\dot{\boldsymbol{\varepsilon}} = \{([\mathbf{I}] - \frac{1}{H_s}[\bar{C}_1]\boldsymbol{\beta}\delta_1^T)^{-1}[\bar{C}_1] + ([\mathbf{I}] - \frac{1}{H_s}[\bar{C}_2]\boldsymbol{\beta}\delta_2^T)^{-1}[\bar{C}_2] + \frac{H_s}{\zeta}[C^e]\}\frac{\zeta}{H_s}\dot{\boldsymbol{\sigma}} \tag{3.29}$$

in which the elastic part of the compliance matrix C^e is given by the following equation.

$$[C^e] = \frac{1}{E}\begin{bmatrix} (1-\nu^2) & -\nu(1+\nu) & 0 \\ -\nu(1+\nu) & (1-\nu^2) & 0 \\ 0 & 0 & 2(1+\nu) \end{bmatrix} \tag{3.30}$$

E and ν are the Young's modulus and Poisson's ratio respectively. Eq. (3.29) represents the constitutive relation for the cracked elements with localized strain.

3.4.3 Hardening, Localized State and Softening

3.4.3.1 Hardening Regime

The constitutive relation for the non localized elements is given by the conventional relation for elasto-plastic strain hardening material (Eq. 3.12) in which case the yield function f and

the plastic potential function g are assumed to be given by the following Mohr-Coulomb criterion with the major principal stress, σ_1 and the minor principal stress, σ_3

$$f = (\sigma_1 - \sigma_3) + (\sigma_1 + \sigma_3)\kappa\,; \qquad g = (\sigma_1 - \sigma_3) + (\sigma_1 + \sigma_3)\eta \tag{3.31}$$

where κ and η are the hardening function and the dilatancy parameter respectively which are assumed as

$$\kappa = \mathrm{Sin}\phi_m = \frac{\kappa_f \xi}{A + \xi}; \qquad \eta = \mathrm{Sin}\psi_m = \frac{\kappa - \kappa_c}{1 - \kappa\kappa_c} \tag{3.32}$$

Here, ϕ_m is the mobilized angle of internal friction, $\kappa_f = \mathrm{Sin}\phi_f$, ϕ_f being the peak friction angle, A is the material constant and ξ is the plastic distortion. ψ_m is the mobilized dilatancy angle, $\kappa_c = \mathrm{Sin}\phi_{cv}$ is a constant defining the zero dilatancy state, ϕ_{cv} being the friction angle at constant volume. The consistency condition yields the hardening modulus H as

$$H = -(\sigma_1 + \sigma_3)\frac{\kappa_f A}{(A + \xi)^2} \tag{3.33}$$

3.4.3.2 Strain Localized State

It is generally believed that localization can occur even in the hardening regime before the peak. However, in this formulation it is assumed that failure precedes the localized shearing. When the yield surface reaches the failure surface, that instant the constitutive relation for the elements is given by Eq. (3.29). The failure surface, F, is assumed to be of Mohr-Coulomb type given by the following equation.

$$F = (\sigma_1 - \sigma_3) + (\sigma_1 + \sigma_3)\sin\phi_f \tag{3.34}$$

3.4.3.3 Response in Softening Regime

On spontaneous loss of homogeneity, the irreversible deformation is assumed to be localized in the two shear bands. Progressive flow within the bands generates plastic strains of finite magnitudes. However, the average non-homogenous strains remain infinitesimal. At the instant of localization, the yield function f_b and the plastic potential function g_b inside the bands in the {n,t} coordinate system are assumed as

$$f_b = \sigma_{nt} + \kappa_s \sigma_n\,; \qquad g_b = \sigma_{nt} + \eta_s \sigma_n \tag{3.35}$$

where κ_s is the softening function assumed to be given by (Pietruszczak and Stolle, 1987).

$$\kappa_s = \eta_s\{1 + \exp[-R(\gamma^p - \gamma_0)]\} \tag{3.36}$$

where η_s is the dilatancy parameter, R is the material constant that determines the rate of softening, γ^p is the plastic shear strain that accumulates within the band after its inception and γ_0 is the value of shear strain when $\gamma^p = 0$. Using the above yield and plastic potential functions, the softening modulus, H_s can be obtained from the consistency condition as

$$H_s = R\sigma_n(\kappa_s - \eta_s) \tag{3.37}$$

3.4.4 Material Parameters

In order to identify the model, the following material parameters need to be specified. The various material constants appeared in the C.S.B. Method described above can be determined from the conventional triaxial tests or plane strain tests.

(1) Elastic moduli E and ν

(2) The deformation parameters which include:

(a) Parameter identifying the failure line denoted by $\kappa_f = \mathrm{Sin}\phi_f$.

(b) The constant A given by $A = \kappa_f \frac{P}{2G}$, where G is the elastic shear modulus and P for conventional triaxial test is given by $P = (\sigma_1 + 2\sigma_3)/\sqrt{3}$

(c) The constant R, which is the slope of the strain softening portion of the stress strain curve and can be determined by performing parametric study.

(3) The dilatancy parameters that includes:

(a) The dilatancy constant $\kappa_c = \mathrm{Sin}\phi_{cv}$, where ϕ_{cv} can be determined from the dilatancy curve. As a rule of thumb, the relation $\phi_{cv} = 0.7\phi_f$ can be used.

(b) The dilatancy constant in the softening regime is given by: $\eta_s = \tan\phi_{cv}$

(4) The smearing parameter ζ can be determined from a parametric study for the problem, which is explained in the chapter about the application of this constitutive model.

3.5 SUMMARY AND CONCLUDING REMARKS

In this chapter, two constitutive relations for modeling the backfill mass of a retaining wall are described. The first one is the conventional elasto-plastic constitutive relation with the Drucker-Prager failure criterion. In it, the hardening is defined by a hyperbolic function, the parameters of which can be determined from the conventional triaxial testing. The other one,

a new formulation named as *Coupled Shear band Method*, is based on the smeared shear band approach and it considers the localized deformation inside the backfill.

Earth pressure phenomenon involves progressive deformation. Thus, the assumption of simultaneous mobilization of the peak strength along the slip surface is not an easily acceptable fact. This necessitates the use of shear band localization in modeling the backfill constitutive laws. Since the triggering of shear band leads to strain softening, the constitutive relation should involve the modeling of the softening regime. Thus, the constitutive relation assuming continuity of stress throughout the entire deformation field, as in the case of the first constitutive description, does not suffice to capture the progressive failure in the backfill.

In most of the existing strain localization models shear banding is entirely attributed to the material instability. These models show sensitivity to different factors such as the discretization of the system, the rate of strain softening etc. Inclusion of the width of the shear band in the constitutive formula, thus taking care of the geometric softening, has shown to render the analysis insensitive to the above factors.

The post localization regime should be modeled by using two shear bands, and the constitutive relation can be formulated by coupling the two bands. The orientations of the bands can be given by Coulomb, Roscoe or Intermediate orientation. The material parameters appeared in the new constitutive law can be easily determined from the conventional triaxial or plane strain tests.

REFERENCES

[1] Anand, L. and Spitzig, W.A. (1980), "Initiation of Localized Shear Bands in Plane Strain", *Journal of Mechanics and Physics of Solids*, Vol. 28, pp. 113-128.

[2] Arthur, J.R.F., Dunstan, T., Al-Ani, Q.A.J.L. and Assadi, A. (1977), "Plastic Deformation and Failure in Granular Media", *Geotechnique*, Vol. 27, pp. 53-74.

[3] De Borst, R. (1988), "Bifurcations in Finite Element Models with a Non-associated Flow Law", *International Journal for Numerical and Analytical Methods in Geomechanics*, Vol. 12, pp. 99-116.

[4] Desrues, J. (1990), "Shear Band Initiation in Granular Material: Experimentation and Theory", In *Geomaterials: Constitutive Equations and Modelling*, Ed. F. Darve, Elsevier Applied Science, London, pp. 283-310.

[5] Drucker, D.C. and Prager, W. (1952), "Soil Mechanics and Plastic Analysis or Limit Design", *Quarterly of Applied Mathmatics*, Vol. 10, 2, pp. 157-165.

[6] Hazarika, H. (1995), "Progressive Failure Analyses of a Retaining Wall-Backfill System Based on Smeared Shear Band Technique", *Proceedings of the 50th Annual Conference of Japanese Society of Civil Engineers*, Matsuyama, Japan, Vol. 3, pp. 986-987.

[7] Hazarika, H. and Matsuzawa, H. (1995), "Coupled Shear Band Method and Its Application to the Seismic Earth Pressure Problems", *Soils and Foundations, Japanese Geotechnical Society* (Submitted for possible publication).

[8] Hazarika, H. and Matsuzawa, H. (1995), "Wall Displacement Modes Dependent Active Earth Pressure Analyses Using Smeared Shear Band Method with Two Bands", *Computers and Geotechnics* (To appear).

[9] Hill, R. (1962), "Acceleration Waves in Solids", *Journal of Mechanics and Physics of Solids*, Vol. 10, pp. 1-16.

[10] Ichikawa, Y., Kyoya, T., Aydan, O., Yoshikawa, K., Kawamoto, T. and Takashiki, N. (1989), "Deformation and Failure of Rocks under "Weak" Cyclic Loading and Incremental Elasto-Plastic Theory", *Memoirs of the Faculty of Engineering, Nagoya University*, Vol. 40, 2, pp. 273-326.

[11] Ichikawa, Y., Ito, T. and Mroz, Z. (1990), "A Strain Localization Condition Applying Multi-Response Theory", *Ingenieur-Archiv*, Vol. 60, pp. 542-552.

[12] Kawamoto, T. and Takeda. N. (1979), "An Analysis of Progressive Failure in Rock Slopes", *Proceedings of the Third International Conference on Numerical and Analytical Methods in Geomechanics*, Aachen, pp. 797-808.

[13] Mandel, J. (1966), "Conditions de Stabilite et Postulate de Drucker", *Proceedings of the IUTAM Symposium on Rheology and Soil Mechanics*, Berlin, pp. 58-68.

[14] Matsuzawa, H. and Hazarika, H. (1995), "Analyses of Active Earth Pressure Against Rigid Retaining Wall Subjected to Different Modes of Movement", *Soils and Foundations, Japanese Geotechnical Society* (Accepted).

[15] Muhlhaus, H.B. and Vardoulakis, I. (1987), "The Thickness of Shear Bands in Granular Materials", *Geotechnique*, Vol. 37, 3, pp. 271-283.

[16] Oka, F., Adachi, T. and Yashima, A. (1994), "Instability of an Elasto-viscoplastic Constitutive Model for Clay and Strain Localization", *Mechanics of Material*, Vol. 18, 2, pp. 119-129.

[17] Ortiz, M., Leroy, Y. and Needleman, A. (1987), "A Finite Element Method for Localized Failure Analysis", *Computer Methods in Applied Mechanics and Engineering*, Vol. 61, pp. 189-214.

[18] Pietruszczak, S. and Mroz, Z. (1981), "Finite Element Analysis of Deformation of Strain Softening Materials", *Intl. Journ. of Num. Meth. in Engg.*, Vol. 17, pp. 327-334.

[19] Pietruszczak, S. and Stolle, D.F.E. (1987), "Deformation of Strain Softening Materials, Part II:", *Computers and Geotechnics*, Vol. 4, pp. 109-123.

[20] Poorooshasb, H.B. and Pietruszczak, S. (1985), "On Yielding and Flow of Sand; A Generalized Two -Surface Model", *Computers and Geotechnics*, Vol. 1, pp. 33-58.

[21] Potts, D.M. and Gens, A. (1984), "The Effect of the Plastic Potential in Boundary Value Problems Involving Plane Strain Deformation", *International Journal for Numerical and Analytical Methods in Geomechanics*, Vol. 8, pp. 259-286.

[22] Rice, J.R. (1976), "The Localization of Plastic Deformation", In *Theoretical and Applied Mechanics*, Ed. W. T. Koiter, North-Holland Publishing Company, Amsterdam, pp. 207-220.

[23] Rice, J.R. and Rudniki, J.W. (1980), "A Note on Some Features of the Theory of Localization of Deformations", *International Journal of Solids and Structures*, Vol. 16, pp. 597-605.

[24] Roscoe, K.H. (1970), "The Influence of Strains in Soil Mechanics", *Geotechnique*, Vol. 20, 2, pp. 129-170.

[25] Rudniki, J.W. and Rice, J.R. (1975), "Conditions for the Localization of Deformation in Pressure-sensitive Dilatant Materials", *Journal of Mechanics and Physics of Solids*, Vol. 23, pp. 371-394.

[26] Scarpelli, G. and Wood, D.M. (1982), "Experimental Observations of Shear Band Patterns in Direct Shear Tests", *Proceedings of the IUTAM conference on Deformation and Failure in Granular Materials*, Delft, pp. 473-484.

[27] Tanaka, T. and Sakai, T. (1993), "Progressive Failure and Scale Effect of Trap-Door Problems with Granular Materials", *Soils and Foundations, JSSMFE*, Vol. 33, 1, pp. 11-22.

[28] Thomas, T.Y. (1961), *Plastic Flow and Fracture in Solids*, Academic Press, New York, U.S.A.

[29] Vardoulakis, I. (1981), "Bifurcation Analysis of the Plane Rectilinear Deformation on Dry Sand Samples", *International Journal of Solids and Structures*, Vol. 17, 11-E, pp. 1085-1101.

[30] Vardoulakis, I., Muhlhaus, H.B. and Aifantis, E.C. (1991), "Continuum Models for localized Deformations in Pressure Sensitive Materials", *Proceedings of the 8th International Conference on Computer Methods and Advances in Geomechanics*, Cairns, Australia, pp. 441-448.

[31] Vardoulakis, I. (1982), "Stability and Bifurcation of Soil Samples", *Proceedings of the International Workshop on Constitutive Relations for Soils*, Grenoble, pp. 477-483.

[32] Vermeer, P.A. (1982), "A Simple Shear-band Analysis using Compliances", *Proceedings of the IUTAM Conference on Deformation and Failure of Granular Materials*, Delft, Holland, pp. 493-499.

[33] Wan, R.G. (1992), "Numerical Modelling of Shear Band Localization in Geomaterials", *Special Lecture in the Symposium on the Recent Problems in Geotechnical Engineering, Chubu Branch of JSSMFE*, Nagoya University, Nagoya, Japan, pp. 1-13.

[34] Yatomi, C., Yashima, A., Iizuka, A. and Sano, I. (1989), "General Theory of Shear Bands Formation by a Non-coaxial Cam-Clay Model", *Soils and Foundations, JSSMFE*, Vol. 29, 3, pp. 41-53.

CHAPTER
FOUR

Modeling the Interface

Nature is indifferent towards
the difficulties it causes
to a mathematician

Fourier

4.1 INTRODUCTION

The interaction between the structure and the geologic media (e.g. soil) is an important aspect of any retaining wall analysis and the response may be affected significantly by the interface between the wall and the backfill (Fig. 4.1b). Whitman and Bielak (1980) define the soil-structure interaction in the following way:

> *If the motion at any point on the soil-structure interface differs from the motion that would occur at this point in the free field if the structure were not present, there is soil-structure interaction. If the interface moves or behaves differently than the corresponding surface in the free field, there is interaction.*

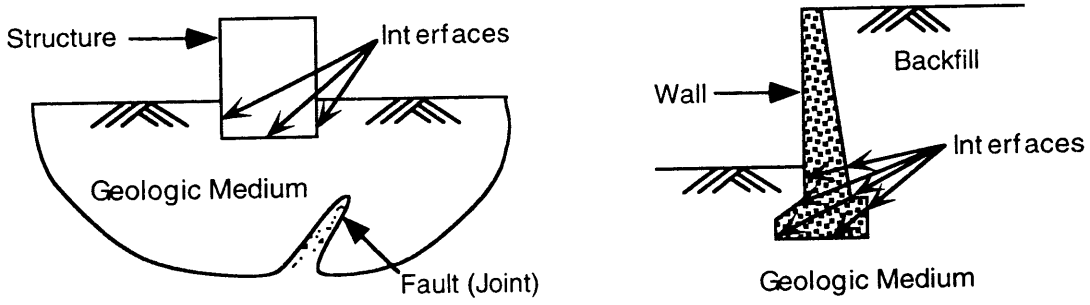

(a) (b)

Fig. 4.1 Typical soil-structure interaction problems (*After* Zaman et al, 1984)

It is now well established that for any realistic evaluation of the behavior of a structural-soil system, subjected to static or dynamic loads, it is essential to allow for the interaction or

coupling between the structural and the geologic media. A number of constitutive or stress-strain models have been proposed in order to simulate the interface behavior, particularly for static loading condition. No model has yet proved to be suitable for general application.

The importance of interaction phenomenon in static and dynamic soil-structure interaction has been recognized and studied by many investigators. It is not intended to present a detailed review herein; comprehensive reviews on various aspects of soil-structure interaction are presented by Desai (1977), Whitman and Bielak (1980). In this chapter some of the well-known interface models, which are widely in use in the Geotechnical Engineering field, are briefly reviewed. Finally, a new interface model, particularly for retaining wall problems, has been presented, the application of which can be referred in the subsequent chapters.

4.2 THEORETICAL BACKGROUND IN MODELING THE INTERFACE

The interface modeling is usually based on the following constitutive relationship for a two-dimensional body:

$$\{\sigma\} = [K_j]\{u_r\} \tag{4.1}$$

where $\{\sigma\}^T = [\sigma_{nn}\ \sigma_{ss}]$ is the vector of normal and shear stresses, $\{u_r\}^T = [u_{nr}\ u_{sr}]$ is the vector of relative displacements (strains) in the normal and shear modes, respectively and $[K_j]$ = matrix containing the stiffness of the interface element, which can be expressed as

$$[K_j] = \begin{bmatrix} K_{nn} & K_{ns} \\ K_{sn} & K_{ss} \end{bmatrix} \tag{4.2}$$

Very often, the cross stiffness K_{ns} and K_{sn} are assumed to be zero, then

$$[K_j] = \begin{bmatrix} K_{nn} & 0 \\ 0 & K_{ss} \end{bmatrix} \tag{4.3}$$

In soil-structure interaction problems, it is usually assumed that the structural and the geologic media may not penetrate each other and hence during the translational model, the value of normal stiffness is assumed to be very high. It is difficult to arrive at an appropriate high value of K_{nn} that would yield consistent and reliable results. Mostly, it is arrived at by performing a parametric study for the problem at hand.

4.3 PROPERTIES OF THE JOINTS AND INTERFACES

The properties that may be assigned to the joints or interfaces, are the shearing and the normal stiffness of the element. They are classified as *dilatant* if the shearing produces joint expansion or contraction and *nondilatant* if the shearing and normal displacement are uncoupled.

4.3.1 Nondilatant Joints or Interfaces

This class of joints is the simplest to model mathematically since there is no volume change due to the shearing strains, and therefore the shear and the normal components of deformation are uncoupled. The stress-strain relations are given by:

$$\begin{Bmatrix} \sigma_n \\ \sigma_s \end{Bmatrix} = \begin{bmatrix} K_n & 0 \\ 0 & K_s \end{bmatrix} \begin{Bmatrix} \varepsilon_n \\ \varepsilon_s \end{Bmatrix} \tag{4.4}$$

In relating the stress to the deformation in the direction normal to the joint, three distinct stages are defined (Fig. 4.2): (1) separation or debonding $K_{nn} = K_{ss} = 0$, when $\varepsilon_n \geq 0$; (2) compression $K_{nn} = E_c$, when $\varepsilon_n < 0$ and (3) contact, $K_{nn} = E_f$.

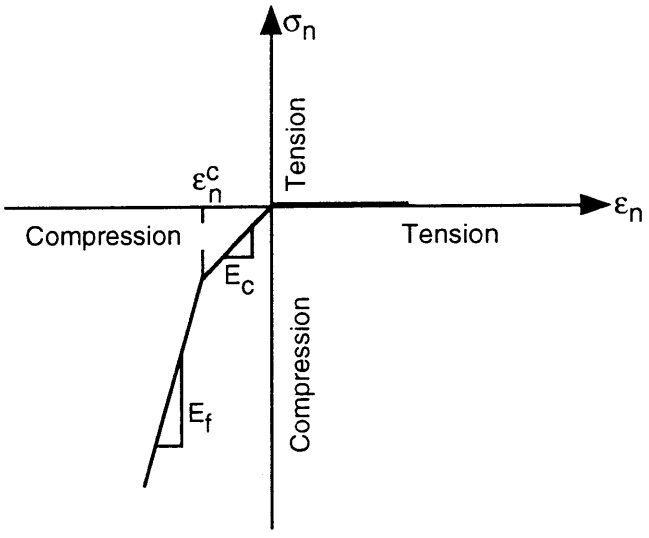

Fig. 4.2 Normal stress-strain relationship (*After* Ghaboussi et al, 1973)

The tangential stress-strain relationship is assumed to be elastic-perfectly plastic using Mohr-Coulomb yield criterion.

4.3.2 Dilatant Joints or Interfaces

Dilatancy at the joints or interfaces is more complicated. One method of representing dilatancy begins by defining nondilatant properties of the joint in terms of p-q coordinate system shown in Fig. 4.3. By transformation of coordinates, the constitutive properties may then be expressed in terms of the n-s system as follows:

$$\begin{Bmatrix}\sigma_n\\ \sigma_s\end{Bmatrix} = \begin{bmatrix}K_q c^2 + K_p s^2 & (K_q - K_p)sc\\ (K_q - K_p)sc & K_q s^2 + K_p c^2\end{bmatrix}\begin{Bmatrix}\varepsilon_n\\ \varepsilon_s\end{Bmatrix} \tag{4.5}$$

in which $c = \cos\gamma$; $s = \sin\gamma$; K_q = normal stiffness in the q direction, perpendicular to the local joint plane; and K_p = shear stiffness in the p direction. The amount of dilatancy, according to this method, thus depends on the intrinsic properties of K_q and K_p as well as on the normal stress.

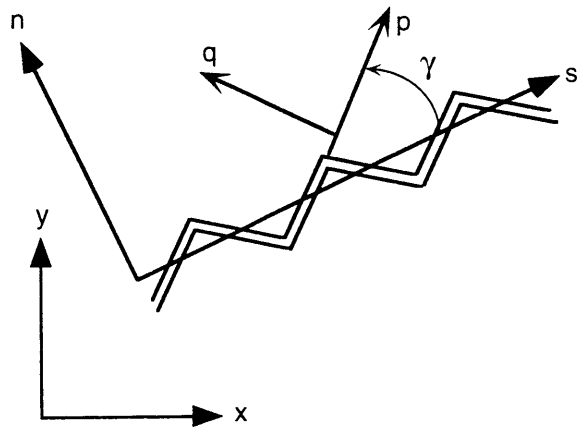

Fig. 4.3 Dilatant joint model (*After* Ghaboussi et al, 1973)

4.4 CLASSIFICATIONS OF INTERFACE

Tatsuoka (1985) pointed out that the interface friction δ between cohesionless soil and another material is upper bounded by two different values (δ_0 and δ^*) depending on the two classes of interface: the first is the case when the interface is a velocity discontinuity, and the second is the case when the interface is not a velocity discontinuity.

When the interface is a velocity discontinuity, the cohesionless soil mass in the immediate vicinity of the interface may or may not be at the limiting stress condition. The value of the friction angle may not be direct function of the mechanical properties of the soil mass, but may be a function of the mechanical properties of the particles and materials in

contact and the roughness of the surface of the material. Fig 4.4 is the case when the interface is a velocity discontinuity.

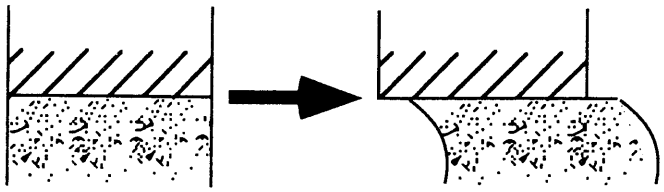

Fig. 4.4 Interface with velocity discontinuity

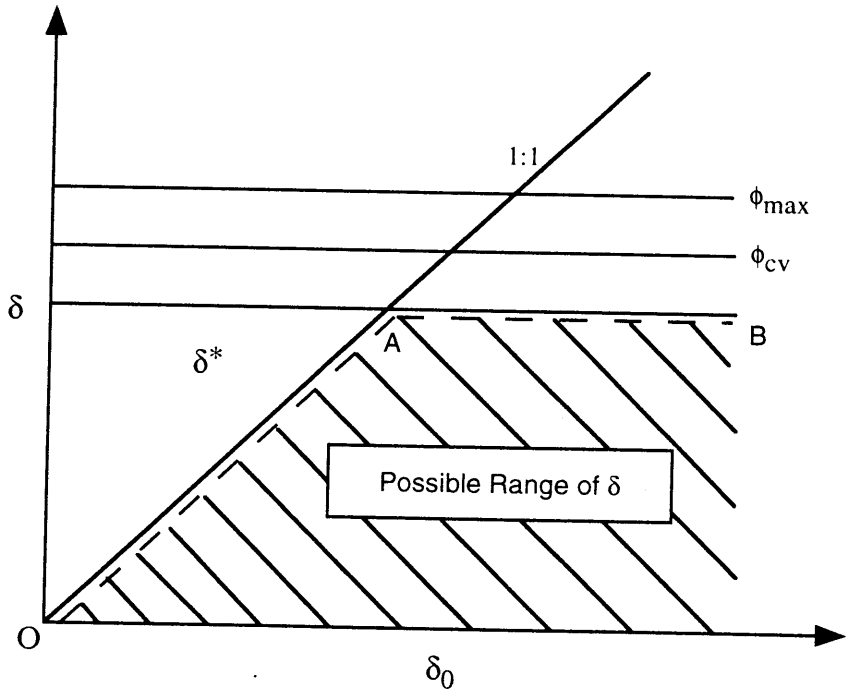

Fig. 4.5 Relationship amongst δ, δ_0 and δ^* (*After* Tatsuoka, 1985)

When the interface is not a velocity discontinuity, the mass of soil moves solely due to its deformation along the interface without producing a velocity discontinuity. The value of the friction angle is a function of the strength and deformation properties of the cohesionless soil and the deformability of the material in contact with the soil.

The relationship between δ, δ_0 and δ^* is illustrated in Fig. 4.5. The range for possible values of δ is upper bounded by two lines OA ($\delta = \delta_0$) and AB ($\delta = \delta^*$). It is to be noted that δ may or may not be mobilized at the failure of the adjacent soil mass.

4.5 INTERFACE MODELS - A REVIEW

Junctions or interfaces between two dissimilar media having widely differing strength properties pose a different problem than the deformation of a continuous medium. In the case of the later, two adjacent points deform in such a way that the continuity of displacements at the points is maintained. However, for the interfaces, continuity may be maintained only up to a certain load level. At higher loads, relative slip and debonding (loss of contact) can occur and the two initially adjacent points may no longer have continuous displacements. Under certain types of loading, the interface may also experience separation or opening and then may close. Thus, the behavior at the interface renders the structural-soil system to deviate from being continuous.

A variety of efforts have been made to account approximately for the foregoing special behavior at interfaces. These have included characterization of behavior of joints in rocks and interfaces in structure-soil systems. Most of the studies towards development and application of models for interfaces and joints have involved static loading and use of such models for cyclic loading is of rather recent origin. Hence for the sake of logical development and completeness, a review of the models for static analysis is presented.

4.5.1 Linkage Element Model

Ngo and Scordelis (1967) presented a linkage element for simulating the cracks in concrete, and described the behavior of a crack in the two-dimensional mass by using springs for normal and shear responses as shown in Fig. 4.6.

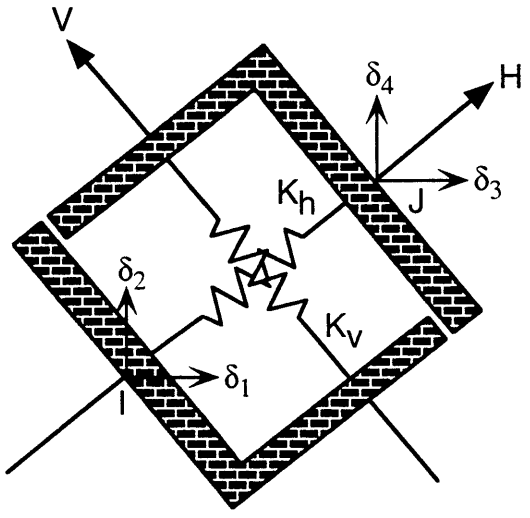

Fig. 4.6. Linkage element (Ngo and Scordelis, 1967)

The linkage element can be conceptually thought of as consisting of two linear springs parallel to a set of orthogonal axes H and V (Fig. 4.6). For generality, the linkage element can be oriented at an arbritary angle θ with the horizontal axis. This type of element is similar to the non-dilatant type of joint element.

To incorporate the linkage element into the finite element computer program, it is necessary to develop the stiffness matrix of the linkage element. Let the springs in the H and V directions have stiffnesses K_h and K_v respectively. The stress-strain relationship will be given by:

$$\begin{Bmatrix}\sigma_h\\ \sigma_v\end{Bmatrix}=\begin{bmatrix}K_h & 0\\ 0 & K_v\end{bmatrix}\begin{Bmatrix}\varepsilon_h\\ \varepsilon_v\end{Bmatrix} \tag{4.6}$$

where ε_h and ε_v are the relative displacement between the points I and J in the H and V directions respectively. The strains and the displacements are related through the displacement transformation matrix T.

$$\{\varepsilon\}=[T]\{\delta\} \tag{4.7}$$

or

$$\begin{Bmatrix}\varepsilon_h\\ \varepsilon_v\end{Bmatrix}=\begin{bmatrix}-c & -s & c & s\\ s & -c & -s & c\end{bmatrix}\begin{Bmatrix}\delta_1\\ \delta_2\\ \delta_3\\ \delta_4\end{Bmatrix} \tag{4.8}$$

where $c = \cos\theta$ and $s = \sin\theta$. Hence the stiffness matrix of the linkage element can be expressed as:

$$[k]=[T]^T[K][T]=\begin{bmatrix}-c & s\\ -s & -c\\ c & -s\\ s & c\end{bmatrix}\begin{bmatrix}K_h & 0\\ 0 & K_v\end{bmatrix}\begin{bmatrix}-c & -s & c & s\\ s & -c & -s & c\end{bmatrix} \tag{4.9}$$

4.5.2 Joint Element Model

Goodman et al (1968) presented a rock joint element by expressing the relative displacement between the two dimensional intact rock masses, and formulated the stiffness matrix for the joint in terms of the normal and shear stiffnesses (Fig. 4.7). The relative displacement vector for the joint element (Fig. 4.7b) is given by:

$$\{w\} = \begin{bmatrix} w_s^{top} - w_s^{bottom} \\ w_n^{top} - w_n^{bottom} \end{bmatrix} \tag{4.10}$$

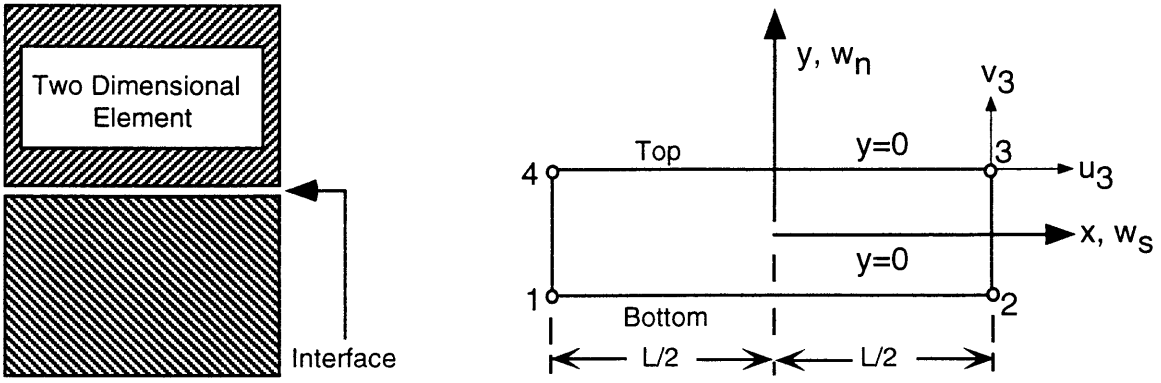

(a) Interface between two elements (b) Interface element

Fig. 4.7 Joint element of Goodman et al (1968)

The vector P (force per unit length) may be expressed in terms of the product of the joint unit stiffness in normal (K_n) and tangential (K_s) directions and the displacement:

$$\begin{Bmatrix} P_s \\ P_n \end{Bmatrix} = \begin{bmatrix} K_s & 0 \\ 0 & K_n \end{bmatrix} \begin{Bmatrix} w_s \\ w_n \end{Bmatrix} \tag{4.11}$$

Considering the energy stored in the element then leads to the following local joint element stiffness matrix

$$[K] = \frac{1}{6} \begin{bmatrix} 2K_s & 0 & 1K_s & 0 & -1K_s & 0 & -2K_s & 0 \\ 0 & 2K_n & 0 & 1K_n & 0 & -1K_n & 0 & -2K_n \\ 1K_s & 0 & 2K_s & 0 & -2K_s & 0 & -1K_s & 0 \\ 0 & 1K_n & 0 & 2K_n & 0 & -2K_n & 0 & -1K_n \\ -1K_s & 0 & -2K_s & 0 & 2K_s & 0 & 1K_s & 0 \\ 0 & -1K_n & 0 & -2K_n & 0 & 2K_n & 0 & 1K_n \\ -2K_s & 0 & -1K_s & 0 & 1K_s & 0 & 2K_s & 0 \\ 0 & -2K_n & 0 & -1K_n & 0 & 1K_n & 0 & 2K_n \end{bmatrix} \tag{4.12}$$

Goodman type joint elements are used not only in the Rock Mechanics problems, but also in Geotechnical Engineering problems, many of which include retaining wall analysis. With Goodman type of joint element, adjacent blocks of continuous elements can penetrate into

each other. Zienkiewicz et al (1970) advocate the use of continuous isoparametric element with simple nonlinear material properties for shear and normal stresses, assuming uniform strain in the thickness direction. Numerical difficulties may arise from ill conditioning of the stiffness matrix due to very large off-diagonal terms or very small diagonal terms, which are generated by this element in certain cases.

Ghaboussi et al (1973) put forward a model similar to above, but used the relative displacement as an independent degree of freedom (Fig. 4.8). They also defined the behavior in terms of the normal and shear stiffness.

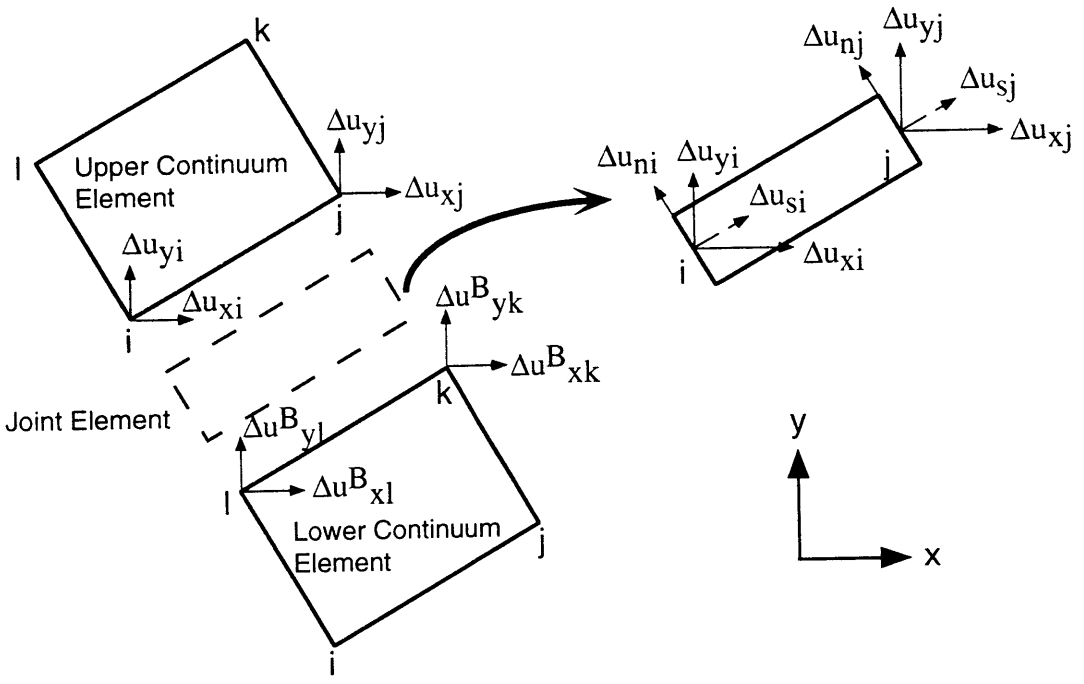

Fig. 4.8 Geometry of joint element (Ghaboussi et al, 1973)

Herrman (1978) presented an algorithm for interface element similar to the aforementioned concepts with certain improvements through constraint conditions. The various modes of the interface behavior such as the sliding and the debonding were discussed, and a numerical algorithm that can provide convergent solutions was proposed. However, still the normal and shear stiffnesses during various modes were chosen arbitrarily.

The computed behavior of an interface under the forgoing procedures and assumptions may work satisfactorily for translation up to the relative slip, but there appears no physical basis for adopting arbitrary values for the normal and shear stiffness, when relative slip and debonding (loss of contact) occur. Because of this, very often, the above interface models involve considerable computational difficulties and the results obtained can not be always relied upon.

4.5.3 Constraint-Interface Model

Katona (1981) has developed a contact-friction interface model based on the virtual work principle modified by a special constraint condition (Fig. 4.9). This element can provide improved conditions at the interface as affected by the state of stress induced during various modes (see Chapter 6 for various modes of an interface), and can be considered to be an improvement over the other previous models.

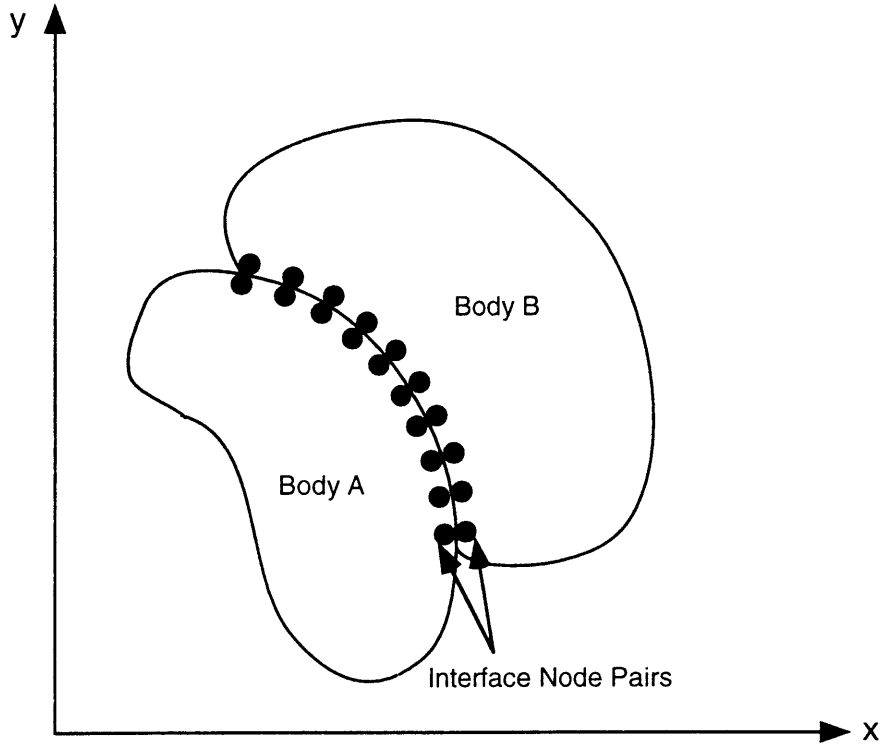

Fig. 4.9 Constraint-interface model (Katona, 1981)

4.5.4 Thin-layer Interface Model

Desai et al (1984) proposed the idea of using a thin solid element at the interface, called a *thin-layer element*, in soil-structure interaction and rock joints. The basic assumption made is that the behavior near the interface involves a finite thin zone (Fig. 4.10) rather than a zero thickness as assumed in previous models described so far. According to this new concept, since the interface is surrounded by the structural and geological materials, its normal properties during the deformation process must depend upon the characteristics of the thin interface zone as well as the state of stress and properties of the surrounding elements. Based on these considerations, it was proposed to express the normal stiffness as:

$$[K_n]_i = \left[K_n(\alpha_m^i, \beta_m^g, \gamma_m^{st})\right] \tag{4.13}$$

where $\alpha_m^i, \beta_m^g, \gamma_m^{st} (m = 1,2,....)$ denote the properties of the interface, geological and structural elements, respectively. The above equation can be written as

$$\left[\overline{K}_n\right]_i = \lambda_1\left[K_n\right]_i + \lambda_2\left[K_n^g\right] + \lambda_3\left[K_n^{st}\right] \tag{4.14}$$

where $\left[\overline{K}_n\right]_i$ denotes normal behavior of the thin interface element and λ_1, λ_2 and λ_3 are the participation factors varying from 0 to 1. One of the simplifications would be to assume $\lambda_2 = \lambda_3 = 0$ and $\lambda_1 = 1$, implying that the normal component is based on the normal behavior of the thin layer element evaluated just as the adjacent soil element.

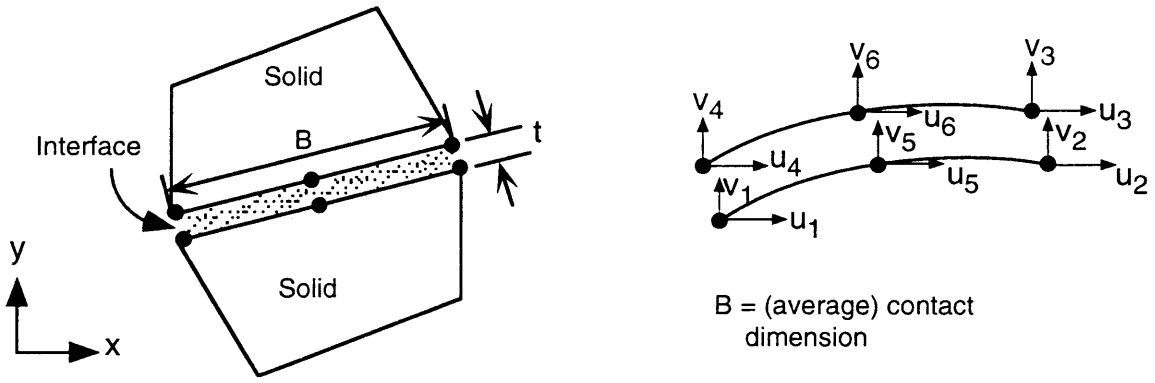

Fig. 4.10 Thin-layer interface element (Desai et al, 1984)

The shear component $\left[K_s\right]_i$ is assumed to be composed of a shear modulus G_i for the interface. The expression used for tangent G_i (Fig 4.11) is given by:

$$G_i(\sigma_n, \tau, u_r) = \frac{\partial[\tau(\sigma_r, u_r)]}{\partial u_r} \times t|\sigma_n \tag{4.15}$$

The quality of simulation of the interface behavior will depend upon a number of factors such as physical and geometrical properties of the surrounding media, non-linear material behavior and the thickness of the thin layer element. If the thickness is too large in comparison with the dimension B, of the surrounding element (Fig. 4.10), the thin layer element will behave essentially as a solid element. If it is too small, computational difficulties may arise. The choice of thickness can, therefore, be an important question and can be resolved by performing parametric studies in which the predictions from various thicknesses are compared with observations. The choice of thickness can become particularly important for dynamic analyses where the mass and damping properties need to be considered. The

developed model was applied to a retaining wall problem. An algorithm for checking the interpenetration of the nodes was also given by the authors.

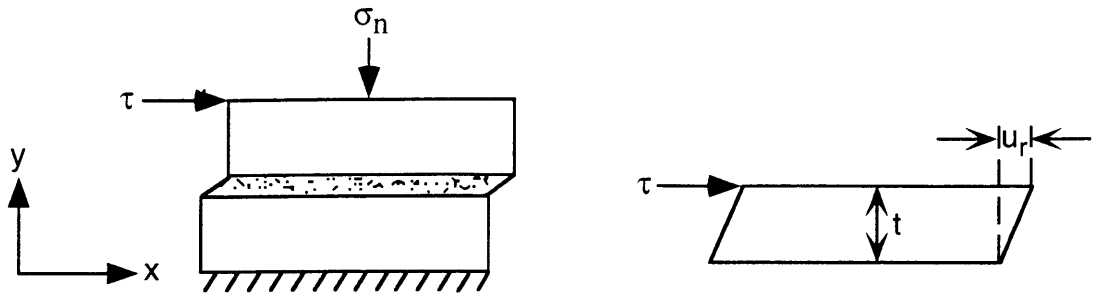

(a) Schematic of direct shear test (b) Deformations at the interface

Fig. 4.11 Behavior at interface

4.6 DEVELOPMENT OF A NEW INTERFACE MODEL

The interface has been modeled until now under two broad assumptions: one assuming to have certain thickness and the other assuming zero thickness. For the application of to soil-structure interaction problems, the thickness of the element is often assumed to be zero. The joint element proposed by Goodman et al (1968) was particularly developed for rock joints. This type of element was used by Clough and Duncan (1971), Bhatia and Bakeer (1989) for the retaining wall problems. Nakai (1985) developed an elasto-plastic joint element based on Goodman type element that can take care of the stick or no slip as well as the slip at the interface between a retaining wall and the backfill soil. However, no explanations were given regarding the assumptions and the physical significance of the different parameters appeared in the material property matrix of the joint element.

4.6.1 Idealization of the Interface

One of the drawbacks of the Goodman type element is the problem of crossing (interpenetration) under compressive load and separation or debonding under tensile loading. In most of the interface models, a high value is assigned for the normal stiffness based on the assumption that the structural and the geological media do not overlap or separate. There is no logical basis for adoption of such values. The *Thin Layer Element* developed by Desai et al (1984) usually does not exhibit the problems of separation or crossing. If the problem occurs, it can be gotten rid of by separating the elements by an arbitrary fraction of the thickness. However, extra calculation time due to iteration is required for this purpose. Added to that, the model itself involves complexity due to the presence of various

parameters, for which parametric studies need to be done. The real challenge is to construct mechanistic models that behave something like the real world; while at the same time striking a balance between rigorous mechanics and engineering simplicity. Thus, what we need is a simplified model with fewest parameters and at the same time a reasonable one to simulate the interface. In the earth pressure analysis, the need for the joint elements with thickness is not of practical significance. From the physical point of view, to simulate the frictional behavior at the interface between the wall and the soil, joints with zero thickness are more appropriate.

An idealized interface model shown in Fig. 4.12 is developed for the soil-structure interaction problems such as the retaining wall-backfill system interaction. The model is based on the concept of linkage element of Ngo and Scordelis (1967) as discussed before. The element has a shear spring in the tangential direction and a slider to represent Coulomb friction.

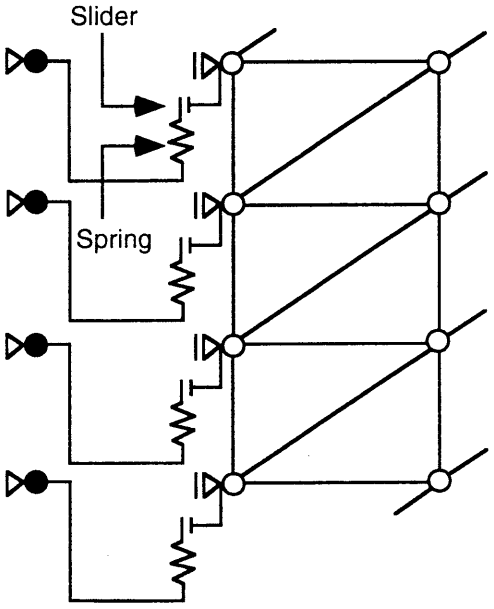

Fig. 4.12 Idealization of the interface

4.6.2 Element Connection

The elements are assumed to have an effective length l with thickness zero (Fig. 4.13a). The elements are introduced connecting the corner nodes of the soil elements and the wall as shown in Fig. 4.13a. The interface is taken to be one producing no velocity discontinuity (Tatsuoka, 1985). In view of the fact that, the friction between the wall and the backfill represents Coulomb's friction between two material surfaces without any dilatancy, interface of non-dilatant type is assumed.

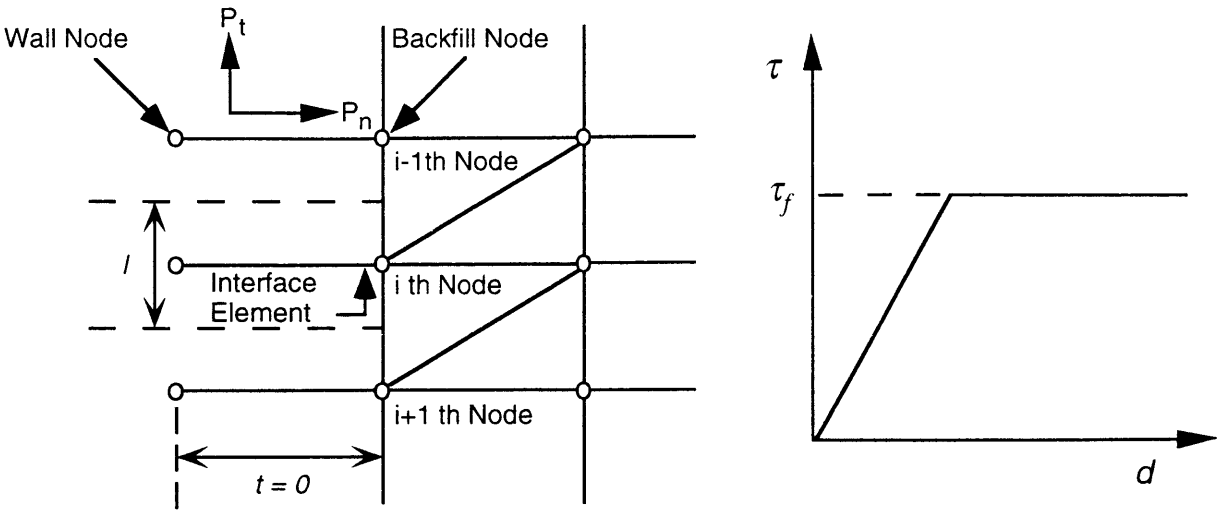

(a) Element's connection (b) Stress-displacement relation

Fig. 4.13 Interface element with zero thickness

4.6.3 Constitutive Relation and Computational Technique

Roscoe's experiment (1970) demonstrated that the interface friction varies with the depth along the interface. However, extensive research to explain this variation is still lacking. In the absence of experimental studies to establish this variation firmly as well as for the sake of simplicity, the same value of friction can be assumed to be maintained by all the interface elements at all depths. The strength characteristics of the interface for the cohesionless backfill can be expressed in terms of the maximum value of the angle of wall friction, δ_f, as

$$\tau_f = -\sigma_n \tan\delta_f \tag{4.16}$$

where τ_f is the shear strength in an element and σ_n is the normal stress acting on that element. The stress-displacement relationship for the interface elements is assumed to be bilinear with elastic-perfectly plastic as shown in Fig. 4.13b. The mobilized value of the friction coefficient, $\tan\delta$ at each incremental displacement can be calculated by $\tan\delta = P_t / P_n$. The tangential force P_t is calculated using the shear stiffness K_v, the effective length l and the relative displacement (v_r) of the interface element in the tangential direction. The normal force P_n is given by the equivalent nodal force for the soil element associated with that interface element.

In the earth pressure analysis, usage of the conventional interface elements leads to opening up of the gap between the wall and the soil elements, when the wall is in active mode. In the passive mode of the wall, the problem of interpenetration of the elements arises. In the developed model, in order to avoid the separation, equal forced displacements

are given to both the wall nodes as well as to the soil element nodes thus keeping the relative displacement in the normal direction between the wall and the backfill always zero. This technique restricts the backfill mass to sliding movement alone along the wall, at the same time keeping its contact with the wall and thus alleviating the necessity of assuming arbitrary values for the normal stiffness of the interface element. The only parameter needed is the shear stiffness, which can easily be obtained from the results of the direct shear test.

4.6.4 Determination of Model Parameters

The shear stiffness of an interface is usually determined by performing direct shear tests, where the geologic material (e.g. soil) and the material of the structure are used in the shear box. However, this type of conventional test does not truly represent the actual stiffness or friction between the two materials, as the deformation characteristics or the dilatancy of the soil affects the ultimate results. In order to minimize the effect of the soil deformation or dilatancy, the tests need to be performed with the minimum possible thickness of the soil sample in the lower box, something which is quite difficult to conduct. Another alternative is to conduct the direct shear tests with various thicknesses and then extrapolate the results to a lower thickness.

However, in the present research the shear stiffness value of the interface between the dry Toyoura sand and the wall is determined to be 22×10^4 kN/m^2 from the test results of the conventional direct shear test by making bilinear assumption as shown in Fig. 4.14.

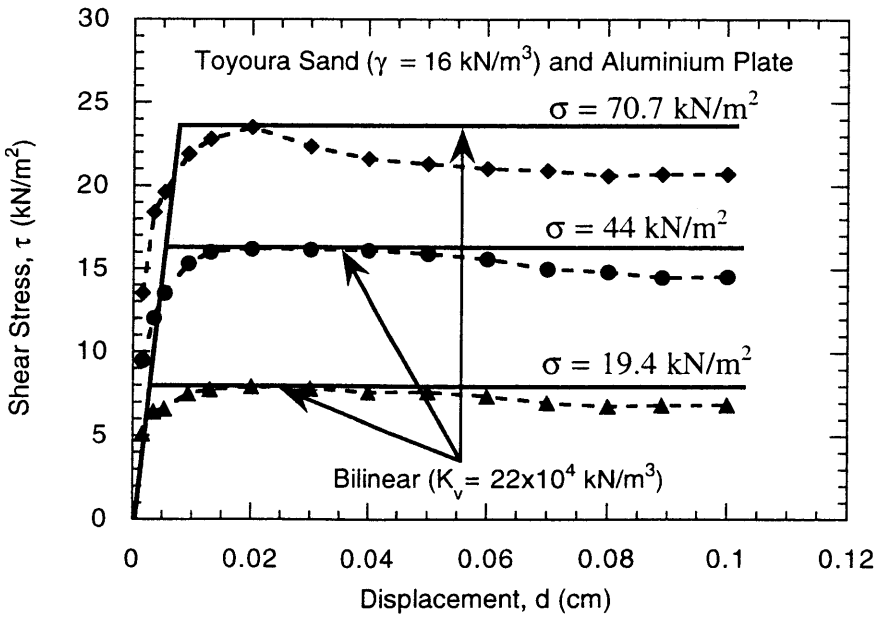

Fig. 4.14 Determination of shear stiffness value for the interface

4.7 CLOSING REMARKS

In this chapter the interface models developed for various applications have been reviewed. The review indicates the need for improved and rational models to account for the interaction effect.

Goodman et al's joint element is widely used in earth pressure calculation. However, this type of element exhibits the problem of separation and/or crossing of two adjacent elements.

Most of the other interface models assume a high value of normal stiffness arbritarily in order to prevent separation or crossing, which has no logical basis. The thin-layer element developed by Desai et al (1984) advocated the need to determine the normal stiffness making it a function of the other interface characteristics. This involves added complexity in an already complex phenomenon of the interface interaction.

The inclusion of relative deformation, such as slip, is essential to simulate the real behavior at the interface. A new interface model is presented, based on the concept of linkage element of Ngo and Scordelis (1967), which can take care of the problem of separation during the active movement of a retaining wall. Slip along the interface can be allowed without opening up of a gap or interpenetration of the wall and the backfill elements. The parameters of the model can be determined from the conventional direct test. The application of this simple interface model can be found in chapter 5 and chapter 6.

REFERENCES

[1] Bhatia, S.K. and Bakeer, R.M. (1989), "Use of the Finite Element Method in Modelling a Static Earth Pressure Problem", *International Journal for Numerical and Analytical Methods in Geomechanics*, Vol. 13, pp. 207-213.

[2] Clough, G.W. and Duncan, J.M. (1971), "Finite Element Analyses of Retaining Wall Behavior", *Journal of Soil Mechanics and Foundation Engineering, ASCE*, Vol. 97, SM 12, pp. 1657-1673.

[3] Desai, C.S. (1981), "Behavior of Interfaces Between Structural and Geologic Media", *Proceedings of the International Conference on Recent Advances of Geotechnical Earthquake Engineering and Soil Dynamics*, St. Louis, Missouri, USA, pp. 619-638.

[4] Desai, C.S. (1977), "Soil-Structure Interaction and Simulation Problems", In *Finite Elements in Geomechanics*, Ed. G. Gudehus, John Wiley and Sons, London, UK.

[5] Desai, C.S., Zaman, M.M., Lightner, J.G. and Siriwardane, H.J. (1984), "Thin-layer Element for Interfaces and Joints", *International Journal of Numerical and Analytical Methods in Geomechanics*, Vol. 8, pp. 19-43.

[6] Ghaboussi, J., Wilson, E.L. and Isenberg, J. (1973), "Finite Element for Rock Joints and Interfaces", *Journal of Soil Mechanics and Foundation Engineering, ASCE*, Vol. 99, SM 10, pp. 833-847.

[7] Goodman, R.E., Taylor, R.L. and Brekke, T.L. (1968), "A Model for the Mechanism of Jointed Rock", *Journal of Soil Mechanics and Foundation Engineering, ASCE*, Vol. 94, SM 3, pp. 637-659.

[8] Herrmann, L.R. (1978), "Finite Element Analysis of Contact Problems", *Journal of Engineering Mechanics, ASCE*, Vol. 104, EM 5, pp. 1043-1057.

[9] Katona, M.G. (1981), "A Simple Contact-Friction Interface Element with Applications to Buried Culverts", *Proceedings of the Implementation of Computer Procedures and Stress-Strain Laws in Geotechnical Engineering*, Chicago, Illinois, pp. 45-63.

[10] Matsuzawa, H. and Hazarika, H. (1995), "Analyses of Active Earth Pressure Against Rigid Retaining Wall Subjected to Different Modes of Movement", *Soils and Foundations, Japanese Geotechnical Society* (Accepted).

[11] Nakai, T. (1985), "Analysis of Earth Pressure Problems Considering the Influence of Wall Friction and the Wall Deflection", *Proceedings of the Fifth International Conference on Numerical and Analytical Methods in Geomechanics*, Nagoya, Japan, pp. 765-772.

[12] Ngo, D. and Scordelis, A.C. (1967), "Finite Element Analysis of Reinforced Concrete Beams", *ACI Journal*, Vol. 64, 3, pp. 152-163.

[13] Roscoe, K.H. (1970), "The Influence of Strains in Soil Mechanics", *Geotechnique*, Vol. 20, 2, pp. 129-170.

[14] Tatsuoka, F. (1985), "On the Angle of Interface Friction for Cohesionless Soil", *Soils and Foundations, JSSMFE*, Vol. 25, 4, pp. 135-141.

[15] Whitman, R.V. and Bielak, J. (1980), "Foundations", In *Design of Earthquake Resistant Structures*, Ed. E. Rosenbleuth, John Wiley and Sons, New York, USA.

[16] Zaman, M.M., Desai C.S. and Drumm, E.C. (1984), "Interface Model for Dynamic Soil-Structure Interaction", *Journal of Geotechnical Engineering, ASCE*, Vol. 110, GT 9, pp. 1257-1273.

[17] Zienkiewicz, O.C., Best, B., Dullage, C. and Stagg, K. (1970), "Analysis of Nonlinear Problems with Particular Reference to Jointed Rock Systems", *Proceedings of the Second Congress of International of Society of Rock Mechanics*, Belgrade, Yugoslavia, pp. 501-509.

CHAPTER
FIVE

Analyses of Static Earth Pressure

Everything takes half as long again,
costs 30 percent more, and can
be improved by 10 percent

Anon

5.1 INTRODUCTION

Most numerical analysis tools for retaining structures are of recent origin; however, the early work of many researchers in the field of Geotechnical Engineering provided the basic information, which is useful in modern analytical tools. The methods of Coulomb and Rankine were the forerunners of the limit approach, which is the basis of several modern analysis techniques. Limit analysis has been used with success to predict collapse loads for earth retaining structures, but it can not predict deformations associated with the limit loads and can not yield information before the limiting state.

Newer numerical methods are oriented toward predicting not only the earth pressures but also the deformations of the backfill mass and retaining structures. This is in recognition of the fact that in many retaining structure problems it is more important to form a reasonable prediction of the deformations that occur in the soil behind the structure than of the earth pressure alone acting on the structures.

Numerical tools, such as the finite element method (FEM), are still not associated by many practicing Geotechnical Engineers with prohibitive time and/or cost effort, in spite of their frequent applications in the area of Geotechnical Engineering. In the past, the increasing complexity of computer codes involved with numerical methods also tended to discourage many ventures beyond conventional analyses involving closed form analytical solutions or simplified limit equilibrium methods. However, in the last two decades, economic finite element computer codes have been developed, and tested so thoroughly that utilizing them even on a limited budget have become feasible.

The advantage of the FEM in the analysis of earth retaining structures lies in its ability to predict both the earth pressures and the deformations with a minimum of simplifying

assumptions. In this chapter, the numerical model comprising of the constitutive relation described in Chapter 3 and the interface model developed in Chapter 4 is applied to analyze the active earth pressure acting against a model retaining wall undergoing various modes of displacement. As of the present, the application is restricted to a model wall, since the idea is to develop a fundamental method through simulation of the model test to examine the efficiency of the model.

5.2 MODEL SIMULATION

5.2.1 Finite Element Discretization and Boundary Conditions

University of Washington's shaking table and retaining wall assembly (Fang and Ishibashi, 1986) is simulated in the analyses. The FE discretization of the experimental model under plane strain condition using constant strain triangular (CST) elements is shown in Fig. 5.1. The wall can undergo three kinds of movement (RB, RT and T) as shown in Fig. 5.2.

As for the boundary conditions, as a general rule the nodes along the lateral boundaries were allowed to have movements only in the vertical direction, while the nodes along the bottom boundaries were restrained against both the horizontal and the vertical movements, with the only exception in the case of the RT mode where the boundary condition changes.

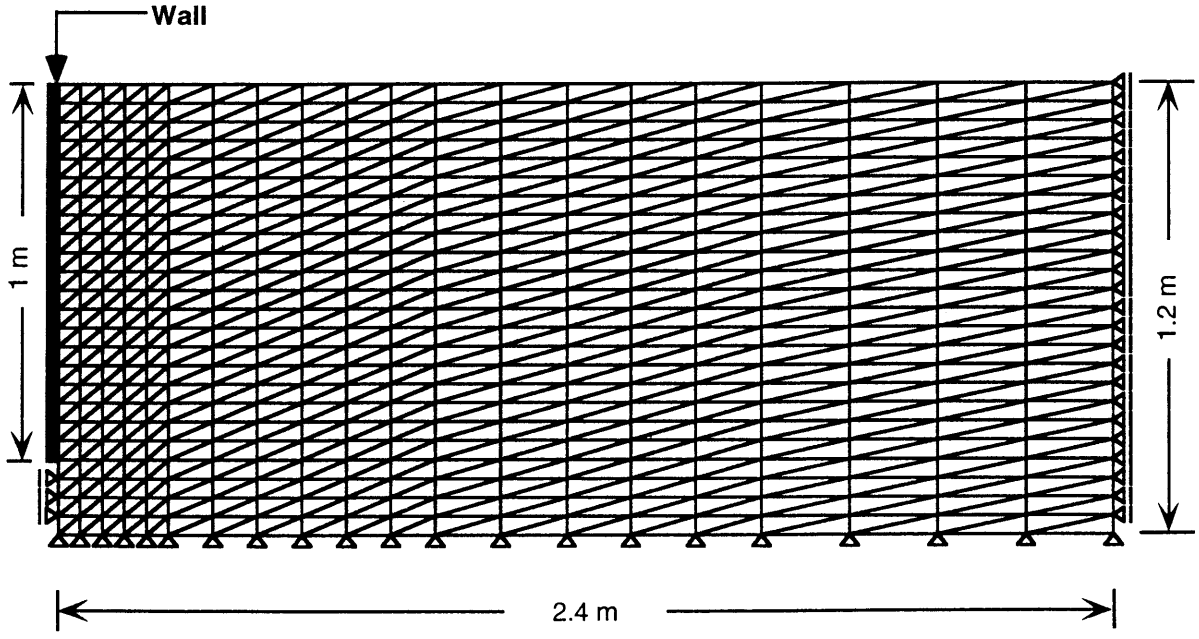

Fig. 5.1 Finite element discretization of the experimental model

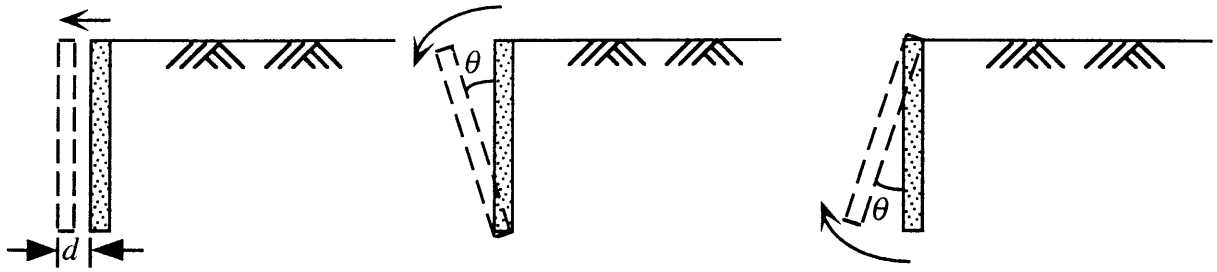

Fig. 5.2 Wall displacement modes considered in the analyses

5.2.2 Interface Model

In the analysis of a rough retaining wall, modeling the interface between the backfill and the wall is an integral part of the analysis. In this analysis, a newly developed interface model reported in Chapter 4 is used to simulate the wall friction. The interface elements are introduced in the boundary between the wall and the backfill. In laboratory condition, friction forces exist between the backfill and the lateral as well as the bottom sides of the soil bin. Hence to simulate the experimental condition it is appropriate to introduce interface elements in these boundaries too. However, to make the model versatile to the real situation this logical view has been ignored in the analyses.

The interface friction is assumed to be the same irrespective of the depth along the interface. The maximum value of the wall friction angle, δ_f, is assumed to be 29° for the T mode and 25° for the RB and the RT mode.

5.2.3 Constitutive Models and Material Parameters

Analyses are completed using two constitutive models, one using the conventional method and the other using the C.S.B. Method, both of which are discussed in Chapter 3.

Same values of the angle of internal friction, ϕ reported in the experimental condition are used in the analyses. The values of κ_f depend on the particular ϕ; and therefore, the friction angle at constant volume, ϕ_{cv}, also differs. The value of R is determined by making parametric studies for the Ottawa sand, which forms the backfill mass. Although, it is advisable to find the value of thickness, d of the shear band from the compression test, in this study a numerical technique is adopted to determine the value. Fig. 5.3 shows the FE mesh used for the calculation. Table 5.1 shows the values of material parameters used in the calculation. In order to simplify the calculation, a smooth wall was considered, a wall that does not need the interface element. The wall was moved in passive translation. The thrust against it was calculated for different values of ζ. It is assumed that the correct value of ζ is the one , for which the peak value of thrust on the wall approximately coincides with the

Rankine value. For $\varsigma = 0.4 \times 10^{-4}$ the peak value of the thrust coincided with the Rankine value, and it was used in the analyses.

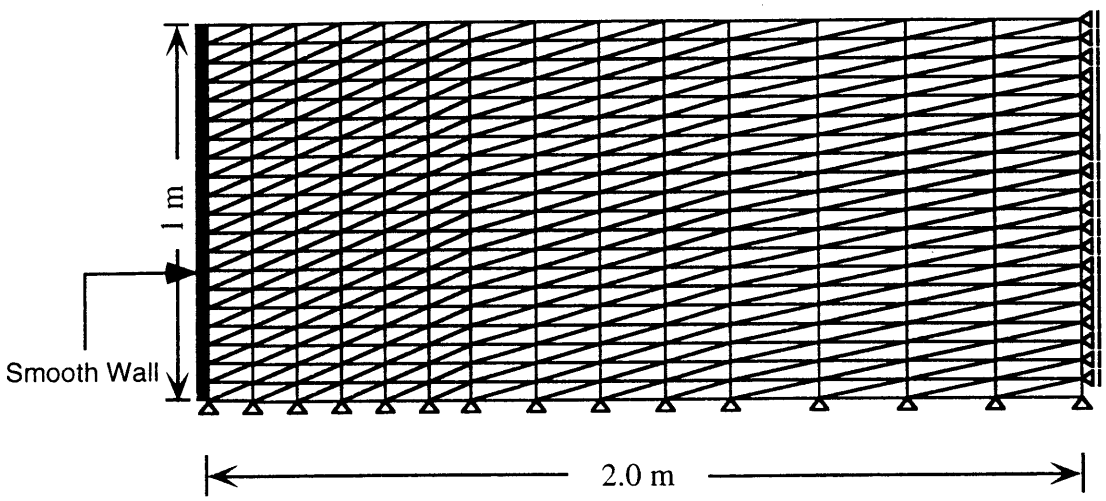

Fig. 5.3 FEM mesh used for determination of the smearing parameter, ζ

Table 5.1 Material parameters of the backfill used for determination of ζ

Parameters	Values
Elastic Parameters	
Young's Modulus, E (kN/m^2)	21000
Poisson's Ratio, ν	0.3
Deformation Parameters	
Angle of Internal Friction, ϕ	40^o
A	0.0037
R	0.05
κ_f	0.642
Dilatancy Parameters	
κ_c	0.491
η_s	0.563

The Material parameters of the backfill used in the remaining analyses are shown in Table 5.2. The coefficient of earth pressure at rest (K_0) is assumed to be 0.6, a value closer to that of the experiments. Hydrostatic distribution is assumed for the initial stress in the backfill. The value of the shear stiffness for the interface element is taken as 22×10^4 kN/m^2. This assumption is a conservative one in view of the fact that the interface stiffness has been

obtained based on the test results of Toyoura sand, whereas the backfill mass in the experimental model simulated is Ottawa sand. However, due to the absence of experimental results, the same value of stiffness is used in the analyses. The material parameters for the backfill have been calculated based on the experimental results of Ottawa sand reported by Ko and Scott (1967, 1968).

Table 5.2 Material parameters of the backfill used in the analysis

Parameters	Values
Elastic Parameters	
Young's Modulus, E (kN/m^2)	21000
Poisson's Ratio, ν	0.3
Deformation Parameters	
Angle of Internal Friction, ϕ	Varies
A	0.0037
R	0.05
κ_f	Varies depending on ϕ
Dilatancy Parameters	
κ_c	Varies depending on ϕ
η_s	Varies depending on ϕ
Smearing Parameter	
ζ	0.4×10^{-4}

5.2.4 Computational Procedure

Analyses are performed in an incremental-cum-iterative scheme using modified Newton-Raphson method. In the static earth pressure analysis, the conventional interface elements suffer from the fact that during the active mode the wall and the backfill separate away, leaving a gap between the wall and the backfill elements, which introduces numerical anomaly. In order to avoid this, equal forced displacements are given to both the wall nodes as well as to the soil element nodes, thus keeping the relative displacement in the normal direction between the wall and the backfill always zero. As mentioned earlier, this technique alleviates the necessity of assuming arbitrary values for the normal stiffness of the interface element. During the analyses, whenever the shear strength in any interface element exceeds its maximum value, it is brought down to that value by reducing the shear stiffness of the interface element in an iterative scheme until convergence is achieved.

5.3 NUMERICAL RESULTS AND DISCUSSION

The results obtained from the *Coupled Shear Band Method* (C.S.B. Method) based numerical analyses, are presented in this section. Comparisons have been made with the experimental results, Coulomb's theory, Dubrova's method and with the numerical results obtained from the conventional strain hardening theory using the Drucker-Prager model discussed in Chapter 3.

5.3.1 Effect of the Wall Displacement on the Earth Pressure Parameters

The three important parameters actively associated with the earth pressure calculations are, (1) the coefficient of the earth pressure, K, (2) the wall friction coefficient, $\tan\delta$, and (3) the relative height of the point of application, h/H, H being the height of the wall. Figs. 5.4-5.6 show the variations of the three parameters with increasing mean wall displacements, for the three modes of the wall displacement (Fig. 5.2) considered, where the mean wall displacement, s, refers to the displacement at the mid-height (H/2) of the wall.

It can be observed that the magnitude and the nature of variations of the parameters depend on the wall movement modes. The different stress conditions that prevail in the backfill resulting from the differences in the boundary conditions for each mode can be attributed for these kinds of behaviors. The numerical results using the C.S.B. Method are showing a better simulation capability as compared to the conventional analysis.

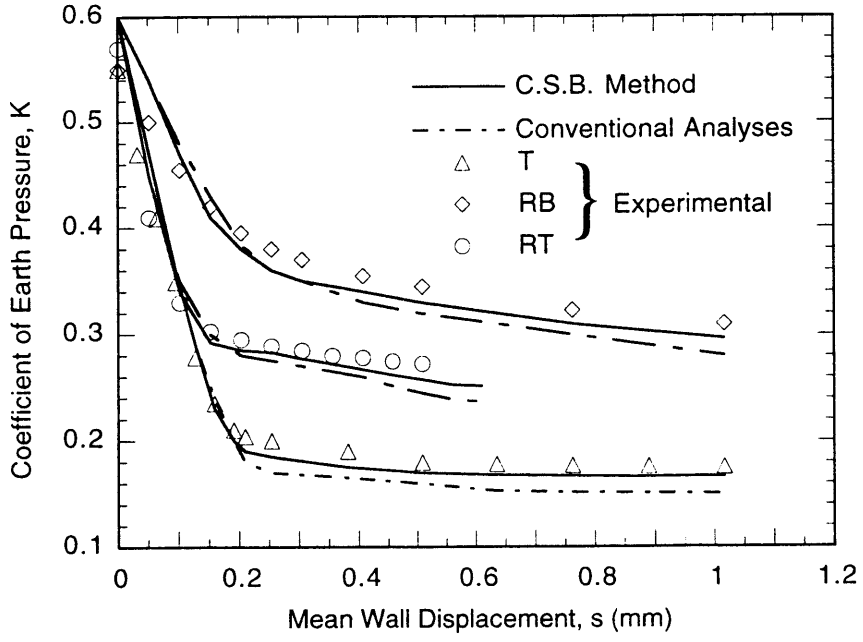

Fig. 5.4 Variation of the coefficient of earth pressure with wall displacement

Fig. 5.4 shows that the experimental tendencies are displayed by the variations of K. The noticeable variation of K among the three modes, is the RB mode, in which the decreasing trend is continued even at larger displacements of the wall. This is due to the fact that the complete active state is difficult to attain, although not impossible, in this particular mode of movement because of the existence of the extra high stress at the base of the wall, as will be evident in the distribution of the active earth pressure discussed in the next subsection.

The variation of the magnitude of the relative height, h/H (Fig. 5.5), is a striking feature as it differs from Coulomb's value of 0.333. Another noticeable point is the dependency of the variation of h/H on the wall movement modes. In the case of the T and the RT mode, the values of h/H increase gradually from the initial value of 0.333 to some particular value, and remain almost constant after certain displacement. The final value is greater than that of the Coulomb value. In the case of the RB mode, the value initially decreases, and then starts to increase to attain the constant value, however, the final value remains less than Coulomb's value. These differences are due to the different patterns of the earth pressure distribution discussed in a subsequent section. It is to be noted that, due to the assumption of hydrostatic distribution for the initial stress, the point of application remains at 1/3 of the wall height for the non yielding wall in each mode of displacement.

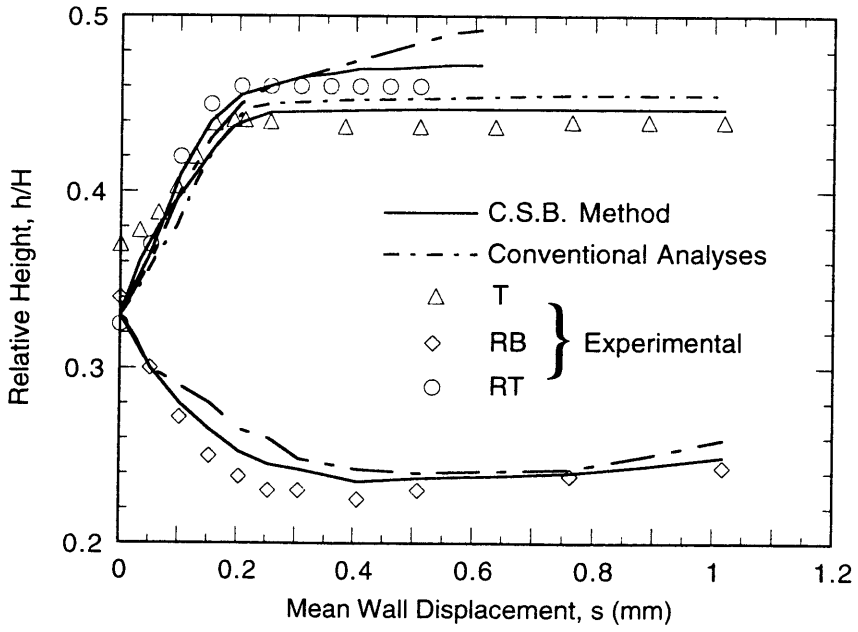

Fig. 5.5 Variation of the point of application of earth pressure with wall displacement

The variation of tanδ (Fig. 5.6) is also found to be dependent on the wall movement modes. The general tendency is to increase gradually with wall displacement, and then attain the peak value. In contrast to the experiments, the numerical results show a drop in the value after attaining the peak value. This may be due to the assumption of equal values of shear

stiffness for all the interface elements irrespective of depths. A slight deviation of the numerical results from those of the experiments has been observed. The disagreement can be attributed to the assumption of the values of shear stiffness for the interface.

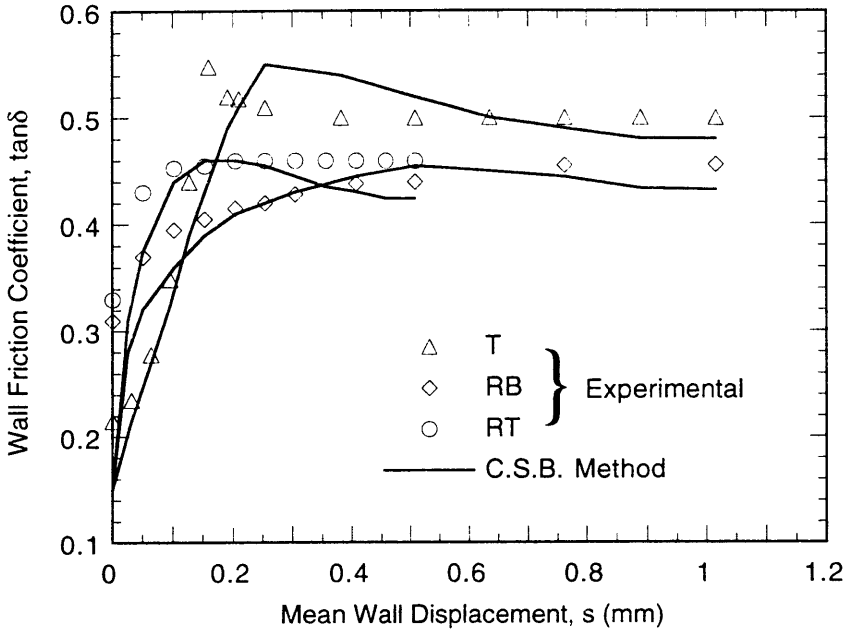

Fig. 5.6 Variation of the coefficient of wall friction with wall displacement

5.3.2 Progressive Failure Pattern and the Active Stress Distribution

Figs. 5.7(a)-5.7(c) show the progression of the failure zone at different stages of wall displacements for each mode of movement. The failure zone of the backfill sand unfolds some remarkable points regarding the active state and the distribution of earth pressure. In the case of the T mode (Fig. 5.7a), the failure develops simultaneously from the top as well as from the bottom, and ultimately joins to reach the final state. In the RB mode of movement (Fig. 5.7b) the failure starts from the top and advances towards the bottom, while in the RT mode (Fig. 5.7c) it initiates at the bottom, and starts moving towards the top of the backfill. The progressive failure eventually culminates in forming the active wedge. It is this pattern of the failure zone progressions, which determines the shape of the distribution curve for the active earth pressure behind the wall discussed in the following paragraph. One can also observe from the failure zones that the RB and the RT modes resemble the Rankine state forming a clear active wedge, while the T mode does not seem to resemble the Rankine state where the failed elements are concentrating in a banded zone.

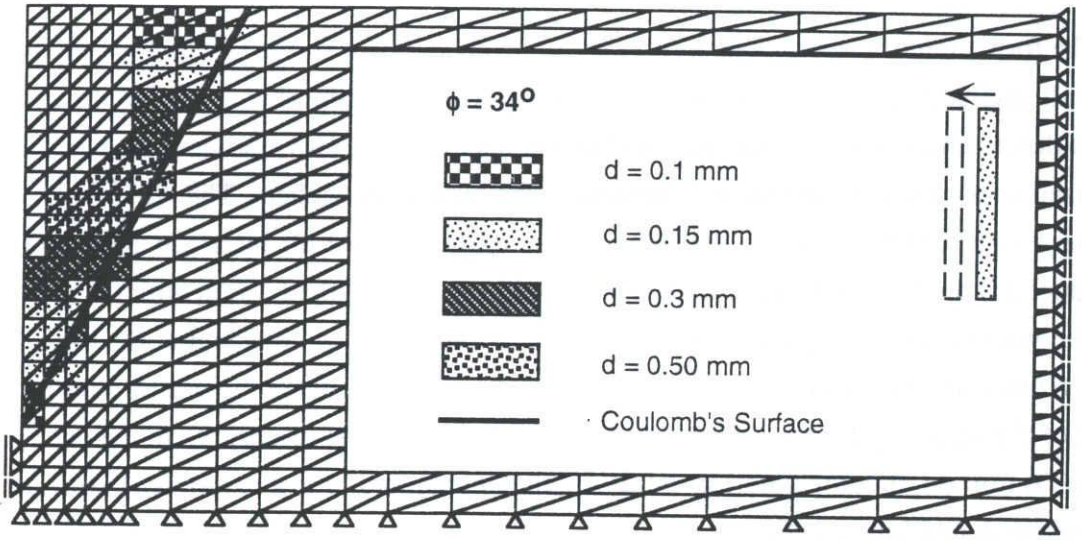

(a) T Mode

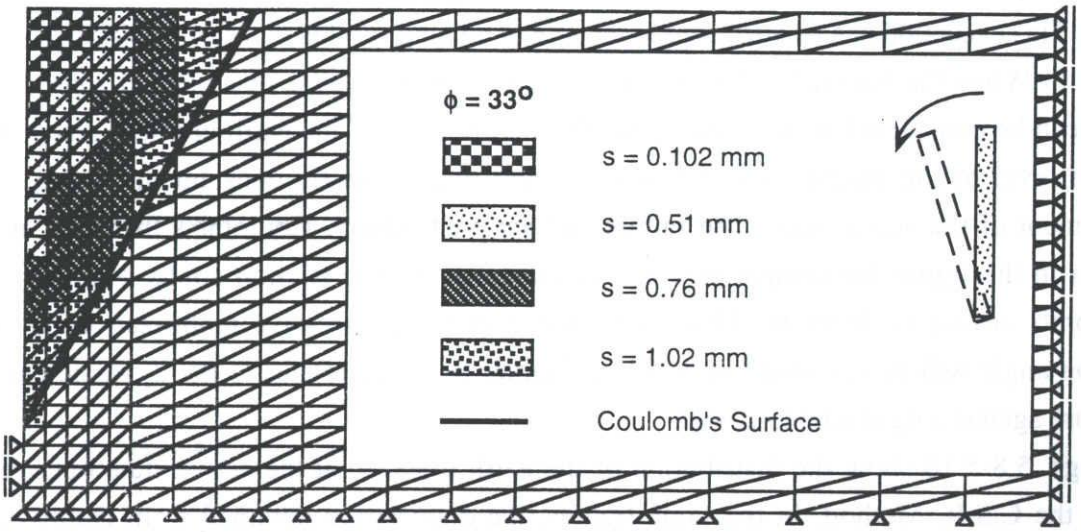

(b) RB Mode

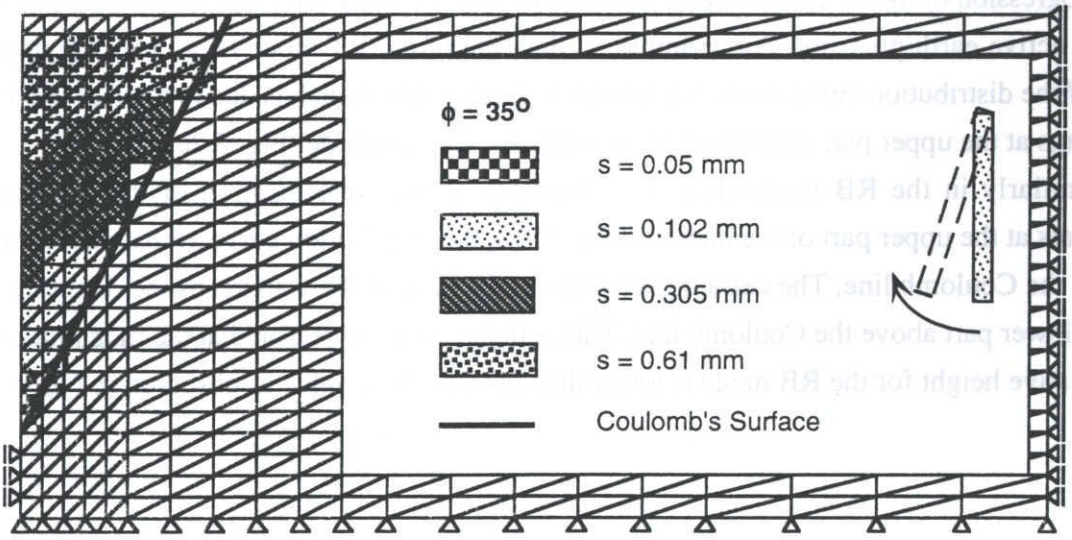

(c) RT Mode

Fig. 5.7 Progressive failure patterns of the backfill for each mode of movement of the wall

The formation of banded zone in the case of T mode, is due to the fact that, in this mode the wall displacement, the active wedge suddenly loses its support along the wall surface, slides down, and forms a weak arch within the backfill soil. Development of a narrower localized zone can be expected, as compared to the results shown here. The wider band may be the results of the effect of the boundary condition, since no interface elements are introduced at the bottom boundaries of the backfill to simulate the friction with the soil bin, and the wall is moved in parallel giving extra freedom to the soil element at the base. The discretization of the FEM mesh will not have a strong effect, since the use of appropriate value of the smearing factor ζ is expected to render the analysis insensitive to the details of discretization in the localization analysis that considers the *geometrical softening* (Pietruszczak and Mroz, 1981).

In the case of the RT mode, it can also be observed that the elements at the top never failed. This exception can be attributed to the role of arching for this mode of displacement of the wall. When the backfill soil forms either a clear failure wedge or a banded zone, that stage can be considered to be active state. The coefficients of the earth pressure reach the lowest level of the magnitudes at this stage, and remain nearly constant, implying the attainment of the active state. The failure surface predicted by Coulomb's theory is also shown in the figure for comparison. The mobilization of the friction angle, ϕ along the Coulomb surface is different. This phenomenon of the progressive mobilization of the friction angle will be discussed in detail in Chapter 6, which relates to the dynamic earth pressure against a rigid retaining wall.

Figs. 5.8-5.10 show the distribution of the earth pressure at the active state obtained using the C.S.B. Method. In the same figures, the distribution obtained from Dubrova's method and Coulomb's theory are also plotted for the purpose of comparisons. The effect of the progression of the failure zones for different modes is clearly reflected in the distributions of the active earth pressure. For example, in the case of the RT mode (Fig. 5.8), the upper part of the distribution curve never reached the Coulomb line, which is due to the fact that the elements at the upper part of the backfill never failed for this mode (Fig. 5.7c).

Similarly in the RB mode (Fig. 5.9), because of the concentration of the localized elements at the upper part of the backfill (Fig. 5.7b), the distribution curve at that part comes below the Coulomb line. The extra higher stress at the base of the wall keeps the distribution at the lower part above the Coulomb line. This is the exactly the reason that the magnitude of the relative height for the RB mode is lower than the Coulomb value as observed in Fig. 5.5.

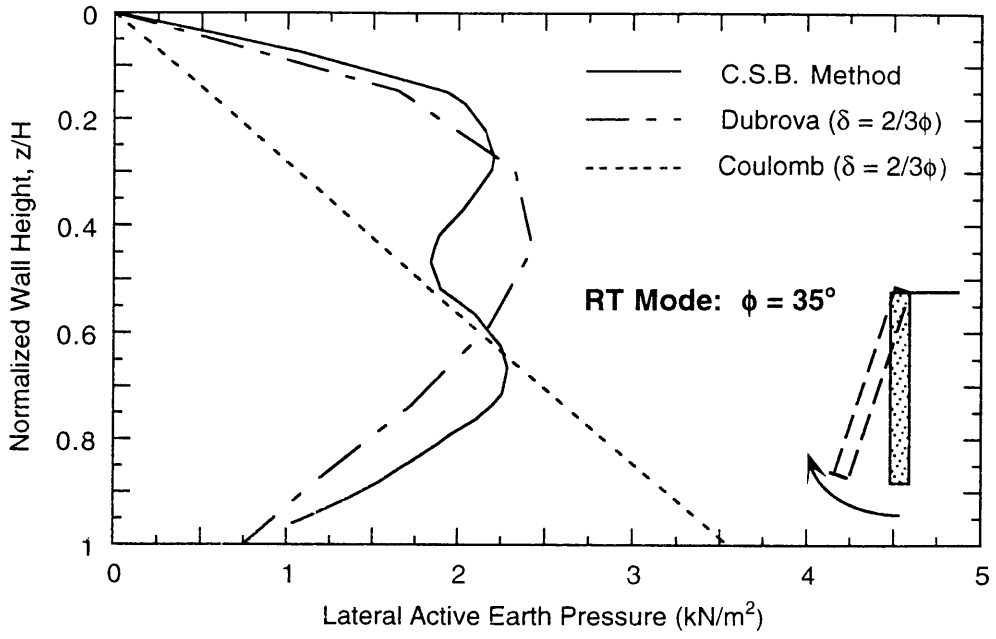

Fig. 5.8 Active stress distribution for the RT mode

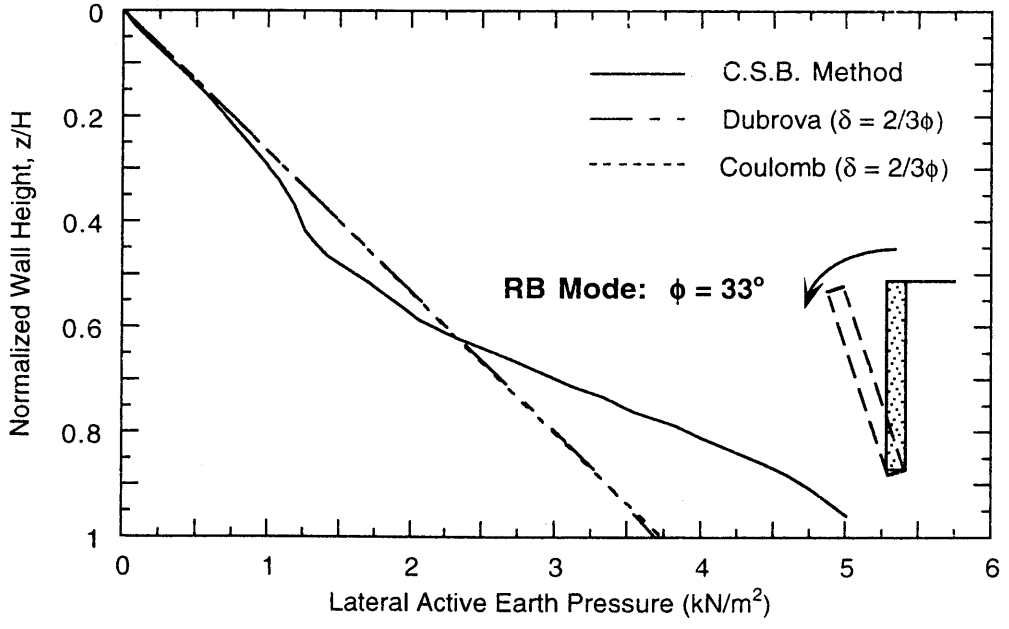

Fig. 5.9 Active stress distribution for the RB mode

In the T mode (Fig. 5.10), the absence of the failed element at the upper part in the vicinity of the wall (Fig. 5.7a) is keeping the distribution curve away from the Coulomb line. From these figures it is seen that the distribution pattern of the active earth pressure depends on the modes of wall displacement due to different mechanisms of the failure. Consequently,

the coefficient of the resultant active thrust and the point of application differ in magnitudes, the discussions of which are made later.

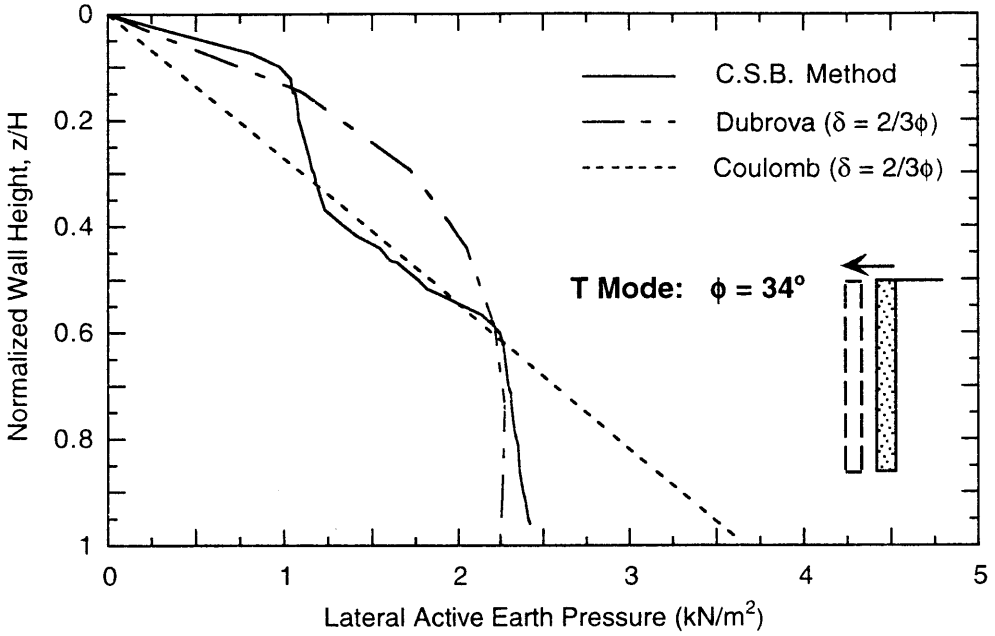

Fig. 5.10 Active stress distribution for the T mode

5.3.3 Effect of the Backfill Strength on the Active Stress Distribution

In order to examine the effect of the soil strength on the distribution pattern of earth pressure, the variation of the active lateral earth pressure behind the wall is plotted as shown in Fig. 5.11 for two particular modes, namely T and RT, for different strengths (angle of internal friction) of the backfill.

It can be observed from Fig. 5.11a that for the translational movement the density of the soil does not effect the pattern of distribution. However, the effect of density is pronounced in the case of the RT mode (Fig. 5.11b). The arching effect at the upper portion of the backfill is known to be responsible for this. The dense backfill is more vulnerable to arching compared to the less dense one. As a result, the dense backfill shows existence of higher stress at the upper part.

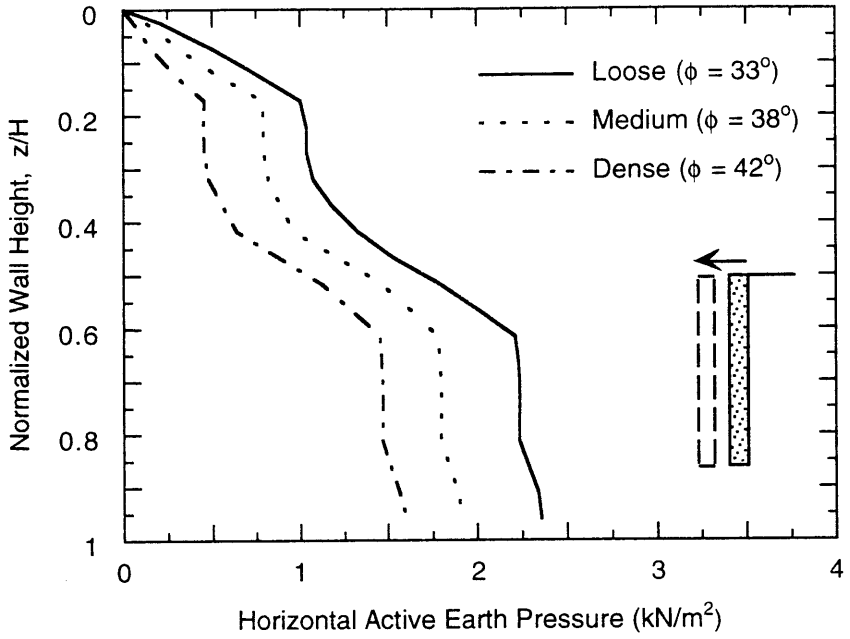

(a) Translational (T) mode

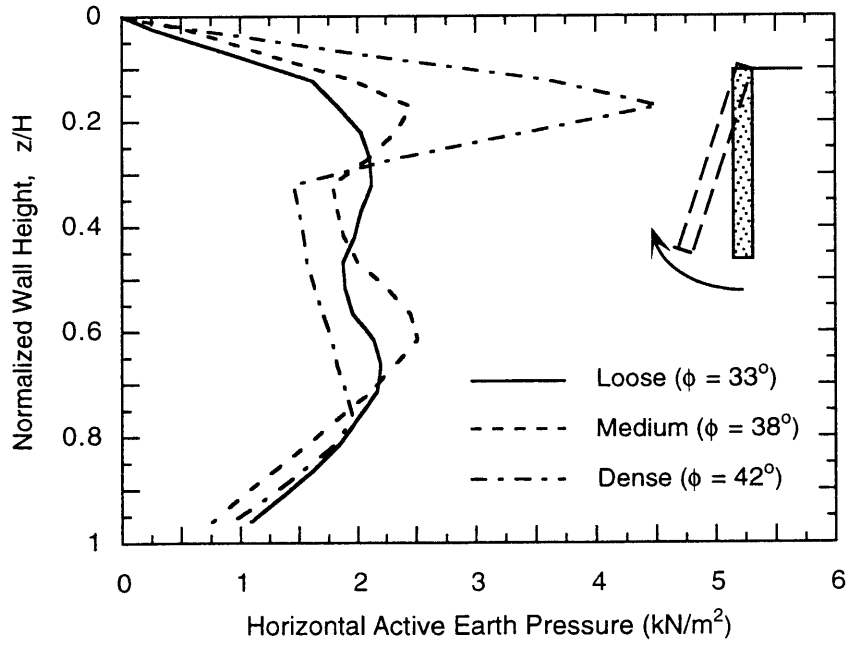

(b) Rotation about the top (RT) mode

Fig. 5.11 Effect of the backfill strength on the distribution of active earth pressure

5.3.4 Coefficient of the Active Stress and Its Point of Application

The computations were performed for various values of the internal friction, ϕ of the backfill sand. The coefficient of the horizontal active thrust, K_A, has been plotted as a function of ϕ for the different modes as shown in Figs. 5.12-5.14. It can be seen that the results from the C.S.B. Method are more close to the experimental values as compared to the results from the conventional method.

In the T mode, the results show a close agreement with the values given by Coulomb's equation as seen in Fig. 5.12. However, in the RB mode (Fig. 5.13) and the RT mode (Fig. 5.14) the values are higher than the Coulomb value, which implies that the total active thrust depends on the wall displacement modes. A remarkable observation from the three figures is that the values given by Dubrova's analytical solution coincide with the Coulomb values, and remain unaltered for all the modes. This is due to the fact that Dubrova assumed the validity of the Coulomb solution (Coulomb's theory considers only the equilibrium condition and the failure mechanism, but not the failure state along the boundary, giving only an *upper bound solution*).

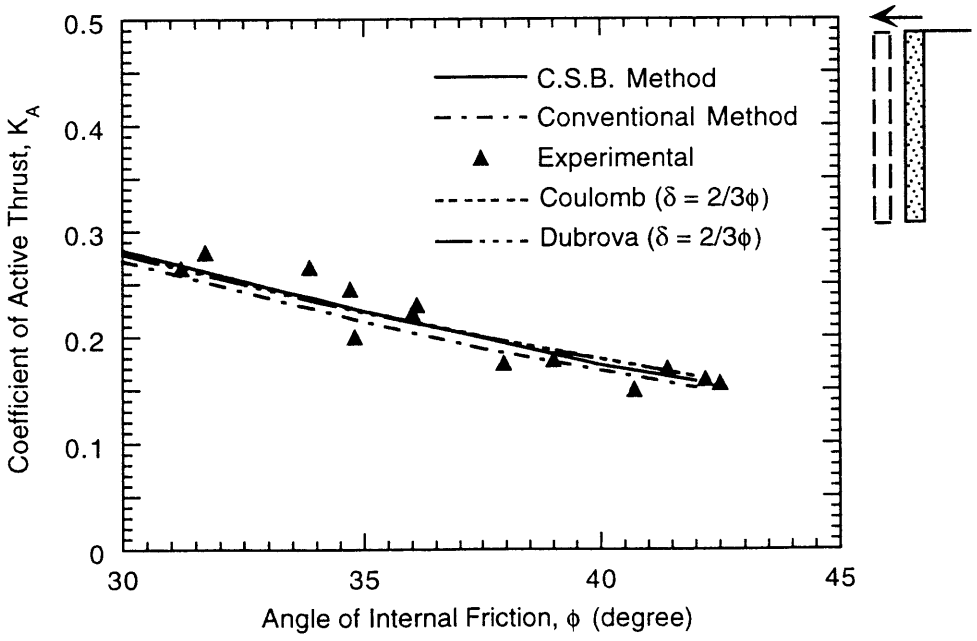

Fig. 5.12 Coefficient of active thrust at various angles of internal friction (T mode)

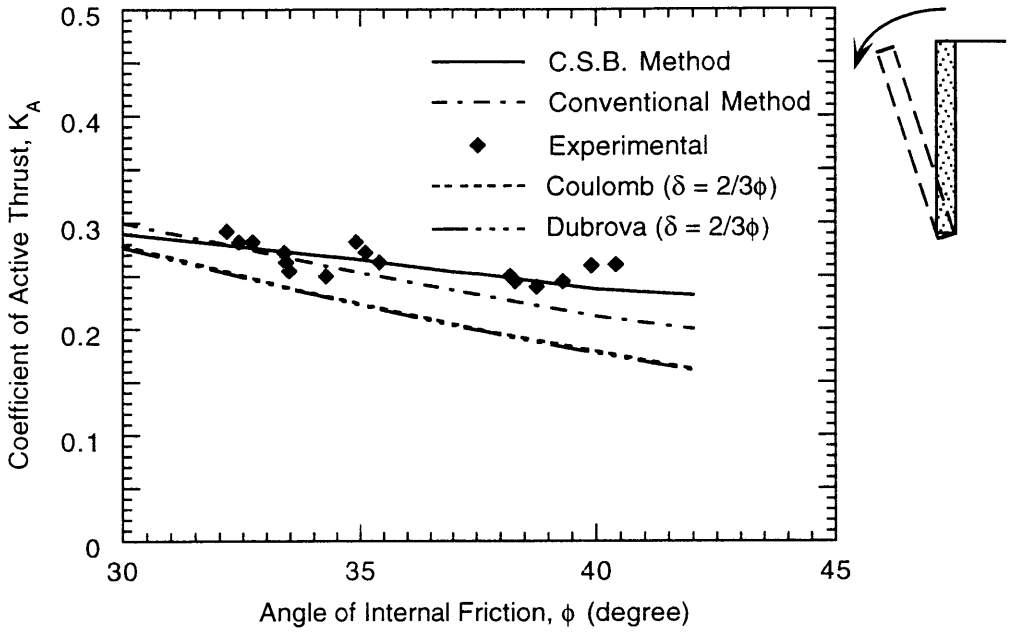

Fig. 5.13 Coefficient of active thrust at various angles of internal friction (RB mode)

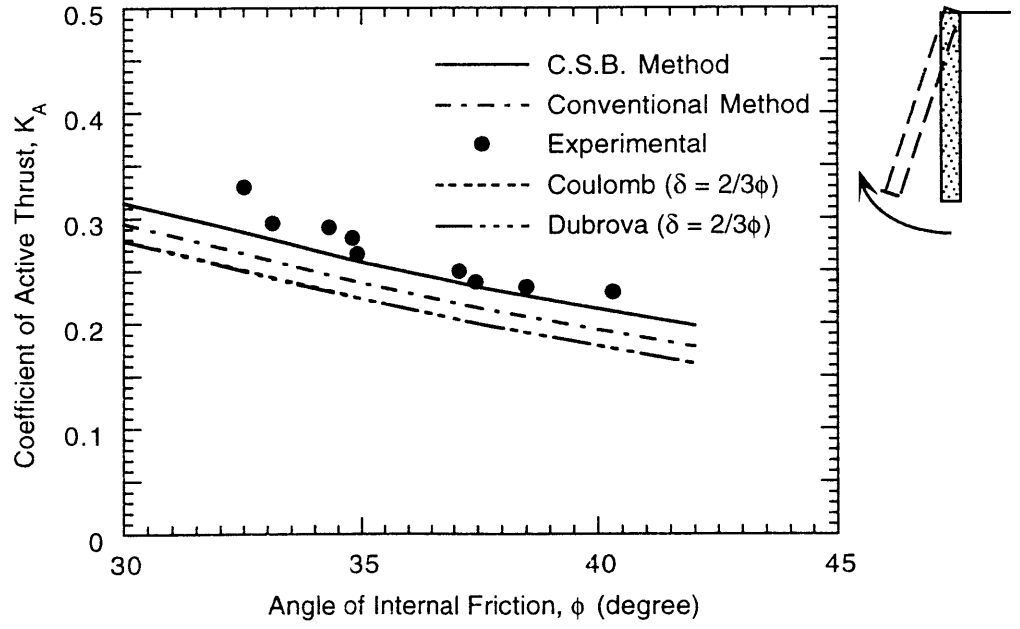

Fig. 5.14 Coefficient of active thrust at various angles of internal friction (RT mode)

Figs. 5.15-5.17 show the variation of the relative height of the point of application of the horizontal active thrust, $(h / H)_A$, for the various modes as a function of the backfill strength. It can be seen that other than the RB mode, both the numerical results and Dubrova's solution agree with the experimental trend. Difference in the case of RB mode is due to proximity of Dubrova's distribution to Coulomb's hydrostatic distribution. Both the magnitude and variation of $(h / H)_A$ differ depending on the wall movement modes. For the same value of ϕ, the RT mode gives the highest value for $(h / H)_A$ and the RB mode gives the lowest value, while the values given by the T mode lying intermediate. With increasing values of ϕ, the $(h / H)_A$ of the RB mode follows a decreasing trend, while those of others are showing an increasing trend with only exception that the RT mode has a steeper gradient.

The exception of the RT mode is due to the effect of arching. The dense backfill exhibits higher arching stress than that of the loose or medium dense backfill. As a result, for dense sand, the upper part of the active distribution curve moves further away from the Coulomb line, while the lower part shows significant reduction of the stress due to free movement of the sand elements near the base of the wall (see Fig. 5.11b). This mechanism of the stress redistribution contributes to the upward movement of the relative height with steep slope.

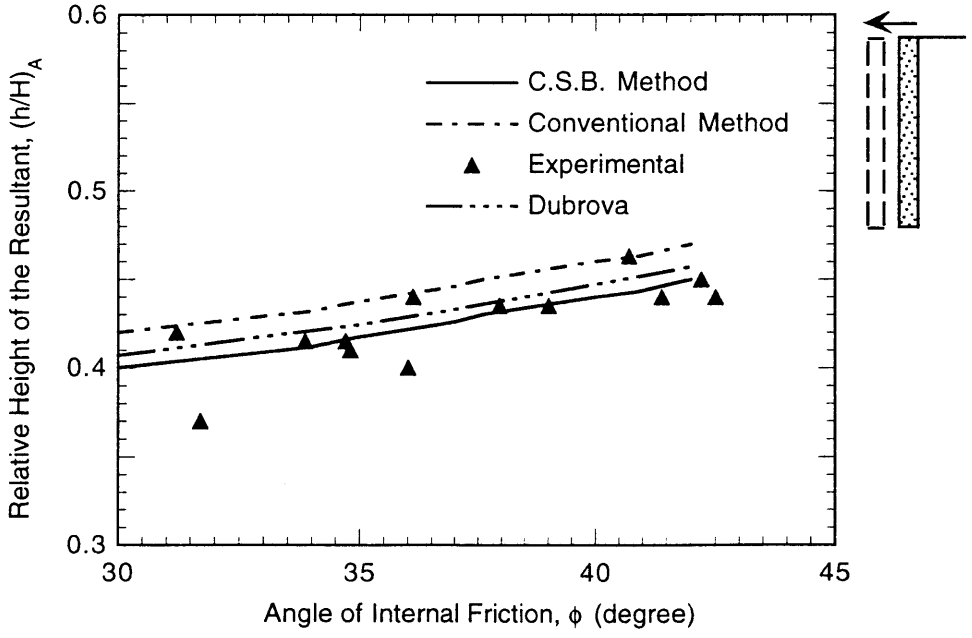

Fig 5.15 Variation of the relative height with angle of internal friction (T Mode)

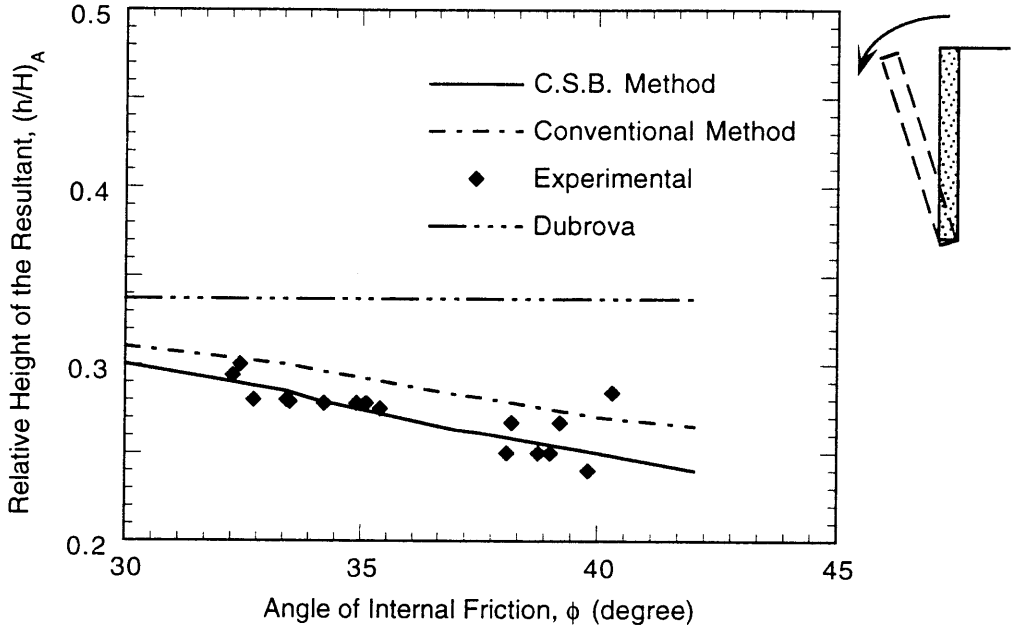

Fig 5.16 Variation of the relative height with angle of internal friction (RB mode)

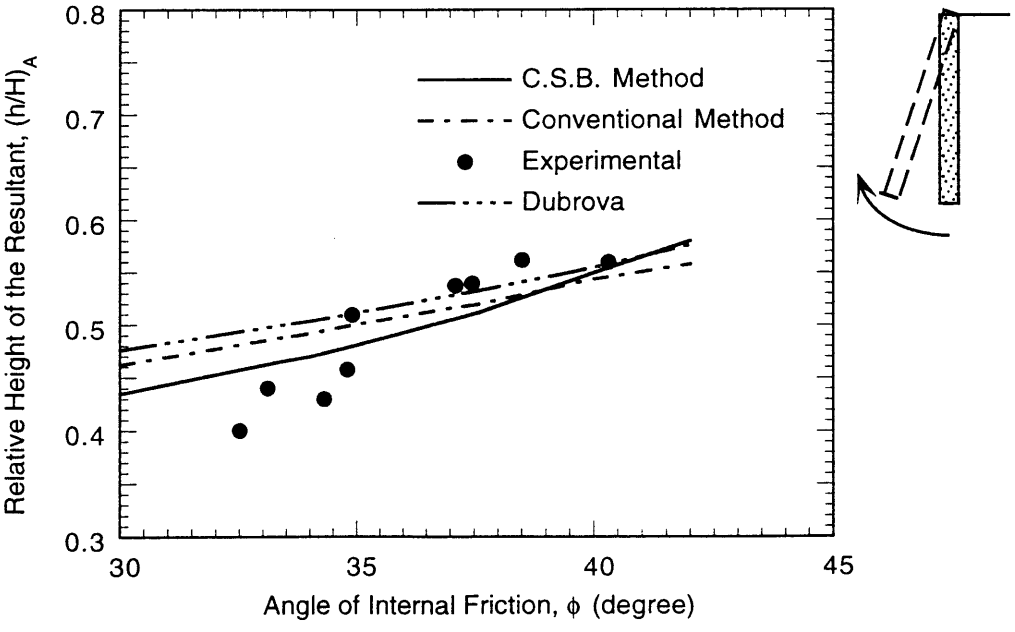

Fig. 5.17 Variation of the relative height with angle of internal friction (RT Mode)

5.3.5 Influence of the Modes of Wall Displacement

Regression analysis of the results obtained from C.S.B. Method renders the following two equations for K_A and $(h/H)_A$ expressing their wall movement modes dependent character for various values of the backfill strength, ϕ.

$$K_A = -0.20 + (\phi - 176.3)M_C - 9667M_C^2 \tag{5.1}$$

$$(h/H)_A = 0.36 + (\phi - 20)M_P - 396M_P^2 \tag{5.2}$$

where, M_C and M_P are the parameters which take different values depending on the wall displacement modes as shown in Table 5.3

Table 5.3 Values of the parameters M_C and M_P for each mode

Modes of Wall Movement	Values of M_C and M_P	
	M_C	M_P
T Mode	-0.0104	0.0043
RB Mode	-0.005	-0.0051
RT Mode	-0.01	0.0123

A comparison is made for the values of the coefficient of the active thrust and the corresponding relative height at $\phi = 40^\circ$, for each wall displacement mode as shown in Table 5.4. It can be seen that in the case of the RB mode a significant difference exists between the numerical values and Dubrova's values. The Table also shows that even though Dubrova's method gives different values of the relative height for wall displacement modes the total active thrusts are independent of the modes. Thus, direct application of Dubrova's method for the retaining wall problems may lead to conservative design.

Table 5.4 Comparative values of the active state parameters

Modes	K_A				$(h/H)_A$			
	C.S.B. Method	Conven. Method	Coulomb	Dubrova	C.S.B Method	Conven. Method	Coulomb	Dubrova
T	0.158	0.168	0.179	0.178	0.440	0.460	0.333	0.447
RB	0.238	0.212	0.179	0.177	0.250	0.270	0.333	0.333
RT	0.214	0.194	0.179	0.179	0.550	0.544	0.333	o.555

5.4 DESIGN PHILOSOPHY

Most of the retaining walls are typically designed based on the active earth pressure distribution. Matsuo et al (1978), based on the field tests of a 10 m high wall, emphasized the importance of the at-rest pressure in designing a retaining wall. Two types of backfill material were used in the investigations: silty sand and slags from industrial production. After the completion of the backfill, the retaining wall was kept in the at-rest state for about two months, and then the wall was rotated about the base (RB Mode). After the wall reaches the active state, this state was held for twenty days, and the change of earth pressure was investigated during this period. It was observed that the earth pressure gradually recovered with time, although the wall was left as it was. The experimental results reported are shown in Fig. 5.18.

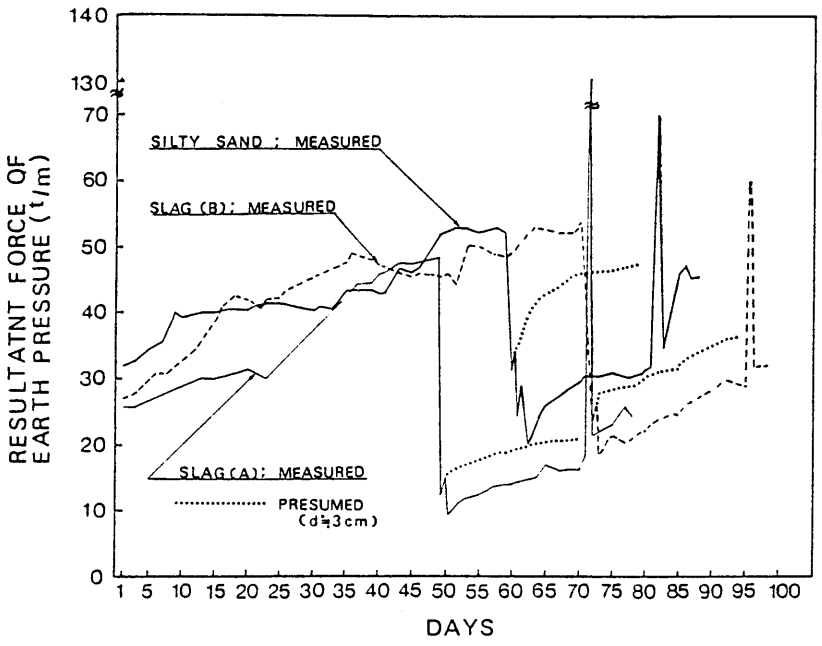

Fig. 5.18 Change of resultant force of earth pressure (*After* Matsuo et al, 1978)

It can be observed from Fig. 5.18 that, from the completion of the backfill to the start of displacement of the wall, there is a gradual increase of earth pressure. This is due to the gradual compaction of the backfill due to its own weight and the influence of the vehicles running around it. The notable point of the figure is that there is a gradual recovery of the earth pressure with time after the wall reaches the active state. By observing the total horizontal earth pressure on the wall, the coefficient of the earth pressure at-rest (K_0) was reported as 0.35~0.45 for the silty sand, 0.30~0.40 for slag A and 0.45~0.55 for slag B. Ichihara and Matsuzawa (1970) based on the laboratory model tests with a backfill of clean sand reported the K_0 value to be 0.4~0.8. The field tests by Matsuo et al (1978) also

indicated that the shape of the distribution of the at-rest pressure is nonlinear, and the shape is not so different from that of the active state.

The recovery of the earth pressure after the active state may be due to the effect of rainfall, which generates seepage flow in the backfill. However, in the analysis of this research, a simplifying assumption of the hydrostatic distribution of the earth pressure at-rest was made. Since dry sand was used as the backfill, and the simulated model was a laboratory model, the assumption made was a justifying one.

The fundamental philosophy of the present design of retaining wall is that it can support the active earth pressure. Expressing this with the mathematical terms, we get:

$$P_d = P_a \times F_s \tag{5.3}$$

where, F_s is the factor of safety, P_d is the design earth pressure and P_a is the active earth pressure. However, in practice, a retaining wall is not intended to serve a short period. With time, as observed in Fig. 5.18, the wall comes to at-rest state again. Hence, Matsuo et al's recommendation can be expressed in the following form:

$$P_d = P_r \times \tilde{F}_s \tag{5.4}$$

where, P_r is the earth pressure at-rest and $\tilde{F}_s$ is the corresponding factor of safety. Observing Eqs. (5.3) and (5.4), it can be said that, for the same design pressure P_d, $\tilde{F}_s$ in Eq. (5.4) can be made almost equal to 1.0, however, in Eq. (5.3) F_s will remain as high as 2.0~3.0. Hence, as a design philosophy the recommendation by Matsuo et al is a justifying concept. However, in order to make such a design possible the characteristics of the at-rest pressure need to be studied in detail, and with the present state of research in this field nothing concrete can be said about it.

On the other hand, the value of K_0 to be used is still a controversial topic. Jaky's equation $(1 - \mathrm{Sin}\phi')$ is valid only for the normally consolidated soil with horizontal ground surface. It is not valid for the over consolidated soil and compacted sand. It also depends on the nature of the backfill and retaining wall. For an infinite horizontal backfill with vertical wall face, the value of K_0 is found to be 0.5 using Mohr's diagram. However, for inclined backfill and inclined retaining wall, the K_0 value is different. Thus, the design based on the at-rest state involves some uncertainties.

In earthquake prone zones, all retaining walls are designed against possible collapse during earthquake. In the design code of Japan, design accelerations of 150-200 gals are used. The corresponding active earth pressure for this range of acceleration will be close to the static at-rest pressure (a detailed discussion of dynamic earth pressure is made in Chapter

6). Thus, walls designed for earthquake loading condition, and walls designed on the basis of the at-rest pressure will have almost the same factor of safety.

5.5 SUMMARY AND CONCLUDING REMARKS

In this chapter a numerical method is presented for the analyses of the active earth pressure against a rigid rough retaining wall, which can adequately capture the progressive deformation of the backfill. The *Coupled Shear Band Method* based analysis is seen to have an edge over the conventional strain hardening analyses especially in regard to its power of capturing the progressive failure, although the capability of the conventional analysis in capturing the same can not be entirely ruled out.

The active state can be defined as that state when the backfill forms a clear failure wedge or a slip surface. The present study shows that the progressive failure pattern of the backfill is influenced by the modes of displacement of the wall, which in turn influences the patterns of the earth pressure distributions. Consequently, the coefficient of the active earth pressure and the point of application of the resultant active thrust depend on the modes of movement of the wall.

The strength of the backfill has a pronounced effect on the distribution of lateral earth pressure only in the case of a wall undergoing rotation about its top (RT mode), which is due to the arching effect for this mode of the wall displacement.

Dubrova's analytical solutions are able to express the different nonlinear distributions of the active stress for various modes. However, the resultant active thrusts given by that method coincide with Coulomb's solution (i.e. irrespective of the wall displacement modes).

Empirical equations expressing the coefficient of active earth pressure and the point of application of the resultant active thrust as functions of wall displacement modes, have been put forward for various values of the backfill strength. Since the two equations are based on the small scale model test analyses, the direct application of them to the field problems may culminate in conservative design. However, the applicability of the two as a preliminary testing mechanism can not be ruled out.

Interface elements with zero thickness, as idealized in this research, can simulate the wall friction satisfactorily, when the appropriate parameters are determined suitably from the experiments. The assumption of equal values of $\tan\delta$ for all the interface elements at different depths may be a gross approximation leading to variations in the behavior of the friction coefficient in the analyses.

REFERENCES

[1] Bang, S. (1985), "Active Earth Pressure Behind Retaining Walls", *Journal of Geotechnical Engineering Division, ASCE*, Vol. 111, 3, pp. 407-412.

[2] Bathe, K.J. (1982), *Finite Element Procedures in Engineering Analysis*, Prentice Hall, Eanglewood Cliffs, New Jersey, USA.

[3] Drucker, D.C. (1950), "Some Implications of Work Hardening and Ideal Plasticity", *Quarterly of Applied Mathmatics*, Vol. 7, pp. 411-418.

[4] Fang, Y.S. and Ishibashi, I. (1986), "Static Earth Pressure with Various Wall Movements", *Journal of Geotechnical Engineering Division, ASCE*, Vol. 112, 3, pp. 317-333.

[5] Girijavallabhan, C.V. and Reese, L.C. (1968), "Finite Element Analysis for Problems in Soil Mechanics", *Journal of Soil Mechanics and Foundation Engineering, ASCE*, Vol. 94, SM 2, pp. 473-496.

[6] Harr, M.E. (1966), *Foundations of Theoretical Soil Mechanics*, McGraw-Hill Book Co., New York, U.S.A.

[7] Hazarika, H., Matsuzawa, H. and Sugimura, M. (1993), "Elasto-plastic Analysis of Static and Dynamic Active Earth Pressure Against Rigid Retaining Wall", *Proceedings of the 48th Annual Conference of Japanese Society of Civil Engineers*, Fukuoka, Japan, pp. 852-853.

[8] Hazarika, H. (1995), "Progressive Failure Analyses of a Retaining Wall-Backfill System Based on Smeared Shear Band Technique", *Proceedings of the 50th Annual Conference of Japanese Society of Civil Engineers*, Matsuyama, Japan, pp. 986-987.

[9] Hazarika, H. and Matsuzawa, H. (1995), "Wall Displacement Modes Dependent Active Earth Pressure Analyses Using Smeared Shear Band Method with Two Bands", *Computers and Geotechnics* (To appear).

[10] Ichihara, M. and Matsuzawa, H. (1973), "Application of Plane Strain Test to Earth Pressure", *Proceedings of the Eighth International Conference on Soil mechanics and Foundation Engineering*, pp. 185-190.

[11] Ichihara, M. and Matsuzawa, H. (1970), "Corelations between Properties of Earth Pressure on Tilting Wall and the Shearing Characteristics of Dry Backfill Sand", *Journal of JSCE*, Vol. 176, pp. 61-74.

[12] Ko, H.Y. and Scott, R.F. (1968), "Deformation of Sand at Failure", *Journal of Soil Mechanics and Foundation Engineering*, Vol. 94, SM 4, pp. 883-898.

[13] Ko, H.Y. and Scott, R.F. (1967), "Deformation of Sand in Shear", *Journal of Soil Mechanics and Foundation Engineering, ASCE*, Vol. 93, SM 5, pp. 283-310.

[14] Matsuo, M., Kenmochi, S. and Yagi, H. (1978), "Experimental Study on Earth Pressure of Retaining Wall by Field Tests", *Soils and Foundations, JSSMFE*, Vol. 18, 3, pp. 27-41.

[15] Matsuzawa, H. (1973), "Earth Pressure Measurement and Static and Dynamic Earth Pressure against Retaining Walls", *Doctoral Thesis (In Japanese)*, Nagoya University, School of Engineering.

[16] Matsuzawa, H., Hazarika, H. and Sugimura, M. (1995), "Wall Movement Modes Dependent Dynamic Active Earth Pressure Analyses Using Cracked Element", *Proceedings of the Third International Conference on Recent Advances in Geotechnical Earthquake Engineering and Soil Dynamics*, Missouri-Rolla, USA, pp. 331-334.

[17] Matsuzawa, H. and Hazarika, H. (1995), "Analyses of Active Earth Pressure Against Rigid Retaining Wall Subjected to Different Modes of Movement", *Soils and Foundations, Japanese Geotechnical Society* (Accepted).

[18] Pietruszczak, S. and Mroz, Z. (1981), "Finite Element Analysis of Deformation of Strain Softening Materials", *Intl. Journ. of Num. Meth. in Engg.*, Vol. 17, pp. 327-334.

[19] Reddy, J.N. (1984), *An Introduction to Finite Element Method*, McGraw-Hill Book Company, Singapore.

[20] Roscoe, K.H. (1970), "The Influence of Strains in Soil Mechanics", *Geotechnique*, Vol. 20, 2, pp. 129-170.

[21] Sherif, M.A., Ishibshi, I. and Lee, C.D. (1982), "Earth Pressure Against Rigid Retaining Walls", *Journal of Geotechnical Engineering Division, ASCE*, Vol. 108, GT 5, pp. 679-695.

[22] Sherif, M.A., Fang, Y.S. and Sherif, R.I. (1984), "K_A and K_0 Behind Rotating and Nonyielding Walls", *Journal of Geotechnical Engineering, ASCE*, Vol. 110, GT 1, pp. 41--56.

[23] Zienkiewicz, O.C. and Taylor R.L. (1989), *The Finite Element Method*, McGraw-Hill Book Company Ltd., London, UK.

CHAPTER
SIX

Seismic Analyses of Earth Pressure

If you can measure what you are
speaking about and express it in
numbers, you know something about it

Lord Kelvin

6.1 INTRODUCTION

In the earthquake prone zones, proper estimation of the seismic earth pressure against retaining structures assumes significant importance, especially in the vicinity of port facilities, where high intensity earthquakes can cause damage to the retaining structures, resulting in catastrophe to the adjoining infrastructures and consequently to human lives. The Great Hanshin Earthquake (in Japan) on 17 January, 1995, in which Kobe port was badly damaged, serves as a stark reminder to both the research and the planning community the enormity of the damage caused by a devastating earthquake, and its repercussions on social and economic front. Thus, the zones frequented by seismic activities need adequate earthquake resistant design.

Retaining walls are damaged in almost every earthquake. The predominant damage occurs in bridge abutments, quay walls, freeway structures etc. Seed and Whitman (1970) gave a brief account (Table 6.1) of the damages in retaining walls during some of the devastating earthquake. Most of these reported damages are due to the increased lateral pressures during earthquake loading, which in turn lead to sliding, overturning and tilting of the structures (Nazarian and Hadjian, 1979).

The huge damages to the retaining walls during the Great Kanto Earthquake in Japan, 1923 gave a wake up call to the research community in the field of earth pressure, leading to the well known Mononobe-Okabe theory which is extensively used till date for the seismic design of the retaining structures. However, Mononobe-Okabe's analytical method is a quasi-static one and it considers only the input acceleration of the ground. A structure under

Table 6.1 Failure and movements of retaining walls in different earthquake (Seed and Whitman, 1970)

Earthquake	Date	Magnitude	Harbor	Epicentral Distance	Damage	Approx. Movement
Kitaizu	Nov. 25, 1930	7.10	Shimizu	30 Miles	Failure of Gravity Walls	26 Feet
Shizuoka	July 11, 1935		Shimizu		Retaining Wall Collapse	16 Feet
Tonankai	Dec. 7, 1944	8.2	Shimizu Nagoya Yokkaichi	110 Miles 80 Miles 90 miles	Sliding of Retaining Wall Outward Movement of Bulkhead with Relieving Platform Outward movement of pile supported deck	- 10 to 13 feet 12 feet
Nankai	Dec. 21, 1946	8.1	Nagoya Osaka Yokkaichi Uno	 125 miles 190 miles	Outward Movement of Bulkhead with Relieving Platform Failure of retaining wall above relieving platform Outward movement of gravity wall	13 feet 14 feet 2 feet
Tokachioki	March 4, 1952	7.80	Kushiro	90 miles	Outward movement of gravity walls	18 feet
Chile	May 22, 1960	8.40	Puerto Montt	70 miles	Complete overturning of gravity walls Outward movement of anchored bulkhead	15 feet 2 to 3 feet
Niigata	June 16, 1964	7.50	Niigata	32 miles	Tilting of gravity wall Outward movement of anchored bulkhead	10 feet 1 to 7 feet

dynamic loading experiences total acceleration (u_t) which is the sum of the input acceleration (u_g) and the response (u) as shown in Fig. 6.1. Thus, earth pressure against retaining wall need to be analyzed numerically taking into account the effect of the response component.

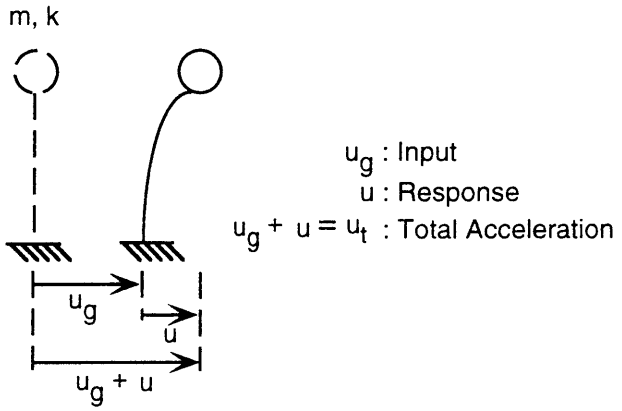

Fig. 6.1 Response of a structure under dynamic loading

The computation of the earth pressures against retaining walls during earthquakes is not so well developed as in the static case, in which case the engineer may use a lot of more or less sophisticated theories. The earth pressure on retaining walls during earthquake is a function of many important parameters such as soil-structure interaction, backfill characteristics, foundation stability, earthquake motion characteristics, structural properties of the wall and the boundary conditions (Prakash, 1981). For increasing magnitudes of the displacements, the soil stresses in the backfill can progressively advance from elastic to elasto-plastic and finally to ultimate state. In addition, non-linear soil-structure interaction is quite important and should be considered in the numerical modeling. Most of the existing numerical methods for dynamic earth pressure analysis limited their attention only to the dynamic component of the earth pressure, whereas the pressure acting on the retaining structures during seismic loading is the total pressure (static + dynamic). A proper constitutive description for the backfill is also found to be lacking in these models. In earthquake engineering design problems, failure and post-failure analysis are very important, and for this purpose consideration of the shear band localization in the backfill assumes importance.

In this chapter, a numerical model is described for the seismic analyses of earth pressure. The model is based on the *Coupled Shear Band Method* described in Chapter 3, which considers the progressive deformation characteristics of the backfill. It also takes care of the interaction between the wall and the backfill at the interface during dynamic loading. Since the soil-structure interaction during dynamic loading play a prominent role in the numerical results, the dynamic soil-structure interaction has also been reviewed here followed by its influence on the seismic earth pressure analysis. The validity of the numerical model is

demonstrated through simulation of a model retaining wall test. In addition, the dependency of the seismic earth pressure on the wall displacement modes is also studied.

6.2 INTERFACE MODEL IN DYNAMIC INTERACTION

The characteristics of the soil-structure interaction are affected not only by the mechanical properties of the constituents but also by the geometrical form and condition of the interface. Often, analysis under dynamic loading is performed by assuming complete bonding at the interface at all stages of loading. Although that assumption usually simplifies an analysis procedure significantly, it can account for the soil-structure interaction effect only to a limited extent, because the relative motions are not included in the analysis.

An interface can experience relative motions under dynamic loading (Fig. 6.2). In the actual system, debonding results at the interface especially at the higher acceleration levels for the active movement of the wall when the minimum inertia force acts away from the wall, in which case the assumption of perfect bonding induces tensile stresses on the contact surface. Thus for a realistic analysis, it may be necessary to incorporate the relative motions of the interface.

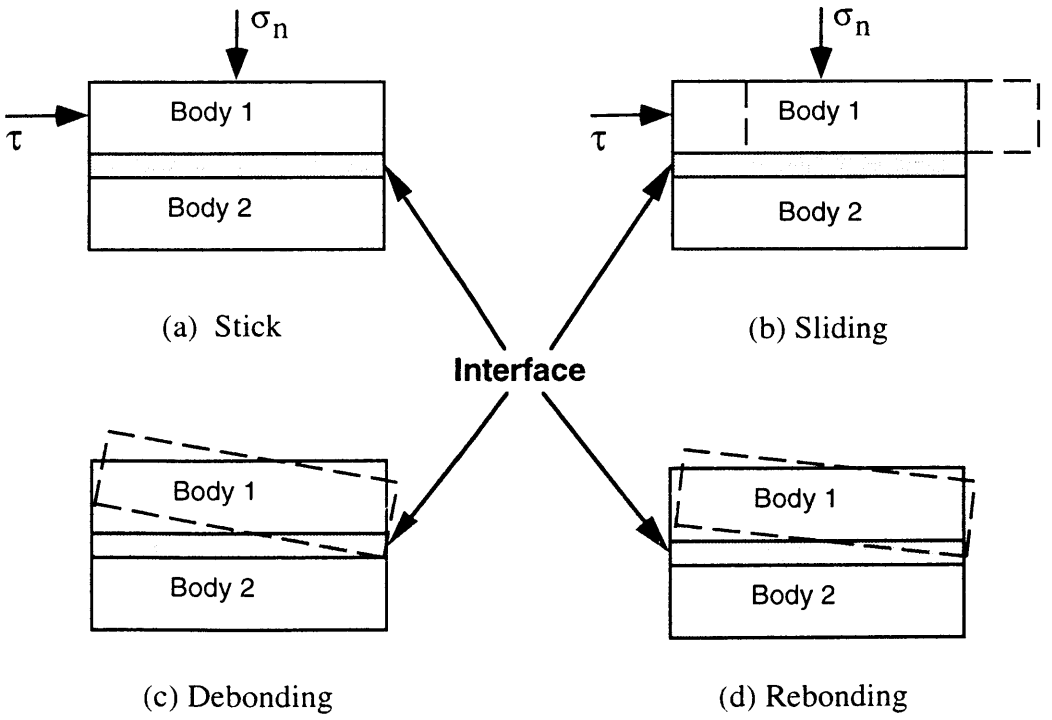

τ: Shear stress

σ_n: Normal Stress

Fig. 6.2 Modes of deformation at the interface

Toki et al (1981) developed a model for the dynamic interaction by considering the separation and the sliding between soil and structure. The joint elements used in the contact surface have a property such that tensile forces are not transmitted between the planes representing the structure and the soil. The dynamic properties governing the sliding were determined by the Mohr-Coulomb failure law determined from the cohesion and the friction angle between soil and structure. The method was applied to: (1) a model nuclear reactor building resting on the surface of a layered soil medium; and (2) a partially embedded pier foundation structure subjected to dynamic excitations. It was observed that, assuming perfect bonding at the contact surface between soil and structure, the structure's motion was restricted by the surrounding subsoil, thus underestimating the actual response of the structure.

Zaman et al (1984) used the thin layer element of Desai et al (1984) for simulation of various modes of deformation in dynamic soil-structure interaction. The numerical procedure was used to predict the behavior of a model structure tested in the field, and the influence of interface behavior on displacements, velocities and accelerations was delineated.

Desai et al (1985) described a modified Ramberg-Osgood model to simulate loading, unloading and reloading response considering the slip mode at the interface. Drumm and Desai (1986) described the cyclic stress-deformation response of dry sand-concrete interfaces using a modified Ramberg-Osgood model. The model permits the description of the interface secant stiffness as a function of the normal stress, shear stress, sand density and number of loading cycles.

A comprehensive review in this general topic is provided by Desai (1981). In recent years, the effects of the relative slip, debonding and rebonding have been identified and analyzed. Appropriate tests are needed to define the constitutive model for the interface, and there appears to be a general lack of testing devices (Desai, 1981).

6.3 A NUMERICAL MODEL FOR ANALYSIS OF SEISMIC EARTH PRESSURE

6.3.1 Constitutive Relation for the Backfill Mass

The constitutive equations, which are used frequently for soil-structure interaction problems, are generally of the visco-elastic type with hysteric damping so that no constraint is imposed on the stress level (yield). It is often recognized that in the area of earth pressure these constitutive equations are inadequate, especially if the distribution of initial earth pressure is close to the active state, and this is certainly the reason that the analyst usually resorts to a simplified theory such as Mononobe-Okabe theory.

In most of the cases of earth pressure analyses, the shear modulus and damping ratio of the backfill are adjusted according to Fig. 6.3a. Nadim and Whitman (1983) used this relationship for certain cases in their analysis. The stress-strain relationship for the backfill is

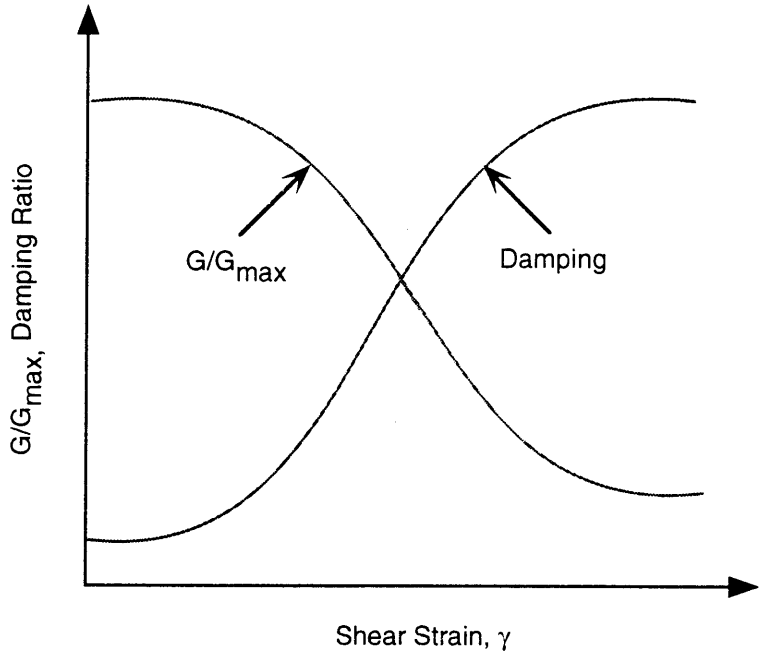

(a) Strain-dependent shear modulus and damping ratio

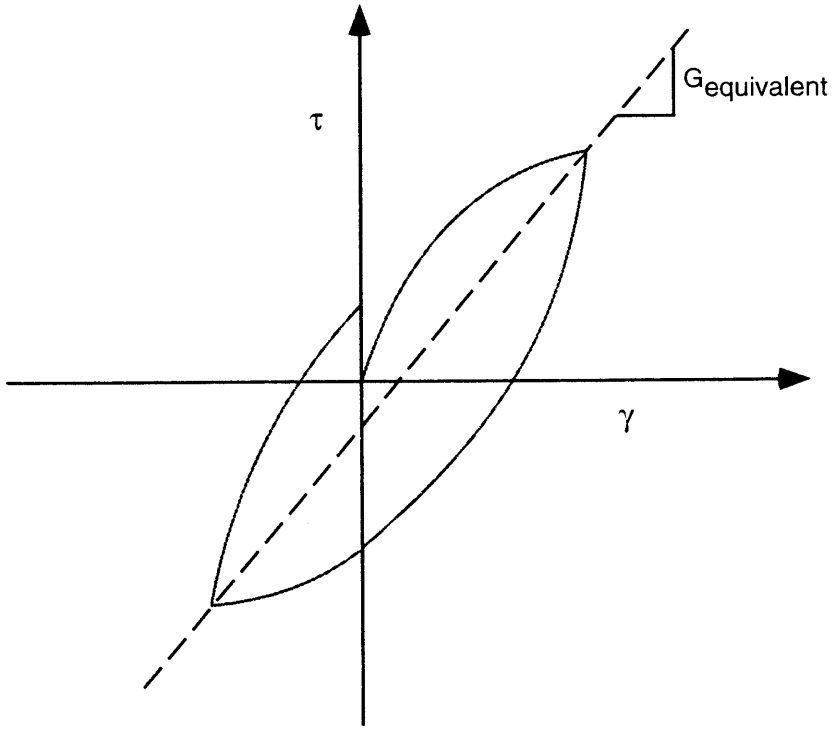

(b) Conventionally assumed stress-strain relationship

Fig. 6.3 Stress-strain relations normally used in dynamic analysis

assumed as shown in Fig. 6.3b using equivalent shear modulus ($G_{equivalent}$). However, the above relations are true only for the pure vibration problems. In the case of seismic earth pressure generation, the stress-strain relationship takes the form shown in Fig. 6.4. The envelope of the response is somewhat similar to the static stress-strain relation. Hence, the same constitutive relation, as for the static analysis, can be applied for the dynamic earth pressure calculation.

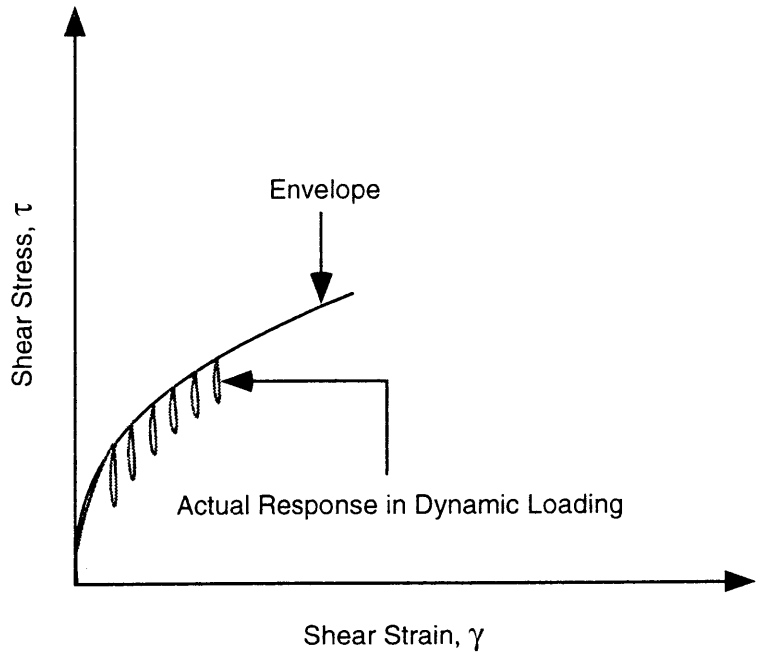

Fig. 6.4 Stress-strain relationship used in this research

The *Coupled Shear Band Method* described in Chapter 3, was derived for the static loading conditions. Needleman (1989) showed that the key features of the phenomenology of shear band development under the dynamic loading conditions are the same as under quasi-static loading conditions, and a delay in shear band development arises due to the inertial effects. The visco-plastic approach has been used by Prevost and Loret (1990) for dynamic localization problems by introducing the artificial viscosity into the rate-independent materials. In this research, the *Coupled Shear Band Method* is applied to analyze model retaining walls under seismic loading. It is recognized that the concept of mixed hardening is more appropriate for the problems involving dynamic loading, however, for simplicity, isotropic hardening is assumed in the analyses.

6.3.2 Interface Model

The assumption of perfect bonding works satisfactorily for the static loading condition. However, the relative movements, such as separation, should be considered for the dynamic soil-structure interaction problems as pointed out earlier. The interface model developed in Chapter 4 can be applied to seismic earth pressure analyses by considering the debonding of the wall and the backfill, when the inertia force acts away from the wall and the wall itself moves away from the backfill, a phenomenon more likely to develop when the wall is in active mode. Debonding can be identified by a criterion based on the sign of the induced force. It can be assumed to occur when the force is tensile. The stress-displacement relationship for the interface element is assumed as shown in Fig. 6.5.

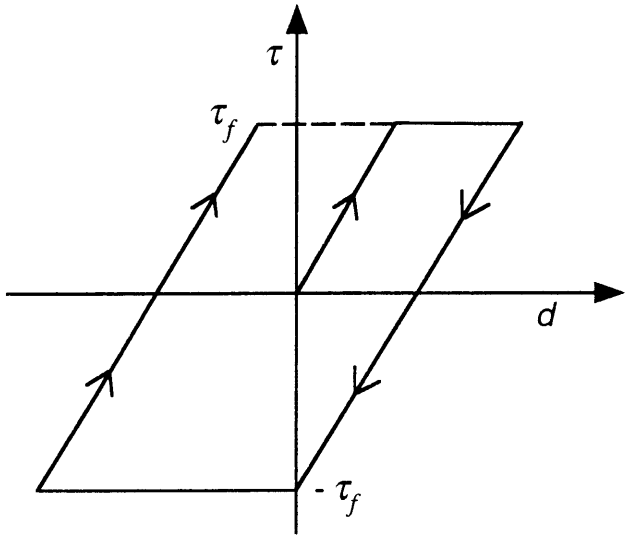

Fig. 6.5 Stress-displacement relationship for the interface

6.4 MODEL OF ANALYSIS AND COMPUTATIONAL PROCEDURE

6.4.1 FEM Model and Method of Analysis

The experimental model developed at Nagoya University's earth pressure laboratory (Ichihara and Matsuzawa, 1973) has been simulated in the FE analyses, the discretization of which is shown in Fig. 6.6a. The wall undergoes the combination of rotation about base and translation (RB-T), and the center of rotation is 20 cm below the wall base as shown in Fig. 6.6b. In this figure, s represents the mean wall displacement of the wall which is the displacement at the mid-height (H/2) of the wall.

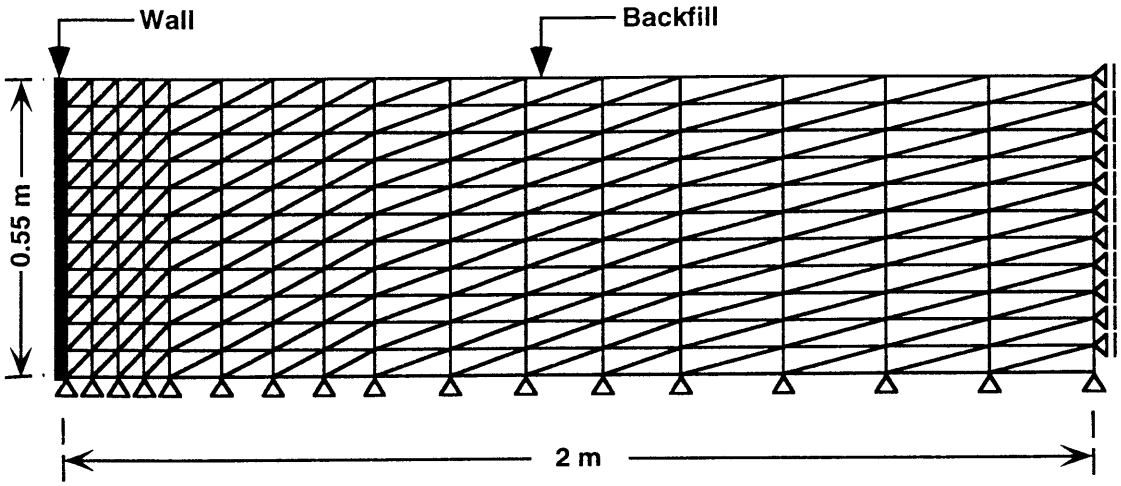

(a) Finite element discretization

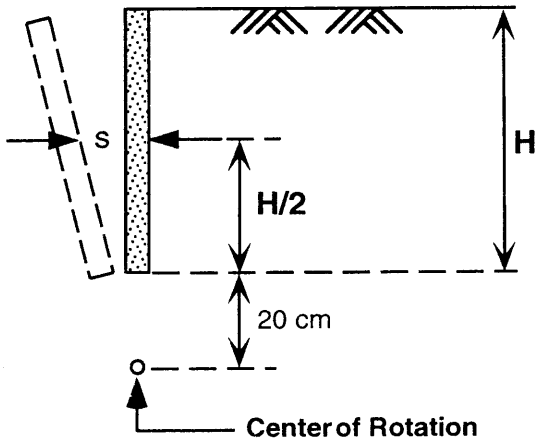

(b) Wall displacement mode

Fig. 6.6 FEM model of the analysis and the mode of wall displacement

The analyses are performed in time domain using Wilson's theta method (for details see Appendix B) to calculate the applied dynamic increment on the model retaining wall. This increment has been added to the static increment due to the displacement of the wall. The updated Lagrangian formulation is used in the stress-strain calculation.

6.4.2 Determination of Material Parameters

Ichihara and Matsuzawa (1973) reported that the plane strain test gives the peak value of the angle of internal friction ϕ_f of the backfill (dry Toyoura Sand) as 42°. However, since the

confining pressure of the experimental model is quite low, the various material parameters appeared in the constitutive relations need to be determined from the experimental data at low confining pressures. The material parameters are determined from the test results of the conventional triaxial compression tests or plane strain tests. Due to limitations of the experimental set up, the experiments for confining pressure less than 10 kN/m^2 could not be performed. Therefore, the parameters are plotted as a function of the confining pressures, and the obtained curve is extrapolated to the low confining zones to determine the parameters. Fig. 6.7 shows the variation of the angle of internal friction at peak ϕ_f with the confining pressures. By extrapolation, the value of ϕ_f corresponding the confining pressure of the experimental set up is found to be 51^0 and this value of ϕ_f is used in the analyses.

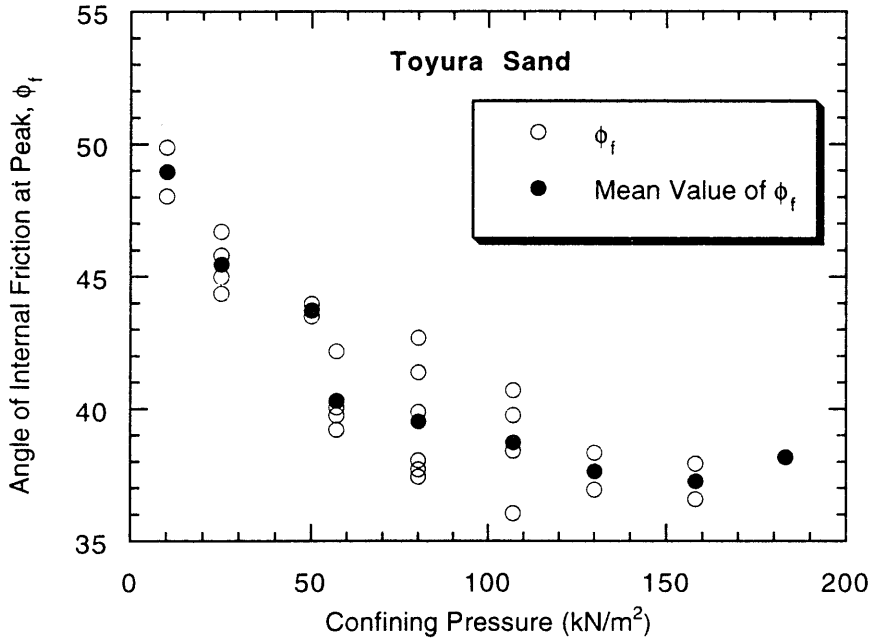

Fig. 6.7 Determination of angle of internal friction

Similarly the constant A (Eq. 3.32, Chap. 3) is determined as shown in Fig. 6.8. Material parameter values of the backfill soil (Toyoura sand) used/assumed in the analyses are tabulated in Table 6.2. The coefficient of the earth pressure at-rest is assumed to be 0.8, and it is assumed to be distributed hydrostatically. The same shear stiffness value, as in the static analysis, for the interface between the dry Toyoura sand and the wall is used (22×10^4 kN/m^2).

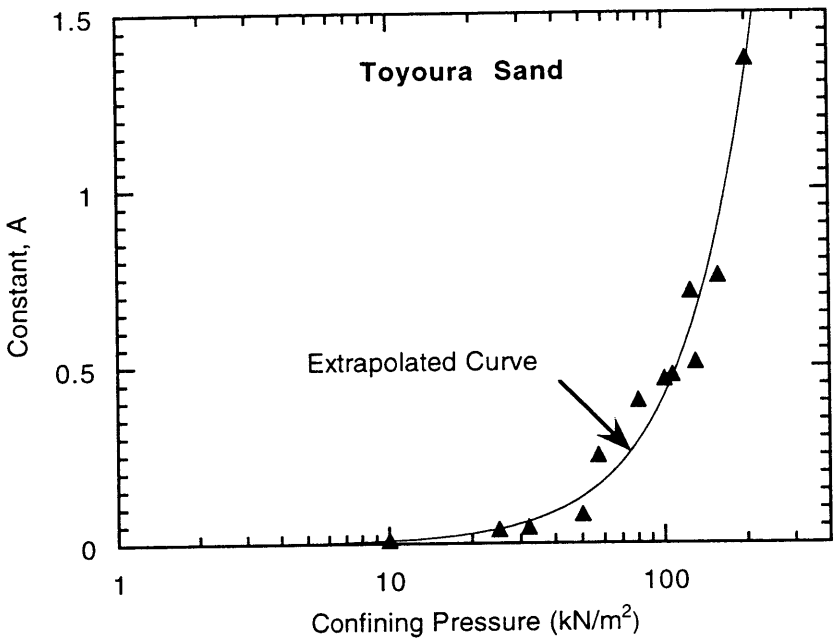

Fig. 6.8 Determination of constant A in Eq. 3.32 (Chapter 3)

Table 6.2 Material parameters of Toyoura sand used in the analyses

Parameters	Values
Elastic Parameters	
Young's Modulus, E (kN/m^2)	22000
Poisson's Ratio, ν	0.3
Deformation Parameters	
A	0.0029
R	0.05
κ_f	0.777
Peak Friction Angle, ϕ_f	51^0
Dilatancy Parameters	
κ_c	0.584
η_s	0.719
Smearing Parameter, ζ	0.32×10^{-5}

6.5 INFLUENCE OF INTERFACE MODES ON SEISMIC ANALYSIS

As discussed in the preceding section, the assumption of perfect bonding at the interface during dynamic loading leads to underestimation of the proper response in the soil-structure interaction system. In this section, the influence of the dynamic interaction on the earth pressure analysis is discussed.

The FEM model shown in Fig. 6.6a is simulated using two interface models to examine the influence of interface behavior on the numerical simulation. In one (Without Debonding), only the sticking and the sliding modes of the interface are considered, while in the other (With Debonding), the separation aspect of the wall and the backfill is also taken into consideration. Whenever debonding occurs, the shear stress is not transmitted through the interface. Therefore, during the analyses at the instant of separation, the particular interface element has been discarded from the finite element assembly by equating the normal stress acting on the element to zero. The equivalent load is added to the element equations. Rebonding can be assumed to occur, when the force becomes compressive again.

The numerical calculation, including the separation and sliding phenomena, shows strong non-linearity and thus the equation of motion must be solved by the step-by-step integration method in the time domain. The stiffness matrix is kept constant during the computation and only the external force is modified so as to satisfy the equilibrium condition.

6.5.1 Influence on Earth Pressure Parameters

Figs. 6.9(a)-(c) show the variation of the coefficient of earth pressure, K, the relative height of the point of application of the resultant, h/H, and the coefficient of wall friction angle, $\tan\delta$, as a function of mean wall displacement, s for the acceleration of 180 gals at the maximum inertia force. It can be observed that initially, the results from both the interface models coincide. However, with increasing wall displacements the differences get increased, with the results from the model considering the debonding aspect at the interface coming more close the experimental values.

Figs. 6.10a-f show the same variations for the acceleration of 360 gals at the maximum and the minimum inertia force. Comparing Figs. 6.9 and Figs. 6.10, it can be observed that for the higher acceleration levels the results from the two models differ even at the small wall displacement, and as the wall displacement increases, the differences of the results obtained using without debonding and the experimental results increase. This implies that the separation mode of the interface plays an active role in the calculation of seismic earth pressure. The influence of the separation becomes crystal clear if we observe the performance of the two models in the case of minimum force as shown in Figs. 6.10(b), (d) and (f). The usage of debonding mode at the interface predicts the experimental trends

satisfactorily, whereas assumption of perfect bonding results in weird variations of the earth pressure parameters K, h/H and tan δ.

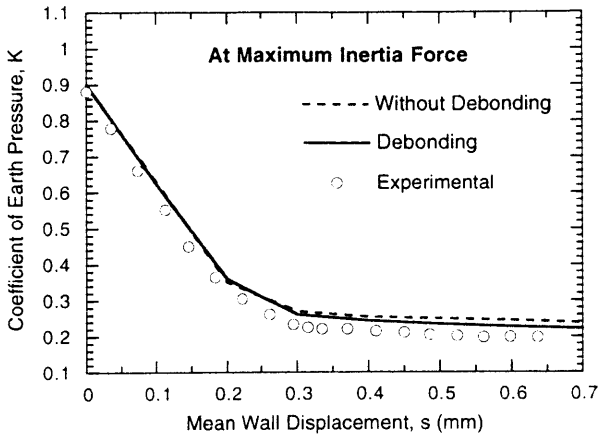

(a) Coefficient of Earth Pressure

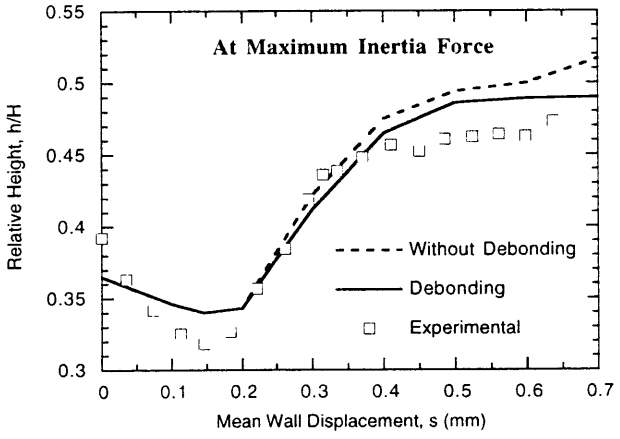

(b) Point of application

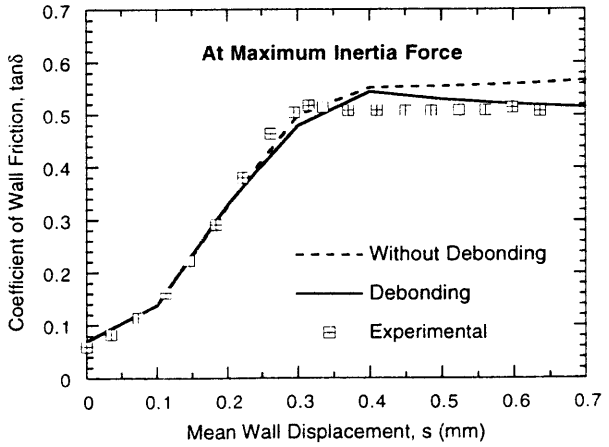

(c) Coefficient of wall friction

Fig. 6.9 Influence of interface interaction on earth pressure parameters (Acceleration = 180 gals)

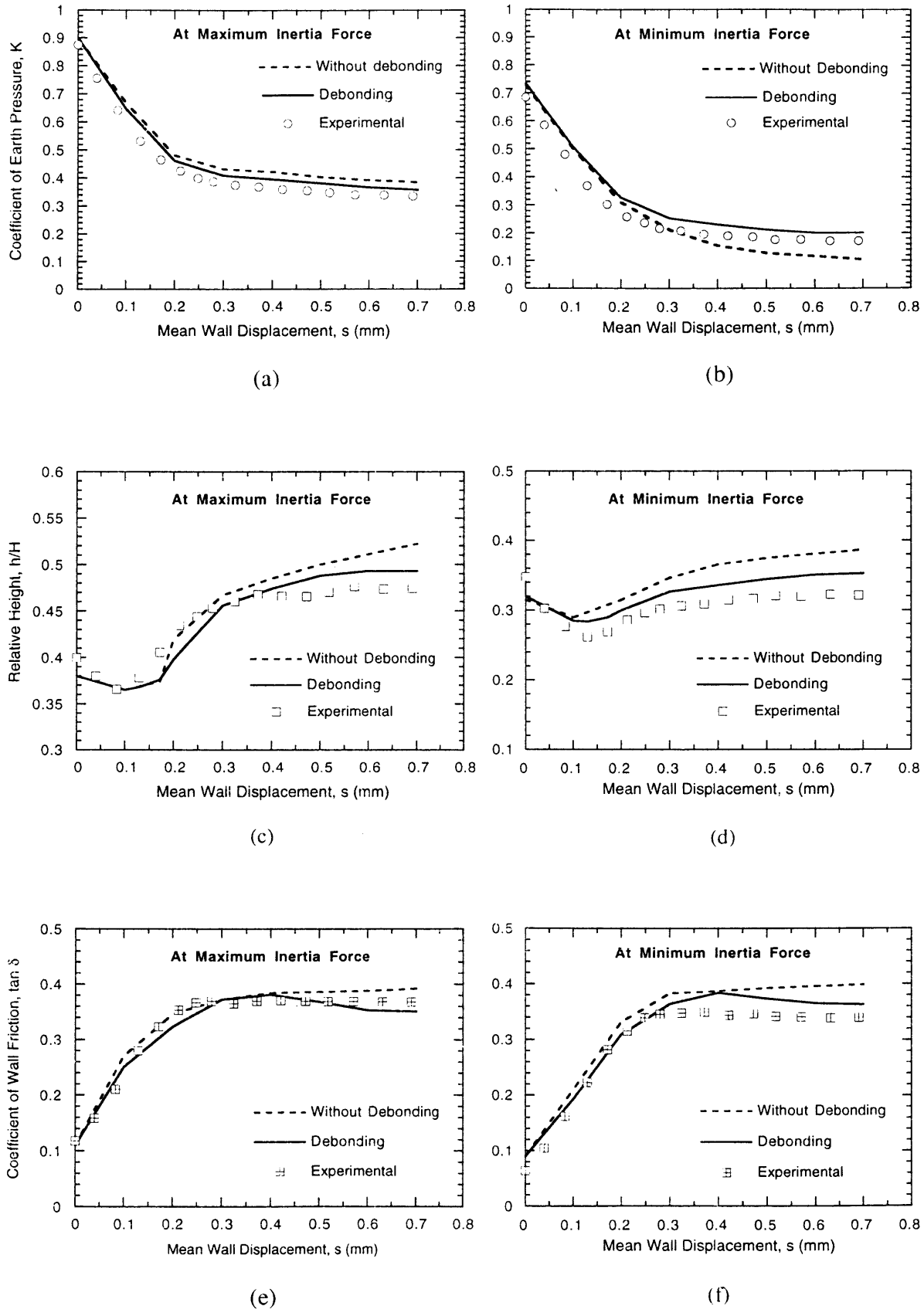

Fig. 6.10 Influence of interface interaction on earth pressure parameters (Acceleration = 360 gals)

6.5.2 Influence on Mean Earth Pressure

Fig 6.11 shows the variation of the mean earth pressure at two different accelerations. This figure too divulges the merit of including the debonding mode and demonstrates that the effect of debonding becomes more pronounced when the acceleration level increases. At the acceleration of 84 gals, the results from both the interface conditions do not exhibit significant differences, however, at the acceleration of 480 gals, there exists a significant difference between the experimental values and the numerical values for the interface model without consideration of debonding. In fact, it was observed during the analyses that at 180 gals of acceleration debonding occurs only at the top interface element (0.09H), whereas at the acceleration of 360 gals debonding spreads till the third element from the top (0.27H).

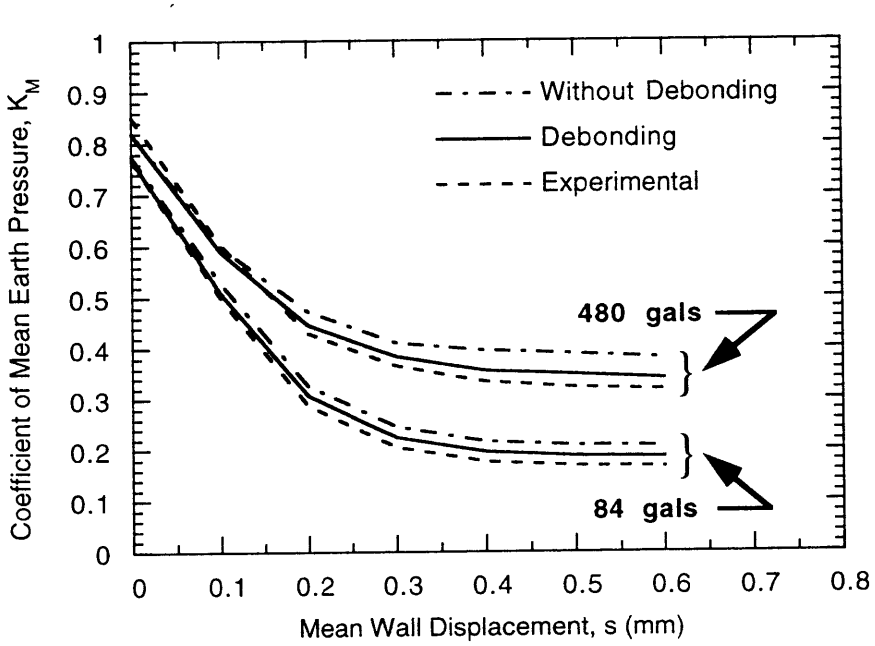

Fig. 6.11 Influence of interface interaction on the mean earth pressure variation

6.6 VALIDATION OF THE NUMERICAL MODEL

In the following subsections, the results obtained from the analyses are discussed with reference to the experimental results. For the retaining walls and similar structures, the action of the earthquake is most dangerous when the horizontal acceleration is directed towards them. Hence, practically, it is sufficient to consider only the effect of the maximum inertia force. Here too, the discussions will be limited to the case of maximum inertia force. The results of the analyses are also compared with the classical Mononobe-Okabe theory and Logarithmic Spiral Method (see Appendix A). The separation between the wall and the

backfill is allowed when the minimum inertia force acts away from the wall. In other words, the interface model permits debonding at the interface.

6.6.1 The Earth Pressure Parameters

The effects of the wall displacement on the seismic earth pressure parameters were observed in Figs. 6.9-6.10. The numerical results exhibit higher values (around 10 %) of the coefficient of the seismic earth pressure as compared with the experiments. Ichihara and Matsuzawa (1970) found that due to the friction between the side walls of the soil bin and the backfill sand the earth pressure against the wall gets reduced by about 10 %.

The non linearity of the earth pressure distribution, which will be discussed in a subsequent section, is responsible for the peculiar variation of the relative height as observed in these figures. The distribution curve changes its shape with displacement of the wall resulting in the characteristic variation.

6.6.2 Progressive Failure of the Backfill and the Active State

The classical Mononobe-Okabe theory based on rigid plastic assumption assumes simultaneous formation of the failure wedge in the immediate vicinity of the retaining wall. However, one should keep in mind that the attainment of the active or the passive state involves progressive deformation of the backfill. The localized deformation analysis is considered to be one of the versatile tool to capture the progression of the deformation pattern, although the capability of the conventional method based on stress continuity in capturing the progressive failure phenomenon can not be entirely ruled out.

Fig. 6.12(a) shows the progression of the failure zone in the backfill at different stages of the wall displacement for the acceleration of 180 gals. The failure initiates from the top of the backfill and spreads downward with displacement. With further displacement of wall the bottom backfill elements near the wall also start to fail, although the dominant failures are still exhibited by the top elements. Finally, a complete failure wedge is formed. This is the characteristic failure mode for this mode of wall displacement, which is RB-T (Fig. 6.6b). Once the failure wedge is completed, even with further movement of the wall the progression of the failure zone ceases, implying the attainment of the active state. The failure surface predicted by the Mononobe-Okabe theory ($\phi = 51^{o}$) is also shown in the same figure. Similar observation has also been predicted for the acceleration of 360 gals as shown in Fig. 6.12(b). Comparing Fig. 6.12(a) and Fig. 6.12(b) it can be seen that the domain of the failure zone increases as the acceleration level increases.

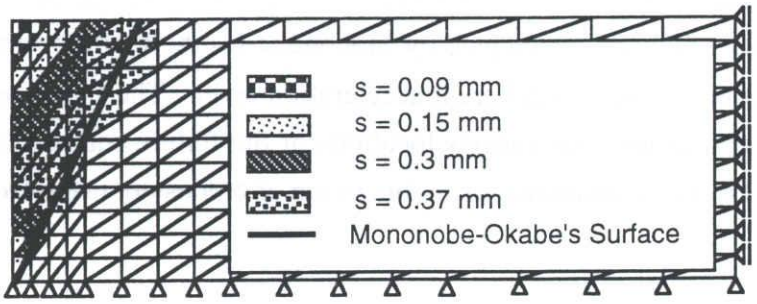

(a) Acceleration = 180 gals

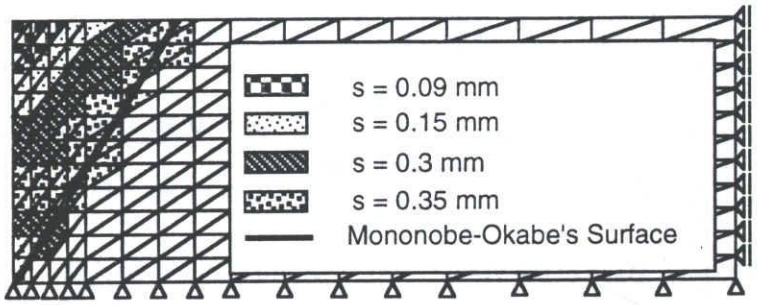

(b) Acceleration = 360 gals

Fig. 6.12 Progression of the failure zone at two different accelerations

6.6.3 Mobilized Angle of Friction and Angle of Wall Friction

The classical theory assumes simultaneous mobilization of the friction angle along the failure line at every location, ΔL (Fig. 6.13). However, the progressive failure of the backfill, as already discussed, does not justify the assumption as the elements intercepted by the M-O failure surface are in a different state of affairs at a particular wall displacement.

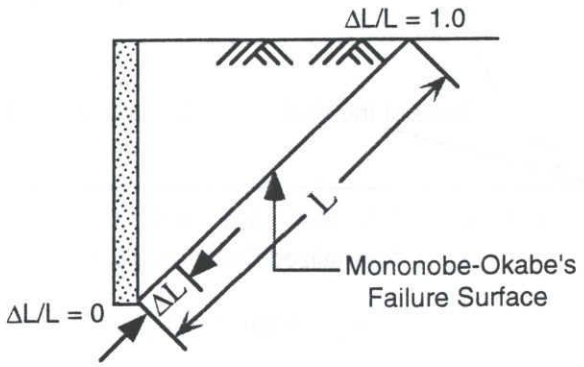

Fig. 6.13 Failure surface in the backfill

Figs. 6.14(a) and 6.14(b) show the mobilized values of the angle of internal friction, ϕ_m, in the elements which are intercepted by Mononobe-Okabe's failure surface, at various mean wall displacements for two different acceleration levels. The figure reveals that, at a particular wall displacement, the various locations of the failure surface exhibit different mobilized value of ϕ. Thus simultaneous mobilization of ϕ does not take place in the failure surface.

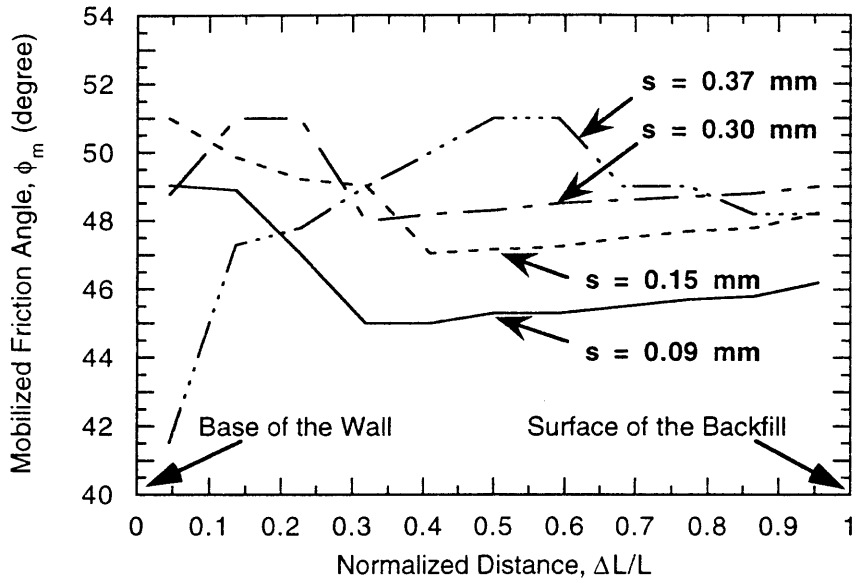

(a) Acceleration = 180 gals

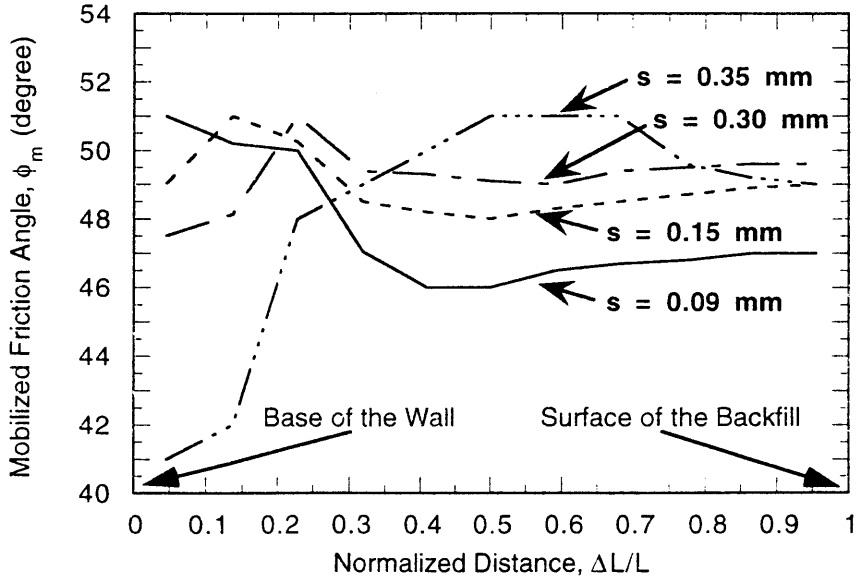

(b) Acceleration = 360 gals

Fig. 6.14 Mobilization of the angle of internal friction, ϕ, at different stages of the wall displacement

Fig. 6.15 shows the mean values of the mobilized friction angle, $(\phi_m)_{mean}$, at various mean wall displacements for the two acceleration levels. It can be observed from this figure that at the small wall displacements the mobilized friction angle differs depending on the accelerations, however, as the wall displacement increases the differences get reduced. The trend of the variation is the same for the two acceleration levels (i.e. initially increases to reach the maximum value and then decreases).

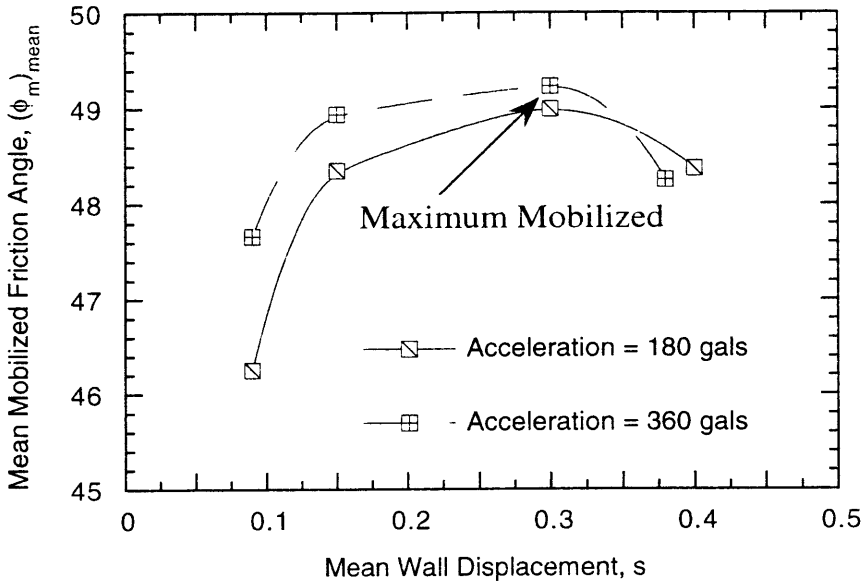

Fig. 6.15 Mean mobilized value of the friction angle for two particular acceleration levels

Fig. 6.16 shows the mobilized values of the wall friction coefficient, tanδ as a function of the mean wall displacement. Although the trend of the variation is the same irrespective of the accelerations, the maximum mobilized values differ. Higher acceleration contributes to the less mobilization of the wall friction. This is reasonable from the point of view of the interface behavior, as at the higher level of acceleration the wall tends to separate away from the wall resulting in the reduced shear strength. The numerical results demonstrate the capability of the present interface model (which can take care of the effects of separation) in simulating the wall friction, even though the mean wall displacement required to reach the peak is different from the experimental ones (Figs. 6.9 and 6.10). Ichihara and Matsuzawa (1973), based on their experimental observation, defined the active state as the stage when the wall friction coefficient tanδ attains its maximum value. Comparing Fig. 6.15 and Figs. 6.9-6.10, it can be seen that the mean wall displacement, s, required in the experiments to reach the maximum value of the mobilized tanδ is almost the same as that at which the mean

of the mobilized ϕ reaches its maximum value, and the value is not significantly affected by the acceleration levels.

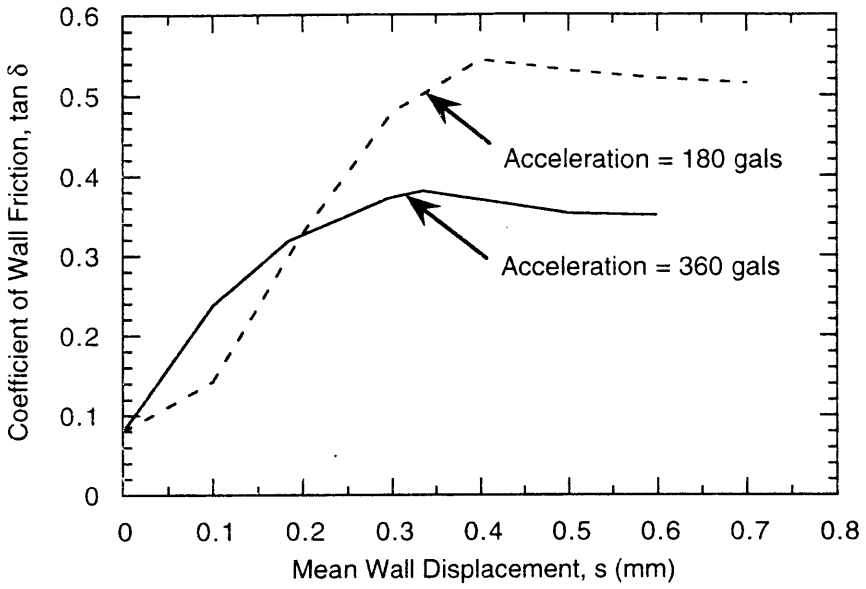

Fig. 6.16 Mobilized angle of wall friction with displacement at two different accelerations

6.6.4 Distribution of the Lateral Active Thrust

Fig. 6.17(a) and Fig. 6.17(b) show the lateral active earth pressure distribution behind the wall at the acceleration of 180 gals and 360 gals respectively obtained from the analyses. In the same figures the hydrostatic distributions given by the Logarithmic Spiral Method (ϕ = 51°) and Mononobe-Okabe's formula (ϕ = 49°; the maximum value of the mean mobilized friction angle given by the analyses (Fig. 6.15)) are also plotted. The effect of the nature of progression of the failure zone discussed in Figs. 6.12 is clearly reflected in the distribution. The presence of the early failed element at the top and the bottom of the backfill contributes to the high reduction of stress at the top and the bottom. The non linearity of the distribution curve results in the characteristic variation of the relative height, (h/H), which was observed in Figs. 6.9 and 6.10. The distribution curve changes its shape with acceleration resulting in the different values of the point of application of the active thrust as will be discussed in the next sub-section.

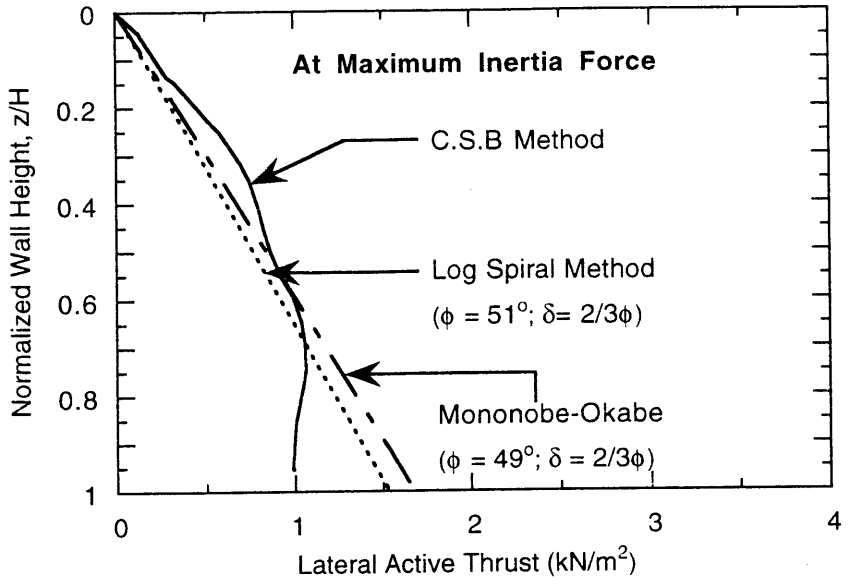

(a) Acceleration = 180 gals

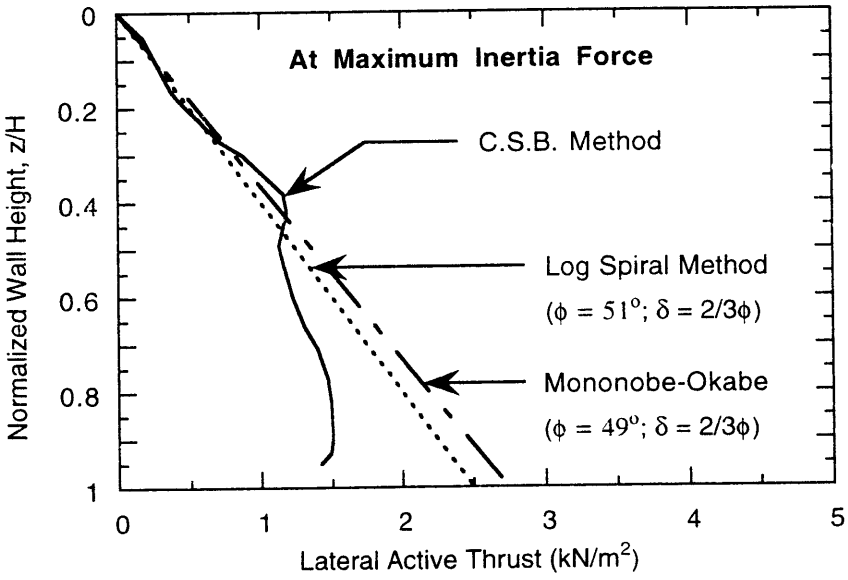

(b) Acceleration = 360 gals

Fig. 6.17 Active earth pressure distribution for two different acceleration levels

6.6.5 Resultant Active Thrust and Its Point of Application

Figs. 6.18a-b show the variation of the coefficient of the lateral active thrust, K_{AE}, as a function of acceleration. A comparison also is made with the Logarithmic Spiral Method and the Conventional Strain-hardening Method (Chapter 3). The numerical results, obtained form

the C.S.B. Method, show fairly good agreement with the experimental trend (nonlinear increase of K_{AE}) as compared to the conventional method. This is because the conventional method is unable to capture the mobilized friction angle along the failure surface efficiently. The Mononobe-Okabe values for the two values of ϕ, discussed in the preceding paragraph, show that the use of the maximum mean mobilized friction angle yields result that is close to the experimental as well as the numerical one (Fig. 6.18b).

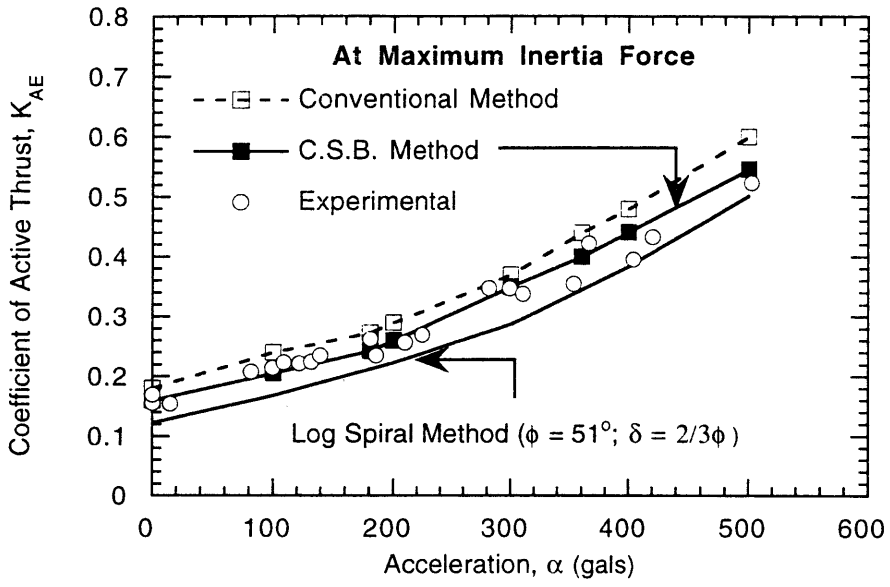

(a) Comparison of the numerical values

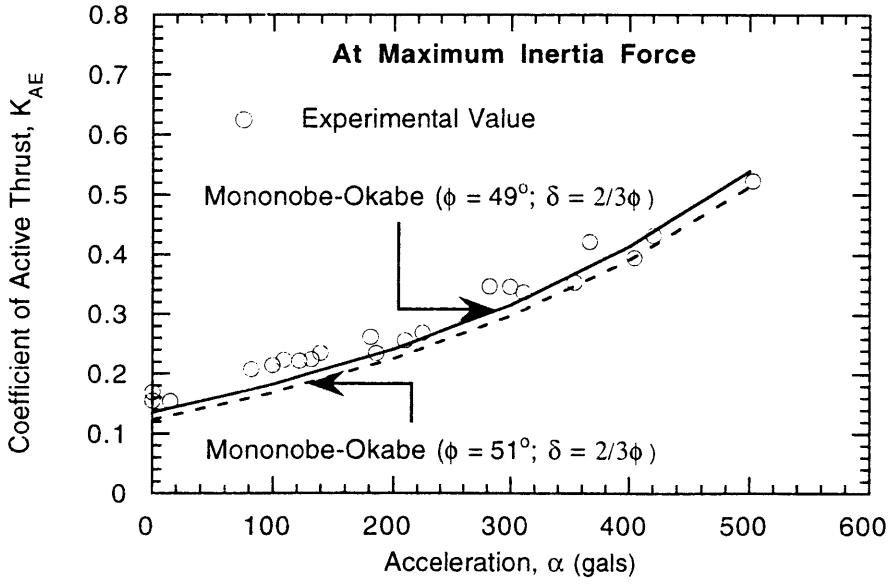

(b) The effect of the mean mobilized friction angle, ϕ_m

Fig. 6.18 Variation of the coefficient of the seismic active thrust with acceleration

The relative height of the point of application of the resultant active thrust, $(h / H)_{AE}$, is plotted as a function of acceleration level as shown in Fig. 6.19. The numerical results using the C.S.B. Method are showing a good agreement with the experimental observations as compared to the conventional method of analyses. With increasing acceleration the active distribution curve gets bulged (Fig. 6.17b) in the middle resulting in the lifting up of $(h / H)_{AE}$.

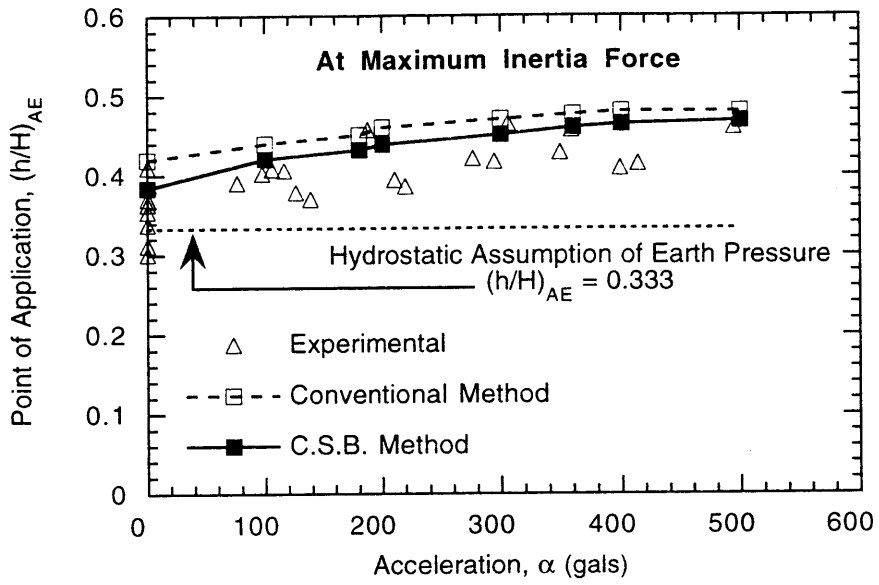

Fig. 6.19 Variation of the point of application of the resultant active thrust with acceleration

6.6.6 Increment of Seismic Active Force and Its Point of Application

The issue of the incremental seismic force and its point of application still remains controversial in the field of dynamic earth pressure. According to Seed and Whitman (1970), the incremental seismic force acts at the height of 0.6H from the base of the wall. Ichihara and Matsuzawa (1973) assumed that the dynamic increment of active thrust can be given by an equivalent surcharge whose point of application acts at the mid-height of the wall. On the other hand, Sherif et al (1982) found from their experiments that the dynamic increment acts at 0.48H from the base of the wall. Therefore, it is felt necessary to elucidate the reality behind this controversy by making use of the numerical values obtained from the analyses.

Fig. 6.20 shows a conceptual drawing used to calculate the total seismic active earth pressure. Generally, the incremental seismic active thrust, ΔP_{AE}, is calculated by using the theory of elasticity, which is not a justified concept for the earth pressure calculations. The seismic increment and its point of application need to be judged based on the calculations using the theories of plasticity.

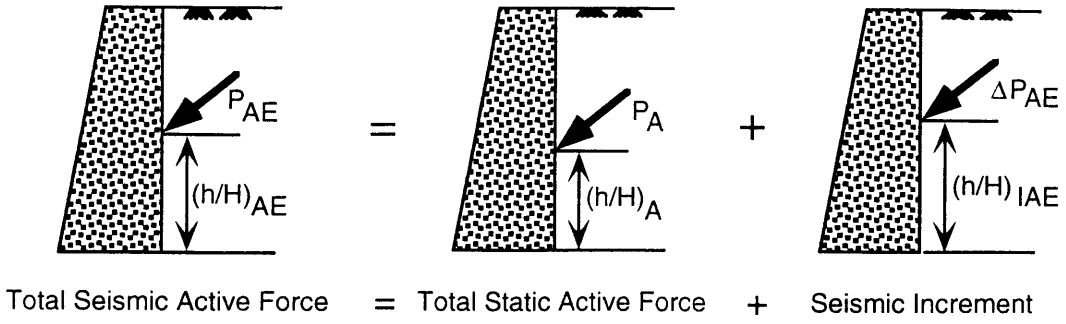

Fig. 6.20 Illustration of the seismic increment

Fig. 6.21 shows the relationship between the calculated incremental coefficient of the lateral active thrust, K_{IAE}, and the acceleration. The relationship shows that the incremental coefficient increases non linearly. As shown in the figure, similar variations have been observed experimentally by Sherif et al (1982) for the translational mode of the retaining wall.

The relationship between the relative height of the incremental active thrust, $(h / H)_{IAE}$, and the acceleration level (Fig. 6.22) divulges that the point of application of the seismic increment fluctuates between 0.5H and 0.55H. The experimental observation of Sherif et al (1982) is also shown in the same figure. It can be inferred from the numerical results that the acceleration levels do not have a significant influence on the point of application of the incremental seismic earth pressure, even though its counterpart does have an effect.

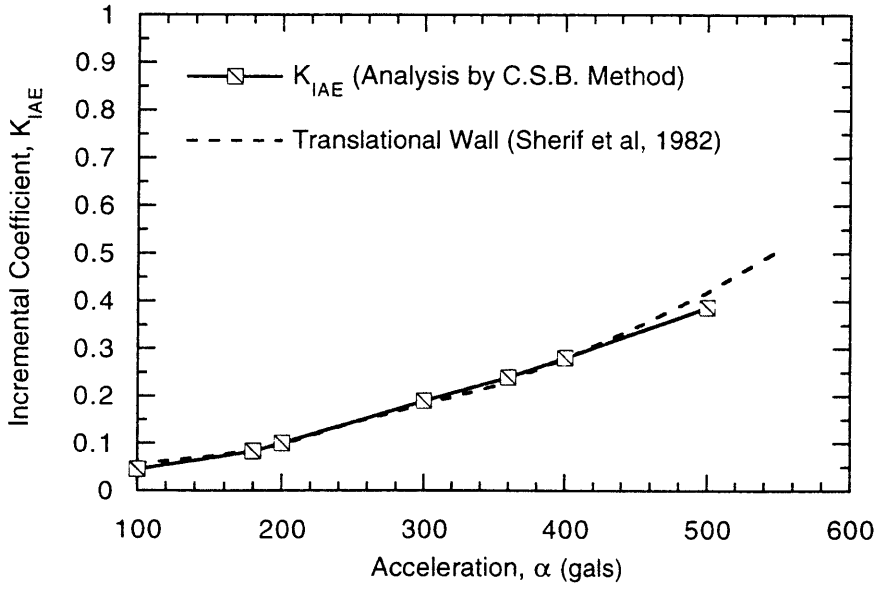

Fig. 6.21 Variation of the incremental active thrust with acceleration

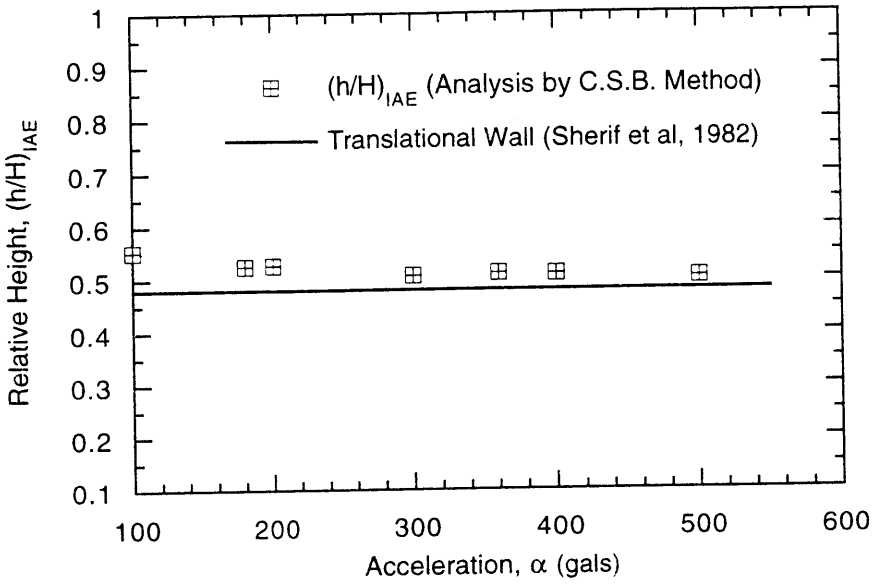

Fig. 6.22 Variation of the point of application of the seismic increment with acceleration

6.7 ANALYSIS CONSIDERING THE WALL DISPLACEMENT MODES

The effect of the wall displacement modes on earth pressure has already been discussed in detail for the static loading condition in Chapter 5. In this section, the same is discussed for the earthquake loading condition using the numerical model described so far.

The well known Mononobe-Okabe theory for earth pressure calculation during earthquake loading is based on the classical Coulomb theory which itself has intrinsic fallacies brought to light by Terzaghi in 1936. In addition, the Mononobe-Okabe theory does not include the effect of the dynamic interaction between the wall and the backfill. It is a theory that considers only the quasi-static force acting on retaining walls, not the pure dynamic loading. Experimental researches on the wall movement modes dependent seismic earth pressure were performed by various researchers (sub-section 2.3.2 in Chapter 2). Analytical expressions have also been put forward (sub-section 2.3.3 in Chapter 2) to explain the nonlinear distribution for various wall movement modes. However, the analytical methods can not explain the exact nature of distribution, particularly because, they seem to ignore the importance of the wall backfill interaction at the interface. Hence, the numerical method that can take care of the effect of interaction was used to analyze the influence of the wall displacement modes on the seismic earth pressure.

6.7.1 FEM Model and the Modes of Wall Displacement

Two wall movement modes (RB and RT) are considered in the analyses. The same FE model, which was adopted for the static earth pressure analyses (Fig. 5.1, Chapter 5), is used here. Comparisons also have been made with the experimental results reported by Ishibashi and Fang (1987). The material parameter values of the backfill sand used/assumed in the analyses are given in Table 6.3.

Table 6.3. Material Parameters of Backfill

Parameters	Values
Elastic Parameters	
Young's Modulus, E (kN/m^2)	21000
Poisson's Ratio, ν	0.3
Deformation Parameters	
A	0.0037
R	0.05
κ_f	0.643
Peak Friction Angle, ϕ_f	40^0
Dilatancy Parameters	
κ_c	0.491
η_s	0.563
Smearing Parameter, ζ	0.40×10^{-4}

6.7.2 Earth Pressure Distribution and the Active State

Figs. 6.23(a) and 6.23(b) show the distributions of the horizontal earth pressure with depth z, at different wall rotations for the RB mode and the RT mode respectively in the case of maximum inertia force. From the results, it can be observed that the distribution pattern depends on the mode of movement of the wall and is highly nonlinear. The noticeable points in the figures are the earth pressure at the top and the base of the wall. In the case of the RB mode, the earth pressure decreases faster at the top, while for the RT mode, the earth pressure shows an increase in value with increasing deformation. On the other hand, at the base portion of the wall, while the RB mode shows existence of higher stress, the RT mode exhibits rapid reduction of stress. This is due to the different mechanism of deformation resulting from differences in stress conditions for each case. The progressive nature of the

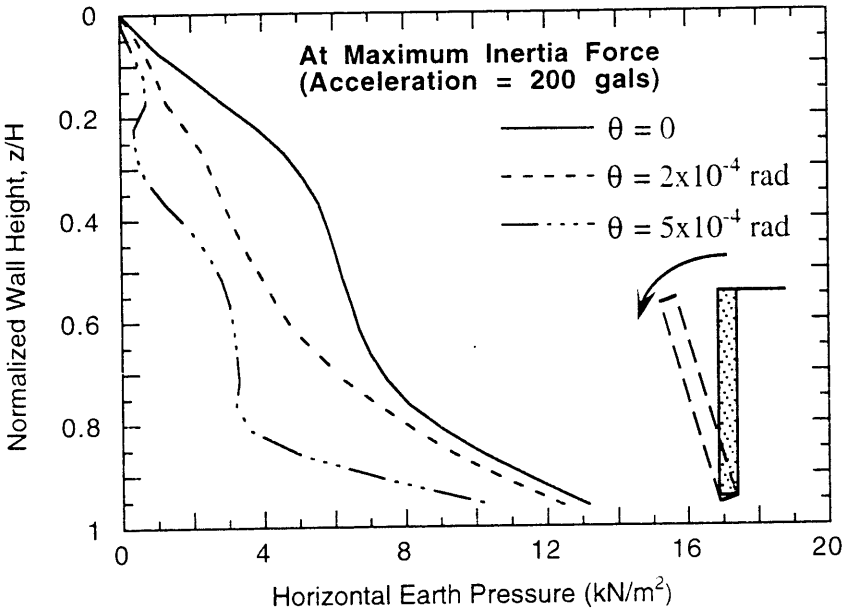

(a) Rotation about base (RB) mode

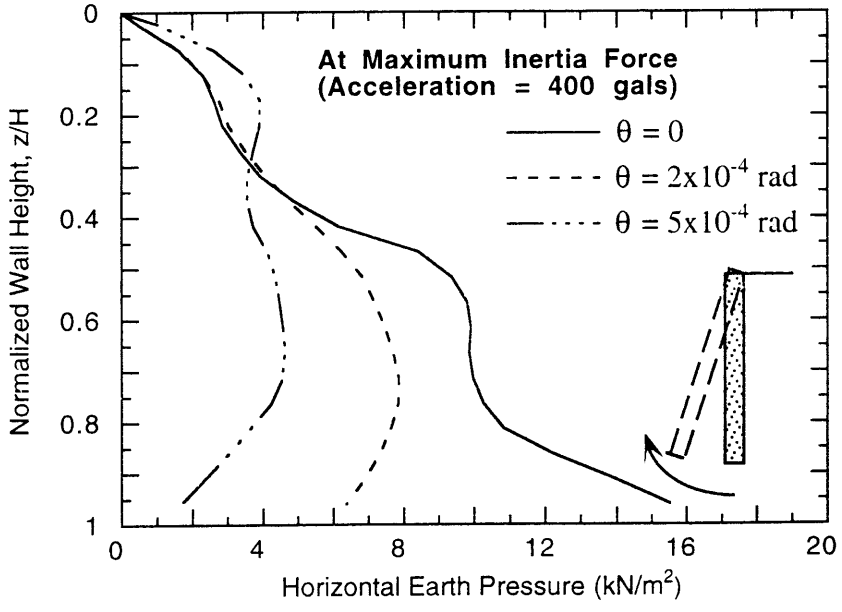

(b) Rotation about top (RT) mode

Fig. 6.23 Distribution of horizontal earth Pressure with the wall rotations

failure pattern of the backfill elements is responsible for this difference in the mechanism of deformations.

Figs. 6.24(a) and 6.24(b) show the progression of the localized zone consisting of the cracked elements at various values of the wall rotation when subjected to an acceleration of

200 gals. The behavior is somewhat similar to the static case discussed in sub-section 5.3.2 of Chapter 5. In the case of the RB mode, as can be seen in Fig. 6.24a, the failure starts from the top and advances towards the base of the wall, finally forming a clear active wedge of Rankine type. However, for the RT mode (Fig. 6.24b), the failure initiates at the base and moves towards the backfill surface. These two figures explain the phenomenon observed in Figs. 6.23a and 6.23b; the early failed backfill elements contribute to the reduction of stress for both the modes, while the arching phenomenon contributes to the higher stress at the top for the RT mode. The extra higher stress at the base for the RB mode comes from the restriction of the movement of the backfill at the base. Mononobe-Okabe's failure surface using constant angle of internal friction ϕ is also shown in the figures. It is to be noted that the elements touched by the Mononobe-Okabe's surface are having different mobilized angles of internal friction at that stage as already discussed in sub-section 6.6.3 for the RB-T mode.

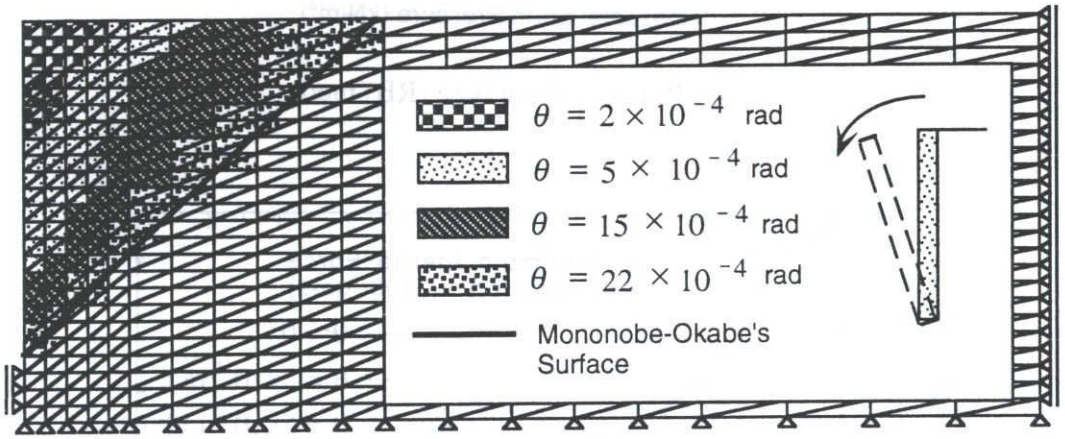

(a) Rotation about the base (**RB**) Mode

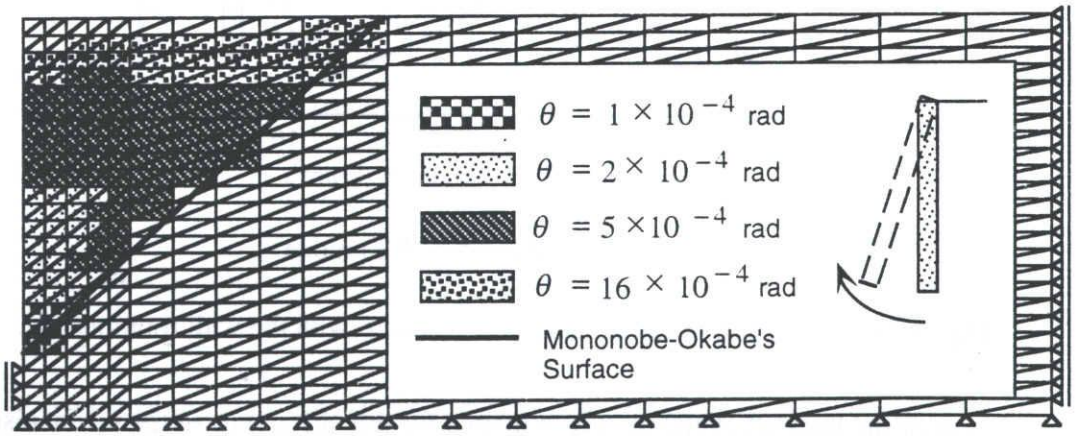

(b) Rotation about the top (**RT**) Mode

Fig. 6.24 Progressive failure pattern of the backfill elements (Acceleration = 200 gals)

6.7.3 Active Earth Pressure Distribution

Figs. 6.25(a) and 6.25(b) show the distributions of the horizontal thrust at the active state for the two modes. The pattern of the distribution curves obtained from the analyses shows reasonable agreement with the experimental trend. For comparison, the active state distribution obtained from Dimarogona's analytical expression is also plotted in the figures along with the hydrostatic distribution obtained using the Logarithmic Spiral Method. Dimarogona's method can only qualitatively express the nonlinear characteristics of the active thrust distribution, and its dependency on the wall movement modes.

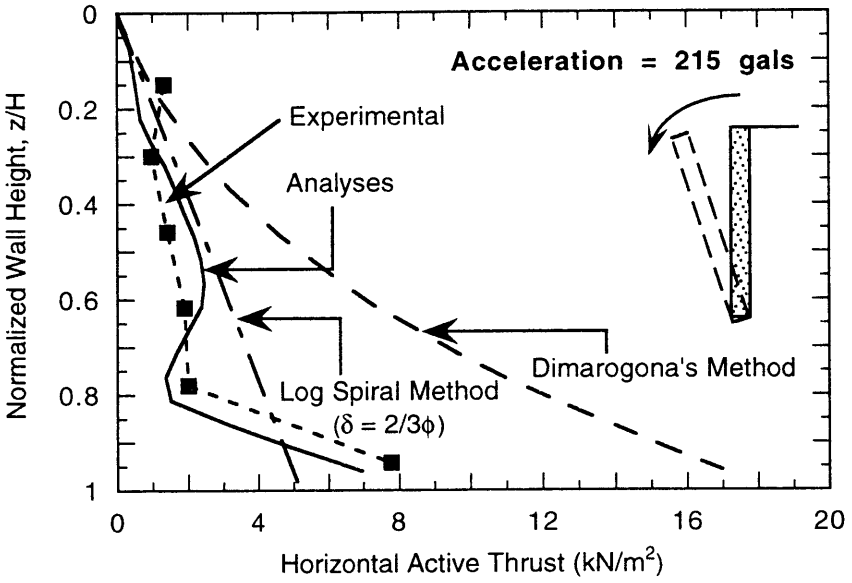

(a) Rotation about base (RB) mode

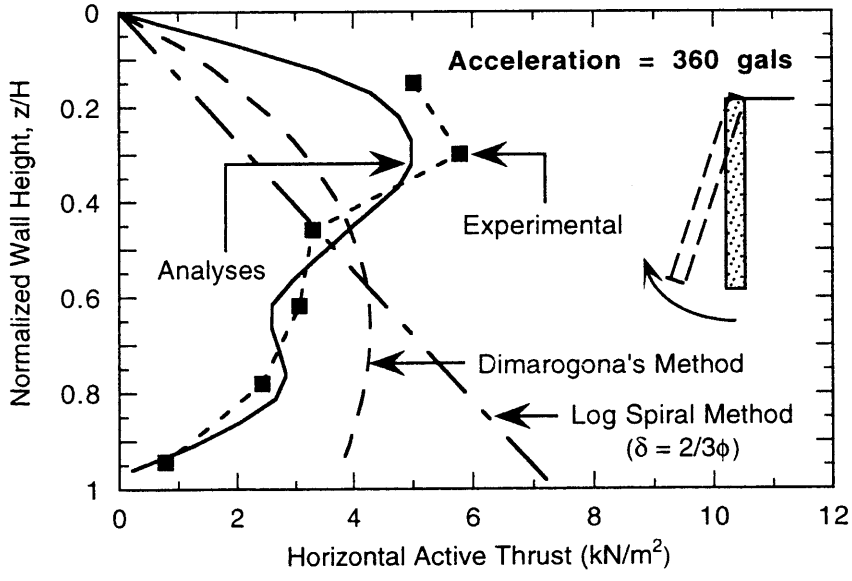

(b) Rotation about top (RT) mode

Fig. 6.25 Seismic active earth pressure distribution for each mode of movement

6.7.4 Coefficient of the Seismic Active Thrust

Fig. 6.26 shows the variations of the horizontal component of the coefficient of seismic active thrust, K_{AE}, as a function of horizontal acceleration, α, along with the values given by Dimarogona's method and Logarithmic Spiral Method. It can be seen that the RB mode gives the highest, and the RT gives the lowest value of K_{AE}. Incidentally, the values given by the RT mode coincide with the values from Logarithmic Spiral Method. While the analyses could explain the experimental trend (nonlinear increase with increasing acceleration) satisfactorily, Dimarogona's method fails to carry any weight quantitatively, which may be due to the fact that the method can not truly capture the progressive failure of the backfill, and can not simulate the soil-wall interaction.

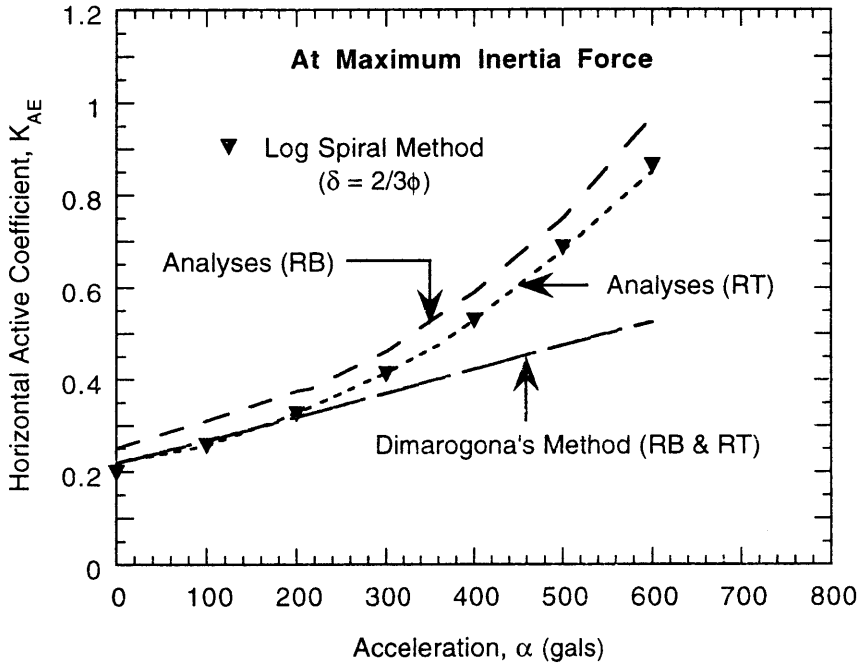

Fig. 6.26 Coefficient of the seismic earth pressure for each mode at various Accelerations

6.7.5 Point of Application of the Resultant Active Thrust

Fig. 6.27 shows the relation between the relative height of point of application of the resultant active thrust, $(h / H)_{AE}$, and the horizontal acceleration, α. A trend similar to the experimental results can be observed; for the RB mode, $(h / H)_{AE}$ increases with acceleration, while for the RT mode, it decreases. Dimarogona's method for RB mode shows negligible increase of the value with accelerations.

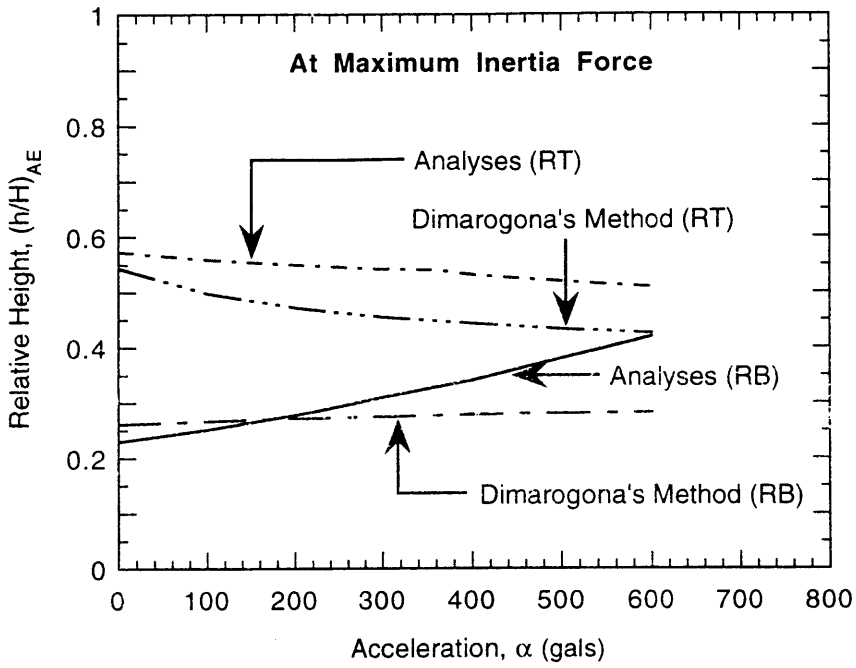

Fig. 6.27 Point of application of the seismic active thrust for each mode as a function of the horizontal acceleration

6.7.6 Effect on the Incremental Seismic Thrust

The discussion of the seismic increment of the active thrust is already made in section 6.6 for RB-T mode of the wall displacement. In this sub-section, the effect of the wall displacement modes on the incremental seismic active thrust is discussed with respect to the RB and the RT mode.

Fig. 6.28 shows the relations between the calculated incremental horizontal coefficient of seismic active thrust, ΔK_{IAE}, and the horizontal acceleration, α, for the two modes. The relationships exhibit a nonlinear pattern (as in the case of RB-T mode) for both the modes. For the same value of acceleration, the RB mode gives the highest value of ΔK_{IAE}.

Similar relationships (Fig. 6.29) for the relative height of the incremental active thrust, $\Delta(h / H)_{IAE}$, reveal that the RB mode results in a lower value and the RT mode results in a higher value of $\Delta(h / H)_{IAE}$ at lower acceleration levels. However, at higher level of acceleration, the values cluster around 0.5, a figure that coincides with the recommendation of Ichihara and Matsuzawa (1973). It can be inferred from this observation of the numerically calculated values that at the higher acceleration levels the wall movement modes do not effect the point of application of the dynamic increment.

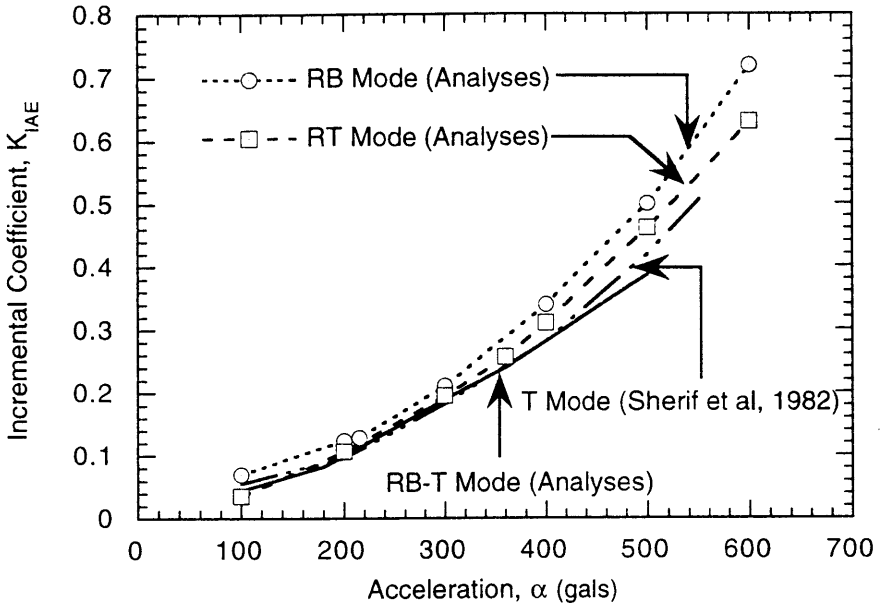

Fig. 6.28 Variations of the coefficient of the incremental seismic active thrust with acceleration and the wall displacement modes

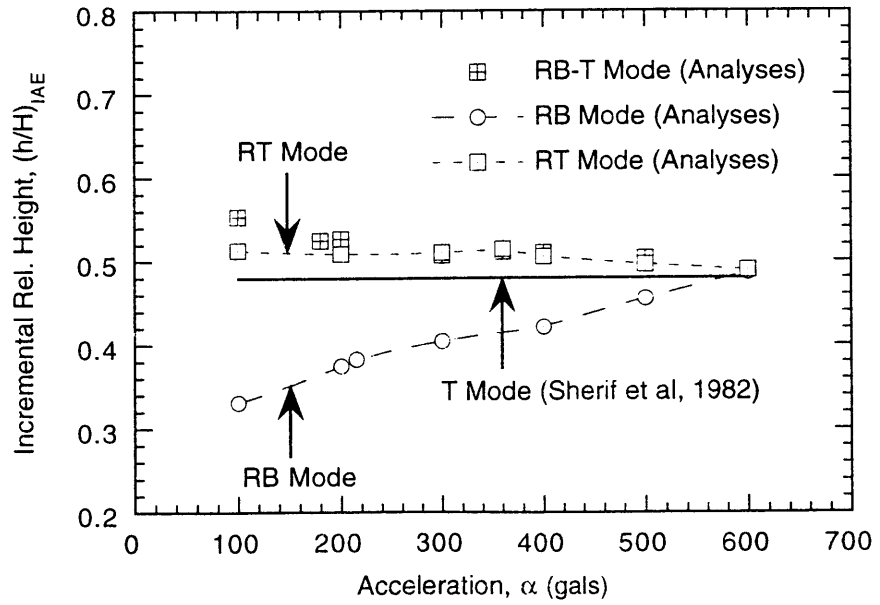

Fig. 6.29 Variations of the point of application of the seismic increment with accelerations and the wall displacement modes

The following empirical equation can be obtained for the variation of the incremental coefficient with acceleration, α, based on the results presented in Fig. 6.28:

$$K_{IAE} = M\alpha^{(0.542M + 0.791)} \tag{6.1}$$

in which M is parameter which takes different values depending on the wall displacement modes as shown in Table 6.4.

Table 6.4 Values of the parameter M

Modes of Wall Movement	M Value
RB-T Mode	0.98
RB Mode	1.45
RT Mode	1.3
T Mode	1.1

6.8 MERITS OF DYNAMIC ANALYSIS

As mentioned earlier, most of the researchers analyzed the dynamic earth pressure in frequency domain by using the equivalent linear stress-strain relationship for the backfill soil. However, their results relate to the amplitude of the dynamic component of the earth pressure and can not express the actual earth pressure (sum of the static component and the dynamic one) along the back face of the wall.

In this research, experimental models are simulated for explaining the mechanism of the dynamic earth pressure generation against a rigid retaining wall supporting dry backfill sand. Dynamic forces similar to those applied in the laboratory tests were used as input motion in the numerical analyses. However, in actual cases, seismic motion is a random one comprising of low frequency motion of small amplitude, and high frequency motion of large amplitude. In the present analyses a pure sinusoidal motion with a frequency of 3.3 Hz was used, which is a low frequency motion. The geometrical scale ratio, (model to prototype) λ_L, can be defined as,

$$\lambda_L = \left(\frac{T_m}{T_p}\right)^2 \tag{6.2}$$

where, T_m and T_p are the periods of vibration in the model and in the prototype, respectively. Since the period of earthquake vibration is in a range of 1 second, the value of

λ_L becomes 1/10.89 for the frequency used in the analyses. Thus, the numerical results can be expected to be valid for a wall of approximately 10 m height. Nevertheless, the purpose of this research is to develop a fundamental methodology, through model test simulation, for the dynamic earth pressure analysis.

On the other hand, Mononobe-Okabe's analytical method for dynamic earth pressure calculation is a quasi-static method in the sense that the dynamic effect is taken into consideration by using the horizontal seismic coefficient k_h as a ratio of the maximum acceleration (α_{max}) to acceleration due to gravity (g). Until now, Mononobe-Okabe's theory is the only method for designing retaining walls under dynamic loading. In spite of the fact that the method makes many simplifying assumptions the results given by it show satisfactory agreement with the experimental results (Ichihara and Matsuzawa (1973), Sherif et al (1982), Ishibashi and Fang (1987), Kawamura et al (1987)), in the case of maximum inertia force. However, in the case of minimum inertia force, the Mononobe-Okabe's theory underestimates the dynamic earth pressure. Therefore, many researchers recommended that a reduced value of the angle of internal friction ϕ should be used for calculating the earth pressure at the minimum inertia force. In this research a pure sinusoidal wave was used as an input motion. Hence, a direct comparison is not expected to give much fruitful conclusions. However, considering the fact that Mononobe-Okabe's quasi-static method is still used in design offices of many countries in the world, the numerical results were compared with the method and drawbacks of the method was brought to the light.

The Mononobe-Okabe theory assumes a linear increase of k_h with increasing maximum acceleration. Noda et al (1975) proposed that for low level of acceleration (acceleration < 200 gals) the relation is acceptable, however, at higher levels the coefficient increases non linearly. Thus,

$$k_h = \frac{\alpha_{max}}{g}; \qquad \alpha_{max} \leq 200 \text{ gals} \tag{6.3}$$

$$k_h = \frac{1}{3}\left(\frac{\alpha_{max}}{g}\right)^{\frac{1}{3}}; \qquad \alpha_{max} \geq 200 \text{ gals} \tag{6.4}$$

Matsuo and Itabashi (1984), based on inverse analysis from the data of maximum ground acceleration of actual earthquakes, proposed the following equation:

$$k_h = 0.072 + 0.332\left(\frac{\alpha_{max}}{g}\right) \tag{6.5}$$

Fig. 6.30 shows the relationship connecting the seismic coefficient and the maximum acceleration given by Eqs. (6.3)-(6.5). Noda et al's proposal shows that after 200 gals of

acceleration Eq. (6.3) overestimates the seismic coefficient. Matsuo and Itabashi's proposal shows that beyond 100 gals of acceleration, the seismic coefficient decreases compared to Mononobe-Okabe's assumption and the relationship is linear.

Ichihara and Yamada (1982), based on the response analysis using SHAKE for the city of Tokyo during the Great Kanto earthquake, proposed expression for the seismic coefficients, which are functions of $\frac{\alpha_{max}}{f}$, called the *pseudo velocity*. The expression takes the following mathematical form:

$$k_h = A \times (\frac{\alpha_{max}}{f})^B \tag{6.6}$$

where, A and B are constant depending on the characteristics of the soil deposit (alluvium or dilluvium), and f is the natural frequency of vibration.

The present design code in Japan uses relations (6.3) and (6.4) for calculating the dynamic earth pressure using Mononobe-Okabe's theory. However, in the strict sense of the seismic motion, this coefficient does not express the magnitude of acceleration; rather it is a coefficient which converts the dynamic effect to a quasi-static load on the structures.

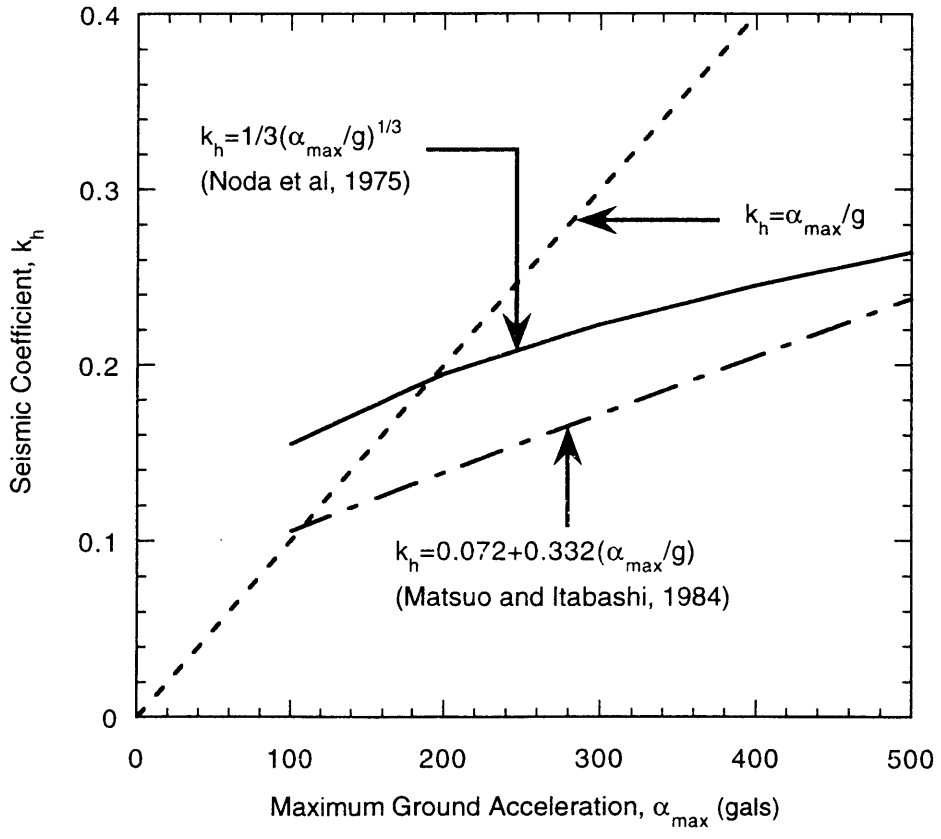

Fig. 6.30 Relation between the seismic coefficient and the maximum acceleration

Another drawback of Mononobe-Okabe's theory is that it does not consider the effect of interaction of the soil and the structure. In order to analyze a soil-structure system, under the dynamic loading with input acceleration $\ddot{u}_g(t)$, the following differential equation needs to be solved.

$$\underset{\text{< Response >}}{\mathbf{M}\ddot{u}(t) + \mathbf{C}\dot{u}(t) + \mathbf{K}u(t)} = \underset{\text{< Input >}}{-\mathbf{M}\ddot{u}_g(t)} \tag{6.7}$$

where **M**, **C** and **K** are the mass, damping and stiffness matrices, and u(t), $\dot{u}(t)$ and $\ddot{u}(t)$ are the response displacement, velocity and acceleration vectors respectively. As shown in Eq. 6.7, the left hand side of the equation represents the response of the structure, and the right hand side represents the input motion. However, Mononobe-Okabe's theory considers only the input or causes using only the maximum acceleration acting on the structure, regardless of the response that is also affected by the soil-structure interaction. In addition, the theory assumes that the displacement is sufficient to mobilize the full shear strength along the failure surface, and the earth pressure is distributed hydrostatically. All these drawbacks could be dealt appropriately by performing dynamic analyses, which was one of the objectives of this research.

6.9 SUMMARY AND CONCLUDING REMARKS

A new methodology is presented, in this chapter, for the seismic analysis of earth pressure against rigid retaining walls. It uses the constitutive model discussed in Chapter 3 (*Coupled Shear Band Method*), and an interface model that allows debonding of the wall and backfill when the inertia force acts away from the wall. The methodology is applied to simulate an experimental research on the seismic earth pressure. The various parameters relating the seismic earth pressures are calculated at different accelerations, and the validity of the developed methodology is described through the comparative discussion. The *Coupled Shear Band Method* demonstrates its efficacy by its power of capturing the progressive deformation characteristics of the sandy backfill more efficiently than the conventional FE analysis.

The assumption of perfect bonding at the interface can not simulate the actual response of the retaining wall-backfill system during dynamic loading. The performance of the interface model in simulating the wall friction could be enhanced by considering the debonding mode at the interface as compared to that where only the sticking and the sliding mode of the interface were considered.

The progressive failure of the backfill culminates in forming the active wedge, and the failure pattern determines the shape of the distribution curve at the active state, which is nonlinear. The domain of the failure zone increases as the acceleration level increases. As in the static case, the progressive failure pattern of the backfill is found to depend on the wall displacement modes.

The mobilization of the friction angle along the failure surface is progressive, not simultaneous. At the active state, the mobilized friction angles at the various locations of the failure surface are different. The coefficient of the seismic active thrust given by Mononobe-Okabe's theory agrees reasonably with the experimental as well as numerical values, if the average value of the maximum mean friction angle is used for the value of ϕ.

The seismic increment of the active thrust varies non linearly with increasing acceleration, and the magnitude depends on the wall displacement modes. However, its point of application is not significantly affected by the acceleration and the wall displacement modes. At the high acceleration levels, the value fluctuates around 0.5H for all the modes, which is in agreement with the experimental findings of other researchers.

REFERENCES

[1] Bakeer, R.M. and Bhatia, S.K. (1985), "Dynamic Earth Pressure behind Gravity Walls Subjected to Sinusoidal Motion", *Proceedings of the Second International Conference on Soil Dynamics and Earthquake Engineering*, pp. 3-12.

[2] Desai, C.S. (1981), "Behavior of Interfaces Between Structural and Geologic Media", *Proceedings of the International Conference on Recent Advances of Geotechnical Earthquake Engineering and Soil Dynamics*, St. Louis, Missouri, USA, pp. 619-638.

[3] Desai, C.S., Somasundaram, S. and Faruque, M.O. (1985), "Constitutive Modelling of Geological Materials: A General Procedure", In *Development in Soil Mechanics and Foundation Engineering - 2, Stress-strain Relation*, Ed. P. K. a. B. Banerjee R., Elsevier Applied Science, pp. 43-67.

[4] Desai, C.S., Zaman, M.M., Lightner, J.G. and Siriwardane, H.J. (1984), "Thin-layer Element for Interfaces and Joints", *International Journal of Numerical and Analytical Methods in Geomechanics*, Vol. 8, pp. 19-43.

[5] Dimarogona, P.D. (1983), "Distribution of Lateral Earthquake Pressure on a Retaining Wall", *Soils and Foundations, JSSMFE*, Vol. 23, 4, pp. 1-10.

[6] Drumm, E.C. and Desai, C.S. (1986), "Determination of Parameters for a Model for the Cyclic Behaviour of Interfaces", *Earthquake Engineering and Structural Dynamics*, Vol. 14, pp. 1-18.

[7] Elgamal, A-W. and Alampalli, S. (1992), "Earthquake Response of Retaining Walls: Full Scale Testing and Computational Analysis", *Proceedings of the 10th World Conference on Earthquake Engineering*, Madrid, Spain, pp. 1671-1676.

[8] Fukuoka, M. and Imamura, Y. (1984), "Researches on Retaining Walls During Earthquakes", *Proceedings of the Eighth World Conference on Earthquake Engineering*, San Francisco, USA, pp. 501-508.

[9] Hazarika, H., Matsuzawa, H. and Sugimura, M. (1993), "Elasto-plastic Analysis of Static and Dynamic Active Earth Pressure Against Rigid Retaining Wall", *Proceedings of the 48th Annual Conference of Japanese Society of Civil Engineers*, Fukuoka, Japan, pp. 852-853.

[10] Hazarika, H., Matsuzawa, H. and Sugimura, M. (1995), "The Influence of Interface Behavior on the Dynamic Earth Pressure Analyses", *Proceedings of the Annual Conference of the Chubu Branch of JSCE*, Nagoya, Japan, pp. 357-358.

[11] Hazarika, H. (1995), "Progressive Failure Analyses of a Retaining Wall-Backfill System Based on Smeared Shear Band Technique", *Proceedings of the 50th Annual Conference of Japanese Society of Civil Engineers*, Matsuyama, Japan, pp. 986-987.

[12] Hazarika, H. (1995), "Seismic Earth Pressure Analyses against a Rigid Retaining Wall Undergoing Various Modes of Movement Based on Coupled Shear Band Method", *Proceedings of the 7th Special Symposium on Dynamic Problems in Geotechnical Engineering, Chubu Branch of Japanese Geotechnical Society*, Nagoya, Japan, pp. 27-34.

[13] Hazarika, H. and Matsuzawa, H. (1995), "Coupled Shear Band Method and Its Application to the Seismic Earth Pressure Problems", *Soils and Foundations, Japanese Geotechnical Society* (Submitted for possible publication).

[14] Iai, S. and Kameoka, T. (1993), "Finite Element Analysis of Earthquake Induced Damage to Anchored Sheet Pile Quay Walls", *Soils and Foundations*, Vol. 33, 1, pp. 71-91.

[15] Ichihara, M. and Matsuzawa, H. (1970), "Corelations between Properties of Earth Pressure on Tilting Wall and the Shearing Characteristics of Dry Backfill Sand", *Journal of JSCE*, Vol. 176, pp. 61-74.

[16] Ichihara, M. and Matsuzawa, H. (1973), "Earth Pressure During Earthquake", *Soils and Foundations, JSSMFE*, Vol. 13, 4, pp. 75-86.

[17] Ichihara, M. and Yamada, K. (1982), "Application of Microzonation for the Damage of Water Pipelines", *Proceedings of the Third International Earthquake Microzonation Conference*, pp. 1665-1676.

[18] Ishibashi, I. and Fang, Y.S. (1987), "Dynamic Earth Pressure with Different Wall Movement Modes", *Soils and Foundations, JSSMFE*, Vol. 27, 4, pp. 11-22.

[19] Kawamura, M., Kuribayashi, E. and Shiga, K. (1987), "Effect of Interactions on Dynamic Active Earth Pressures", In *Development in Geotechnical Engineering- Soil Dynamics and Liquefaction*, Ed. A. S. Cakmak, Elsevier, Amsterdam, Holland, pp. 103-110.

[20] Loret, B. and Prevost, J.H. (1990), "Dynamic Strain Localization in Elasto-(visco)plastic Solids, Part 1. General Formulation and One-Dimensional Examples", *Computer Methods in Applied Mechanics and Engineering*, Vol. 83, pp. 247-273.

[21] Matsuo, M. and Itabashi, K. (1984), "Study on Aseismicity Evaluation of Slopes and Earth Structures", *Journal of JSCE*, Vol. 352, III-2, pp. 139-147 (In Japanese).

[22] Matsuzawa, H. (1973), "Earth Pressure Measurement and Static and Dynamic Earth Pressure against Retaining Walls", *Doctoral Thesis (In Japanese)*, Nagoya University, School of Engineering.

[23] Matsuzawa, H., Hazarika, H. and Sugimura, M. (1994), "Elasto-plastic Analysis of Dynamic Active Earth Pressure Considering the Wall Movement Modes", *Proceedings of the Eighth International Conference on Computer Methods and Advances in Geomechanics*, West Virginia, USA, pp. 2471-2476.

[24] Matsuzawa, H., Hazarika, H. and Sugimura, M. (1995), "Seismic Earth Pressure Analyses Considering the Localized Deformation of the Backfill Sand", *Proceedings of the International Workshop on Wind and Earthquake Engineering for Offshore and Coastal Facilities*, Berkeley, USA, pp. 367-372.

[25] Matsuzawa, H., Hazarika, H. and Sugimura, M. (1995), "Wall Movement Modes Dependent Dynamic Active Earth Pressure Analyses Using Cracked Element", *Proceedings of the Third International Conference on Recent Advances in Geotechnical Earthquake Engineering and Soil Dynamics*, Missouri-Rolla, USA, pp. 331-334.

[26] Nadim, F. and Whitman, R.V. (1983), "Seismically Induced Movement of Retaining Walls", *Journal of Geotechnical Engineering, ASCE*, Vol. 109, GT 7, pp. 915-931.

[27] Nazarian, H.N. and Hadjian, A.H. (1979), "Earthquake-Induced Lateral Soil Pressures on Structures", *Journal of the Geotechnical Engineering Division, ASCE*, Vol. 105, GT 9, pp. 1049-1066.

[28] Needleman, A. (1989), "Dynamic Shear Band Development in Plane Strain", *Journal of Applied Mechanics, ASME*, Vol. 56, pp. 1-9.

[29] Noda, S., Uwabe, T. and Chiba, T. (1975), "Relation Between Seismic Coefficient and Ground Acceleration for Gravity Quaywall", *Report of the Port and Harbor Research Institute, Japan*, Vol. 14, 4, pp. 67-111 (In Japanese).

[30] Owen, O.R.J. and Hinton, C. (1980), *Finite Elements in Plasticity*, Pineridge Press, Swansea, UK.

[31] Pietruszczak, S. and Poorooshasb, H.B. (1985), "On Modelling of Cyclic Behaviour of Soils", In *Developments in Soil Mechanics and Foundation Engineering - 2, Stress-strain Modelling of Soils*, Ed. Banerjee and Butterfield, Elsevier Applied Science, pp. 139-184.

[32] Prakash, S. (1981), "Analysis of Rigid Retaining Walls During Earthquakes", *Proceedings of the International Conference on Recent Advances in Geotechnical Earthquake Engineering and Soil Dynamics*, Rolla, Missouri, USA, pp. 993-1019.

[33] Prevost, J.H. and Loret, B. (1990), "Dynamic Strain localization in Elasto-(visco-)plastic Solids, Part 2. Plane Strain Examples", *Computer Methods in Applied Mechanics and Engineering*, Vol. 83, pp. 275-294.

[34] Seed. H.B. and Whitman, R.V. (1970), "Design of Earth Retaining Structures for Dynamic Loads", *Proceedings of the Special Conference on Lateral Stress, Ground Displacement and Earth Retaining Structures*, Ithaca, New York, pp. 103-147.

[35] Sherif, M.A., Ishibshi, I. and Lee, C.D. (1982), "Earth Pressure Against Rigid Retaining Walls", *Journal of Geotechnical Engineering Division, ASCE*, Vol. 108, GT 5, pp. 679-695.

[36] Toki, K., Sato, T. and Miura, F. (1981), "Separation and Sliding Between Soil and Structure During Strong Ground Motion", *Earthquake Engineering and Structural Dynamics*, Vol. 9, pp. 263-277.

[37] Zaman, M.M., Desai C.S. and Drumm, E.C. (1984), "Interface Model for Dynamic Soil-Structure Interaction", *Journal of Geotechnical Engineering, ASCE*, Vol. 110, GT 9, pp. 1257-1273.

[38] Zienkiewicz, O.C., Leung, K.H. and Pastor, M. (1985), "Simple Model for Transient Soil Loading in Earthquake Analysis. I. Basic Model and Its Application", *International Journal of Numerical and Analytical Methods in Geomecahnics*, Vol. 9, pp. 453-476.

CHAPTER
SEVEN

Summary and Conclusions

The point is not to pocket
the truth, but to chase it

Elio Vittorini

7.1 SYNOPSIS

The analytical methods for earth pressure calculation, based on the classical theory and the others with rigid-plastic assumption, can not capture the progressive deformation phenomenon such as earth pressure development against a retaining wall. Hence, researchers resort to numerical methods. In this dissertation, a numerical method is presented for the analysis of a retaining wall-backfill system that considers the progressive deformation characteristics of the backfill such as localization.

The three main issues of interests, in this dissertation, were:

(1) Modeling of the Backfill Considering the Localized Deformation

(2) Development of a Simple Interface Model

(3) The Wall Displacement Modes Dependent Earth Pressure (both static and dynamic)

A new constitutive formulation was derived, based on smeared shear band technique, utilizing two shear bands (named *Coupled Shear Band Method*), in order to capture the progressive deformation of the backfill mass. In contrast to the conventional shear band formulation, the *Coupled Shear Band Method* considers two shear bands inside a localized element. The constitutive relation was formulated by coupling the two bands. It contains the width of the shear bands, which represents the "geometric softening".

Various interface models with varying degree of complexity are available in the literature till date. A new simplified interface model from the point of view of the earth pressure analysis was also presented in this thesis. The merit of this interface model lies in its simplicity and minimum material parameters to describe it.

Earth pressure (both the static and the dynamic) acting against model retaining walls was analyzed using the described computational model. The influence of the wall displacement

modes on the static as well as the dynamic earth pressure was discussed in detail. Based on the results of the numerical analyses, empirical equations were put forward expressing the wall displacement modes dependent character of the earth pressure, which are functions of the backfill strength (ϕ) and the acceleration (α). Thus, the total seismic active earth pressure (K_{AE}) can be calculated from the total static active earth pressure (K_A) and the seismic increment (K_{IAE}) for each mode, which can be expressed in the following way:

$$K_{AE} = K_A(\phi, M_1) + K_{IAE}(\alpha, M_2) \tag{7.1}$$

where, M_1 and M_2 are the parameters that take different values depending on the wall displacement modes.

7.2 CONCLUSIONS OF THIS RESEARCH

The key findings of this research can be summarized as follows:

(1) The earth pressure development against retaining structures involves the phenomenon of progressive deformation. Hence, numerical analysis of retaining structures should adopt constitutive description that can adequately express the deformation that takes place progressively in the backfill. The constitutive relation based on the localized deformation can capture the progressive deformation more efficiently than that of the conventional strain-hardening constitutive relation.

(2) The progressive failure patterns of the backfill are influenced by the modes of displacement of the wall, which in turn influence the patterns of the earth pressure distributions. In earthquake loading condition, the domain of the failure zone increases as the acceleration level increases.

(3) The active state can be defined as that state of the backfill when it forms a clear failure wedge or a slip surface.

(4) The mobilization of the friction angle along the failure surface is progressive, not simultaneous. At the active state, the mobilized friction angles at the various locations of the failure surface are different. The mean values of the mobilized friction angle are not significantly affected by the acceleration levels.

(5) The coefficient of the active earth pressure and the point of application of the resultant active thrust depend on the modes of movement of the wall.

(6) Dubrova's analytical solutions (static earth pressure) are able to express the different nonlinear distribution of the active stress for various modes. However, the resultant active thrusts given by that method coincide with Coulomb's solution (i.e. irrespective of the wall displacement modes). Dimarogona's analytical method for the seismic earth

pressure calculation has similar drawbacks too. It can express the nonlinear distribution of the earth pressure, for various modes of wall movement, only qualitatively.

(7) The seismic increment of the active thrust varies non linearly with increasing acceleration, and the magnitude depends on the wall displacement modes. However, its point of application is not strongly affected by the acceleration and the wall displacement modes; the value converges towards the mid-height of the wall for all the modes at the high acceleration level.

(8) Interface elements with zero thickness as idealized in this research, can simulate the wall friction satisfactorily when the appropriate parameters are determined suitably from the experiments. The assumption of equal values of $\tan\delta$ for all the interface elements at different depths may be a gross approximation leading to variation in the behavior of the friction coefficient in the analyses. An experimental study in this regard will be a big boon to this field of research.

7.3 FINALE

The present study relates to the active movement of the retaining wall. The efficacy of the computational model should be more pronounced if applied for the passive condition in which case the shear band consideration would be indispensable as the continuity of the stress field within the backfill, under no circumstances would prevail due to large displacements involved.

Complexity was sacrificed in favor of simplicity in certain cases. However, this should not always be case, as A.N. Whitehead said, "The only simplicity to be trusted is the simplicity on the far side of the complexity".

Considering the fact that many important retaining structures are constructed on waterfronts, the model can be extended to include saturated backfill (submerged soil). In addition, the application of the described model to practical retaining wall problem will continue to offer insight into the importance and relevance of various governing mechanisms of backfill deformations. New ideas will definitely make room for the improvement of the present model. To put it into the words of the Greek philosopher Heraclitus - **Τα παντα ρει** (Everything flows).

APPENDIX
A

Logarithmic Spiral Method

A1 EARTH PRESSURE CALCULATION BASED ON CURVED FAILURE SURFACE

Mononobe-Okabe's theory for the dynamic earth pressure calculation assumes the rupture surface of the failure wedge as a plane surface. However, experiments and theoretical investigations established the fact that the sliding surface is composed of a curved part in the lower section and of a plane part which corresponds to the Rankine state. The exact equation of the curved part has not yet been found - it is likely that the respective differential equations can not be solved in a closed form. Therefore, in practice, the real curve is replaced by simple curve. Two types of slip curves are mainly in use: the circle and the logarithmic spiral.

Ichihara et al (1973) analytically derived expressions for calculation of the passive earth pressure coefficient during earthquake by assuming the slip surface to be composed of a logarithmic spiral and a straight line. It has been proved that the active coefficient for the static earth pressure using curved slip surface does not differ significantly from that of the straight line surface even though their counter part (the passive coefficient) does differ. The same can not be true for the dynamic active earth pressure calculation, where the effect of the inertia force enters into the governing equations. The Logarithmic Spiral Method proposed by Ichihara et al (1973) is extended to compute the dynamic active earth pressure coefficient, the details of which follow.

A2 LOGARITHMIC SPIRAL METHOD FOR CALCULATING THE ACTIVE EARTH PRESSURE

An Inclined retaining wall with vertical height H is shown in Fig. A1. The sliding surface is approximated to be consisting of a logarithmic spiral BD (convex spiral) and a straight line DC. Within the soil mass ADC, the state of stress is same as the Rankine active pressure. The dynamic force acting on the vertical section FD are P_{DN} and P_{DS} as shown in Fig. A1. The center of the logarithmic spiral is at O.

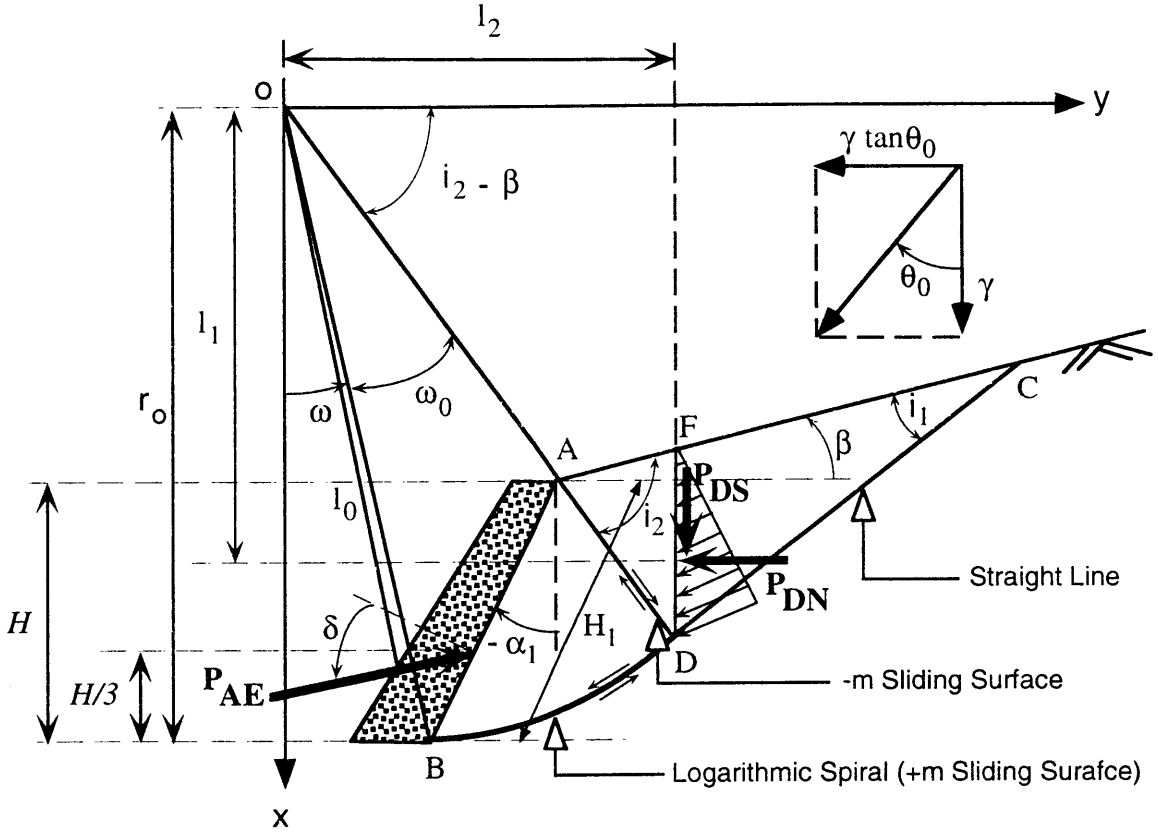

Fig. A1 Backfill with composite sliding surface

From the moment equilibrium, the following equation can be obtained.

$$P_{AE} l_0 = -M_1 + M_2 + M_3 + M_4 \qquad \text{(A1)}$$

Here, l_0 = Arm length of the resultant active earth pressure, P_{AE}

M_1 = Moment about O of the assumed soil mass of ΔOBA including the seismic effect

M_2 = Moment about O of the assumed soil mass of sector OBD including the seismic effect

M_3 = Moment about O of the assumed soil mass of ΔADF including the seismic effect

M_4 = Moment about O of the active Rankine earth pressure including the seismic effect acting upon the vertical section FD.

Moment M_1

Assuming only the horizontal component of the input acceleration, α, we get:

$$M_1 = S_{OBA}(x_{G1}k_h + y_{G1}) \tag{A2}$$

where $k_h = \tan\theta_0 = \frac{\alpha}{g}$, g being the acceleration due to gravity. The area S_{OBA} and the center of gravity (x_{G1}, y_{G1}) of ΔOBA can be obtained from the simple geometry.

Moment M_2

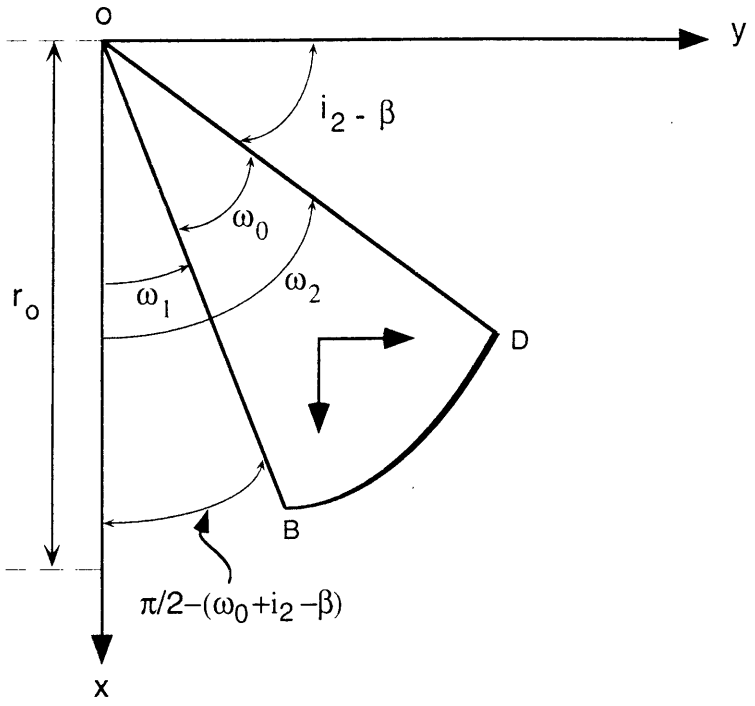

Fig. A2 Illustration of calculating the moment M_2

The equation of the sliding surface is given by,

$$r = r_0 e^{-\omega \tan\phi} \tag{A3}$$

here, ω is the angle of vector r from r_0 and is considered positive if measured counterclockwise. The moment M_2 is given by:

$$M_2 = M_x + M_y \tag{A4}$$

where M_x and M_x are derived to be,

$$M_x = \frac{\frac{1}{3}r_0^3}{1+C_1^2}[e^{C_1\omega}(C_1\sin\omega - \cos\omega)]_{\omega_1}^{\omega_2} \tag{A5}$$

$$M_y = \frac{\frac{1}{3}r_0^3\tan\theta_0}{1+C_1^2}[e^{C_1\omega}(C_1\cos\omega + \sin\omega)]_{\omega_1}^{\omega_2} \tag{A6}$$

$C_1 = -3\sin\phi$, ϕ is the angle of internal friction of the backfill. The vector r_0 can be derived as,

$$r_0 = \frac{\cos(\beta - i_2 - \alpha_1)}{\sin\omega_0}H_1 e^{(\frac{\pi}{2}-(\omega_0+i_2-\beta))\tan\phi} \tag{A7}$$

Moment M_3

The moment M_3 is given by,

$$M_3 = S_{ADF}(k_h x_{G3} + y_{G3}) \tag{A8}$$

where (x_{G3}, y_{G3}) is the center of gravity of ΔADF (Fig. A1) and S_{ADF} represents the area of ΔADF.

Moment M_4

The forces acting on the soil mass in the active Rankine zone during earthquake is shown in Fig. A1. The Mohr circle for the plastic equilibrium state is shown in Fig. A3. Using this figure, The normal resultant force, P_{DN} and the shear force, P_{DS} (both the forces are considered positive in the shown direction) are calculated to be,

$$P_{DN} = \frac{\gamma\overline{FD}^2\cos\beta}{2\cos^2\phi\cos\theta_0}[1 - \sin\phi\cos(\Delta_0 + \theta_0 - \beta)]C_2 \tag{A9}$$

$$P_{DS} = \frac{\gamma\overline{FD}^2\cos\beta}{2\cos^2\phi\cos\theta_0}\sin\phi\sin(\Delta_0 + \theta_0 - \beta)C_2 \tag{A10}$$

where, $\sin\Delta_0 = \frac{\sin\beta_0}{\sin\phi}$; $C_2 = \cos\beta_0 - \sqrt{(\cos^2\beta_0 - \cos^2\phi)}$ and $\beta_0 = \beta + \theta_0$ ($\beta_0 \le \phi$).

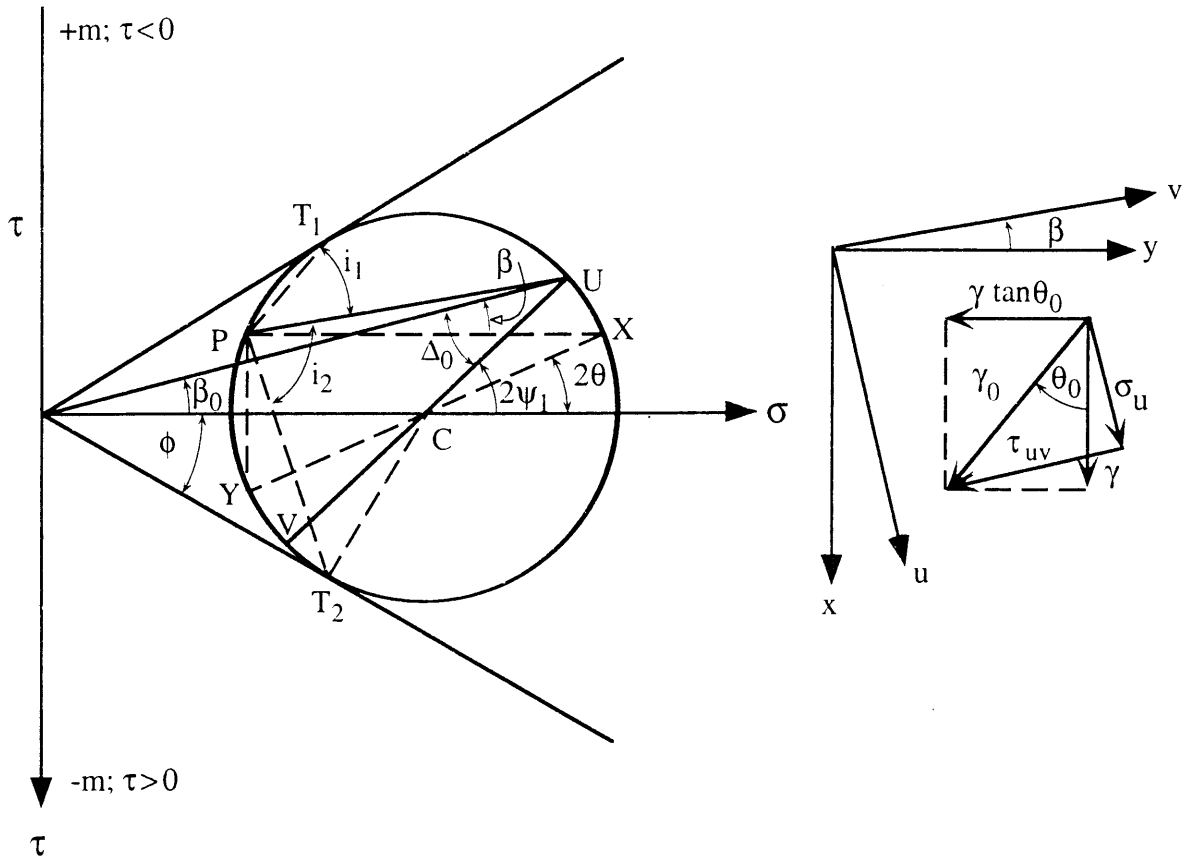

Fig. A3 Calculation of the moment M_4

The arm lengths l_1 and l_2 are given by

$$l_1 = \overline{OD}\sin(i_2 - \beta) - \tfrac{1}{3}\overline{FD} \tag{A11}$$

$$l_2 = \overline{OD}\cos(i_2 - \beta) \tag{A12}$$

Hence the moment M_4 is given by

$$M_4 = l_1 P_{DN} + l_2 P_{DS} \tag{A13}$$

Arm Length l_0

The arm length l_0 of P_{AE} can be obtained as follows.

$$l_0 = \overline{OB}\sin(\delta + \omega_0 + i_2 + \alpha_1 - \beta) - \tfrac{1}{3}H_1\cos\delta \tag{A14}$$

Angle between the Backfill Surface and the Sliding Surfaces

Considering the Mohr diagram (Fig. A3) and from geometry we get,

$$i_1 = \frac{\pi}{4} + \frac{\phi}{2} - \frac{(\beta_0 + \Delta_0)}{2} \tag{A15}$$

$$i_2 = \frac{\pi}{4} + \frac{\phi}{2} + \frac{(\beta_0 + \Delta_0)}{2} \tag{A16}$$

Angle between the X Axis and the Sliding Surface AD

The angle α_2 between the X-axis and the sliding surface AD can be obtained as

$$2\alpha_2 = \frac{\pi}{2} - \phi + \beta - \Delta_0 - \theta_0 \tag{A17}$$

The clockwise moments are considered positive throughout the formulations. Substituting the values of M_1, M_2, M_3, M_4 and l_0 given by the above equations in Eq. A1, the resultant force of active earth pressure can be obtained from the maximum value of P_{AE} for various values of ω_0 shown in Fig. A1. If the wall is forced down with reference to the backfill, for instance by the action of a heavy load on its crest, the value of δ becomes negative and the curvature of the lower part of the failure surface is reversed (i.e. concave spiral). In that case the above equations need to be reformulated using the concave logarithmic spiral, the details of which is not discussed here.

REFERENCES

[1] Ichihara, M., Mori, N., Nakane, S. and Hirano, I. (1973), "Passive Earth Pressure Coefficient During Earthquake", *Memoirs of the Faculty of Engineering Nagoya University*, Vol. 25, 2, pp. 129-179.

[2] Matsuzawa, H., Hazarika, H. and Sugimura, M. (1994), "Elasto-plastic Analysis of Dynamic Active Earth Pressure Considering the Wall Movement Modes", *Proceedings of the Eighth International Conference on Computer Methods and Advances in Geomechanics*, West Virginia, USA, pp. 2471-2476.

APPENDIX
B

Solution of Equilibrium Equation in Dynamic Analysis

B1 NONLINEAR DYNAMIC ANALYSIS

The finite element equation for a dynamic system is represented by:

$$\mathbf{M}\ddot{u}(t) + \mathbf{C}\dot{u}(t) + \mathbf{K}u(t) = \mathbf{R}(t) \tag{B1}$$

where **M**, **C** and **K** are the mass, damping and stiffness matrices; R is the external load vector; and u(t), $\dot{u}(t)$ and $\ddot{u}(t)$ are the displacement, velocity and acceleration vectors of the finite element assemblage.

The Wilson θ method renders the following equation of motion for the finite element assemblage:

$$\mathbf{M}\left\{\frac{6}{(\theta\Delta t)^2}\hat{\Delta}u(t) - \frac{6}{\theta\Delta t}\dot{u}(t) - 3\ddot{u}(t)\right\} + \mathbf{C}\left\{\frac{3}{\theta\Delta t}\hat{\Delta}u(t) - 3\dot{u}(t) - \frac{\theta\Delta t}{2}\ddot{u}(t)\right\} + \mathbf{K}\hat{\Delta}u(t) = \hat{\Delta}\mathbf{R}(t) \tag{B2}$$

where,

$$\hat{\Delta}u(t) = u(t+\theta\Delta t) - u(t) \tag{B3}$$

$$\hat{\Delta}\mathbf{R}(t) = \mathbf{R}(t+\theta\Delta t) - \mathbf{R}(t) \tag{B4}$$

On rearranging the terms, Eq. B2 takes the following form:

$$\overline{K}(t)\hat{\Delta}u(t) = \hat{\Delta}\overline{\mathbf{R}}(t) \tag{B5}$$

where,

$$\overline{\mathbf{K}}(t) = \mathbf{K} + \mathbf{M}\frac{6}{(\theta\Delta t)^2} + \mathbf{C}\frac{3}{\theta\Delta t} \tag{B6}$$

$$\hat{\Delta}\overline{\mathbf{R}}(t) = \hat{\Delta}\mathbf{R}(t) + \mathbf{M}\left\{\frac{6}{\theta\Delta t}\dot{u}(t) + 3\ddot{u}(t)\right\} + \mathbf{C}\left\{3\dot{u}(t) + \frac{\theta\Delta t}{2}\ddot{u}(t)\right\} \tag{B7}$$

In the formulations described above $\theta = 1.4$ and Δt is a suitably chosen time increment.

B2 SOLUTION OF NONLINEAR EQUATIONS

The solution of Eq. B5 gives the values of $\hat{\Delta}u(t)$ at time $t + \theta\Delta t$. In order to calculate the variables $u(t)$, $\dot{u}(t)$ and $\ddot{u}(t)$ at time $t + \Delta t$, the following procedure is adopted.

(1) From the solution of Eq. B5, calculate $\hat{\Delta}\ddot{u}(t)$, employing Eq. B8 which is of the form:

$$\hat{\Delta}\ddot{u}(t) = \frac{6}{(\theta\Delta t)^2}\hat{\Delta}u(t) - \frac{6}{\theta\Delta t}\dot{u}(t) - 3\ddot{u}(t) \tag{B8}$$

(2) Calculate $\Delta\ddot{u}(t)$ using the equation

$$\Delta\ddot{u}(t) = \frac{1}{\theta}\hat{\Delta}\ddot{u}(t) \tag{B9}$$

(3) Calculate $\Delta\dot{u}(t)$ and $\Delta u(t)$ employing the following equations.

$$\Delta\dot{u}(t) = \ddot{u}(t)\Delta t + \Delta\ddot{u}(t)\frac{\Delta t}{2} \tag{B10}$$

$$\Delta u(t) = \dot{u}(t)\Delta t + \ddot{u}(t)\frac{\Delta t^2}{2} + \Delta\ddot{u}(t)\frac{\Delta t^2}{6} \tag{B11}$$

(3) Calculate the values at time $t + \Delta t$ by employing the following equations

$$u(t + \Delta t) = u(t) + \Delta u(t) \tag{B12}$$

$$\dot{u}(t+\Delta t) = \dot{u}(t) + \Delta\dot{u}(t) \tag{B13}$$

$$\ddot{u}(t+\Delta t) = \ddot{u}(t) + \Delta\ddot{u}(t) \tag{B14}$$

The equilibrium equation to be solved, in nonlinear analysis, at time t + Δt using modified Newton-Raphson method (k = 1,2,3....) can be written (neglecting the damping matrix **C**) in the following form.

$$\mathbf{M}^{(k)}\ddot{u}(t+\Delta t) + \mathbf{K}^{(k)}\Delta u(t) = \mathbf{R}(t+\Delta t) - {}^{(k-1)}\mathbf{F}(t+\Delta t) \tag{B15}$$

$${}^{(k)}u(t+\Delta t) = {}^{(k-1)}u(t+\Delta t) + {}^{(k)}\Delta u(t) \tag{B16}$$

B3 LOADING AND UNLOADING CRITERIA

For Backfill Element:

Loading Condition

When $(\sigma_1 - \sigma_3) = (\sigma_1 - \sigma_3)_{max}$ and

$d(\sigma_1 - \sigma_3) > 0$

Unloading condition

When $(\sigma_1 - \sigma_3) \leq (\sigma_1 - \sigma_3)_{max}$

$d(\sigma_1 - \sigma_3) < 0$

For Interface Element:

Loading Condition

When $\tau = \tau_{max}$ and $d\tau > 0$

Unloading condition

When $\tau \leq \tau_{max}$ and $d\tau < 0$

VITA

The author was born in Jorhat, a city in the North Eastern State of Assam, India on January 13, 1968. He is the youngest son of Swarnalata and Sreemanta Ram Hazarika. He passed his H.S.L.C. (High School Leaving Certificate) Examination in 1983 with first division from Balya Bhavan High School, Jorhat. He finished his Pre-Degree (Science) in 1985 from J.B. College, Jorhat standing 9th in the university. The author joined Indian Institute of Technology (IIT), Madras in 1986, and obtained his B.Tech degree in Civil Engineering in 1990.

In the year 1991, the author joined at Nagoya University earning his Master's Degree in Geotechnical Engineering in 1993 with the financial support from the ministry of education and culture, Japan, and continued his research for the Degree of Doctor of Engineering.